# From Landscape to Inflationary Perturbations

**Dissertation**
**zur Erlangung des Doktorgrades**
**des Department Physik**
**der Universität Hamburg**

vorgelegt von
Cecelie Hector
aus Hamburg

Hamburg
2012

| | |
|---|---|
| Gutachter des Dissertation: | Prof. Dr. L. Covi |
| | Prof. Dr. G. Sigl |
| Gutachter der Disputation: | Prof. Dr. L. Covi |
| | Dr. J. Kersten |
| Datum der Disputation: | 02. 04. 2012 |
| Vorsitzender des Prüfungsausschusses: | Dr. G. Steinbrück |
| Vorsitzender des Promotionsausschusses: | Prof. Dr. P. Hauschildt |
| Leiter des Departments Physik: | Prof. Dr. D. Pfannkuche |
| Dekan der Fakultät für Mathematik, Informatik und Naturwissenschaften: | Prof. Dr. H. Graener |

## Abstract

We discuss a quantum tunneling event in a piecewise potential where the false vacuum part is either linear or quartic and the true vacuum is described by a quartic potential. We find exact solutions for these tunneling processes and explain how exact tunneling solutions can give information about the local shape of the string theory landscape. We investigate the existence of bounce solutions for effective potentials with sharp minima and maxima. We also partly derive the two-point correlation function for a $\lambda\phi^4$-theory on a de Sitter background for a massless minimally coupled scalar field $\phi$.



## Zusammenfassung

Wir untersuchen den Tunnelprozess in gestückelten Potentialen, bei denen das falsche Vakuum entweder durch ein lineares oder ein quartisches Potential, das echte Vakuum in beiden Fällen durch ein quartisches Potential beschrieben wird. Wir finden exakte Lösungen für diese Tunnelprozesse und erklären, wie diese exakten Lösungen Hinweise auf die lokale Form der Stringtheorie Landscape geben. Außerdem gehen wir genauer auf die Existenz von Tunnellösungen bei effektiven Potentialen mit 'Knicken' an den Minima und Maxima ein. Ebenfalls haben wir teilweise die Zweipunkt Korrelationsfunktion für eine $\lambda\phi^4$-Theorie berechnet auf einem de Sitter Hintergrund für ein masseloses, minimal gekoppeltes, skalares Feld $\phi$.

# Contents

# 1. Introduction

Humor ist der Knopf, der verhindert, dass uns der Kragen platzt.

*(Joachim Ringelnatz)*

Over the last 20 years cosmology underwent an enormous change from being a very vague field of research to becoming a powerful area of precision science. This development has also been recognized by a number of Noble Prizes starting in 1978 with Penzias and Wilson 'for the discovery of the cosmic microwave background radiation', followed by Mather and Smoot in 2006 'for the discovery of the blackbody form and anisotropy of the cosmic microwave background', complemented in 2011 with the Prize for Perlmutter, Schmidt and Riess 'for the discovery of the accelerating expansion of the Universe through observations of distant supernovae' [1].

On the very theoretical side of cosmology it connects to string theory, which gives the motivation for the first two projects of this thesis. String theory is the leading candidate for a UV-complete theory describing our universe. Taking string theory for granted, we have to deal with a vast amount of different vacua, the number usually quoted is $10^{500}$ [2, 3]. At the time of the big bang, the energy per unit volume was very high, and the state of the universe was very far from any vacuum, true or false. As the universe expanded and cooled down, it might well have settled into a false vacuum instead of a true one. It then might travel through the string theory landscape via first order phase transitions [4, 5]. In this case, the scalar field potential possesses a number of local minima. A field that is initially trapped in a higher energy vacuum jumps to a lower energy vacuum via a quantum tunneling process.

Studies of these processes are often done using the thin-wall approximation. This is often not justified, especially not in string theory. There the differences of the potentials are usually too large for this approximation. Therefore, it is important to know exact solutions. So far, there were exact solutions only known for a small number of potentials. We found solutions for additional potentials. We also comment on what one can learn from these results about the local shape of the string theory landscape.

In a further step, we go into more detail on potentials with sharp minima and maxima, which need a different treatment.

The more observational side of cosmology motivates the last project of this thesis. The cosmic microwave background (CMB) radiation provides a lot of information about the universe. The anisotropies in the CMB go back to quantum fluctuations, which are stretched to classical fluctuations during inflation. Over the years, the quality of the

data on the CMB improved enormously from COBE to PLANCK. This pushes theorists to have a closer look at the theoretical background of these fluctuations. For example, one hopes to determine the right model of inflation with the help of these analyses.

Investigations of these perturbations are normally done by solving classical equations of motion, although it is not clear if this is a valid approximation. In [6] this was tested up to one-loop for a cubic inflaton potential. They calculated the two-point function for a scalar field. In the context of the CMB this corresponds to the temperature power spectrum. For tree-level and one-loop the approximation turned out to be valid, but it was not expected to be valid for two-loop. As an extension of this work we study a model with quartic inflaton potential up to two-loop corrections. The highly improved quality of CMB data from PLANCK demands the extension of the analysis to the next loop-level.

We do this using the closed time path formalism. We calculate the cosmological correlation functions after horizon exit for $\phi^4$-theory on a de Sitter background for a massless minimally coupled scalar field $\phi$. The calculation of the two-loop corrections is much more complicated than the oneloop corrections. One peculiarity here is that IR $\times$ UV-divergent terms can appear.

The thesis is organized as follows. In the next Chapter, we give an introduction to the field of cosmology and motivate the research work in the following Chapters. In Chapter 3 we present new exact tunneling solutions for specific potentials [7]. We discuss the existence of tunneling solutions in general and analyze in which cases potentials with kinks can be approximated with caps [8]. We calculate inflationary perturbations in Chapter 4 for a $\phi^4$-theory [9]. Finally, we conclude in Chapter 5.

# 2. The Universe

Above us only sky.

*(John Lennon)*

The purpose of this Chapter is to give a short introduction to the basics of modern cosmology. We start with general FRW cosmology focussing on the inflationary phase. We then give an introduction to the theory of density fluctuations. Finally we explain how these perturbations were created and how we can measure them today using the CMB. For a more comprehensive review we recommend [10–12].

## 2.1. General FRW cosmology

In Einstein's equations gravity is interpreted as curvature of space-time

$$R_{\mu\nu} - \frac{1}{2} g_{\mu\nu} R = 8\pi G T_{\mu\nu} + \Lambda g_{\mu\nu}, \quad \mu, \nu = 0 \ldots 3. \tag{2.1}$$

Here, $R_{\mu\nu}$ is the Ricci tensor and $R$ the Ricci scalar, both derived from the metric $g_{\mu\nu}$. $T_{\mu\nu}$ is the energy-momentum tensor and represents the matter content of the universe. $\Lambda$ stands for a (possible) cosmological constant, $G$ is Newton's constant giving the coupling.

Cosmological experiments measure an expanding universe that is homogeneous and isotropic (on large scales). This is described by the Friedmann-Robertson-Walker metric [13–16]

$$\mathrm{d}s^2 = \mathrm{d}x^\mu \mathrm{d}x^\nu g_{\mu\nu} = \mathrm{d}t^2 - a(t)^2 \left[ \frac{\mathrm{d}r^2}{1 - kr^2} + r^2 (\mathrm{d}\theta^2 + \sin^2\theta \mathrm{d}\phi^2) \right]. \tag{2.2}$$

$a(t)$ is the scale factor that describes the expansion of the universe. $k$ determines the geometry of the universe. For $k = -1$ we have an "open" universe, $k = 0$ means flat (favoured by observations), $k = 1$ means closed. We can rewrite the metric using conformal time $\mathrm{d}\tau \equiv \mathrm{d}t/a(t)$ as

$$\mathrm{d}s^2 = a^2(\tau) \left[ \mathrm{d}\tau^2 - \frac{\mathrm{d}r^2}{1 - kr^2} - r^2 \left( \mathrm{d}\theta^2 + \sin^2\theta \mathrm{d}\phi^2 \right) \right]. \tag{2.3}$$

Assuming this isotropic and homogeneous metric, the energy-momentum tensor of the universe is the one of a perfect fluid

$$T_{\mu\nu} = -p g_{\mu\nu} + (p + \rho) u_\mu u_\nu, \tag{2.4}$$

with pressure $p$ and energy density $\rho$. $u_\mu$ is the four-velocity of a comoving observer.

With Eq. (2.4), Einstein's equations (2.1) decouples into two independent components, the Friedman equations

$$\begin{aligned} H^2 = \left(\frac{\dot{a}}{a}\right)^2 &= \frac{8\pi G}{3}\rho + \frac{\Lambda}{3} - \frac{k}{a^2} \\ \frac{\ddot{a}}{a} &= -\frac{4\pi G}{3}(\rho + p) + \frac{\Lambda}{3}. \end{aligned} \tag{2.5}$$

$H$ is the Hubble parameter and gives the rate of expansion of the universe. The dot denotes the derivative with respect to $t$. Conservation of energy follows from Eq. (2.4) with $T_{\mu\nu_{|\nu=0}}$:

$$\partial_0 \rho = -3\frac{\dot{a}}{a}(p + \rho). \tag{2.6}$$

From now on, we assume a n-component ideal fluid, each component with an assigned pressure $p_i$ and density $\rho_i$. From the equation of state

$$p_i = w_i \rho_i \tag{2.7}$$

together with Eq. (2.6) we find a relation between the scale factor and the energy density

$$\rho_i \propto a^{-3(1+w_i)}. \tag{2.8}$$

We distinguish three different kinds of components: relativistic matter/radiation ($w = \frac{1}{3}$), nonrelativistic matter ($w = 0$) and vacuum energy/cosmological constant ($w = -1$). We define the critical density

$$\rho_{crit} = \frac{3H^2}{8\pi G}, \quad \Omega_i = \frac{\rho_i}{\rho_{crit}} \tag{2.9}$$

and rewrite Eq. (2.5) as

$$1 - \sum_i \Omega_i = -\frac{k}{a^2 H^2}. \tag{2.10}$$

The values of the $\Omega_i$ have been measured [17, 18] to be $\Omega_\Lambda = 0.73$: dark energy, $\Omega_{DM} = 0.22$: dark matter, $\Omega_M = 0.05$: baryonic matter, summing up to

$$\sum_i \Omega_i = \Omega_{total} \approx 1, \tag{2.11}$$

which corresponds to a flat universe.

## 2.2. Inflation

Inflation is a period of exponentially fast expansion of the universe. It was first introduced by Guth and Linde [19, 20]. The main motivation was to solve a number of puzzling measured properties to the universe. Inflation solves the **horizon** problem (Question: How can the universe be so homogeneous and isotropic, although it should consist of $10^5$ causally disconnected patches? Answer: During inflation, the universe expanded so fast that these patches are actually causally connected.) and the **flatness** problem (Question: Why is $\Omega_{total}$ so close to 1? This looks like extreme finetuning. Answer: The exponentially fast expansion drives the value towards 1.).

In the following discussion we will use $8\pi G = M_p^{-2} = 1 = \bar{h} = c$. We begin with the Einstein Hilbert action plus a scalar field in a FRW universe

$$S = \int \mathrm{d}^4 x \sqrt{|g|} \left( \frac{1}{2}\mathcal{R} + \frac{1}{2}\dot{\phi}^2 - V(\phi) \right). \tag{2.12}$$

In the flat case $k = 0$, we find

$$H^2 = \frac{1}{3}\left( \frac{1}{2}\dot{\phi}^2 + V(\phi) \right), \qquad \dot{H} = -\frac{1}{2}\dot{\phi}^2. \tag{2.13}$$

The equation of motion for the scalar field is

$$\ddot{\phi} + 3H\dot{\phi} + \partial_\phi V(\phi) = 0 \tag{2.14}$$

including the $\dot{\phi}$ friction term. Accelerated expansion, i.e. inflation, means

$$\frac{\ddot{a}}{a} = \dot{H} + H^2 > 0. \tag{2.15}$$

During inflation, the universe expands exponentially fast

$$a(t) \approx e^{Ht}, \quad H \approx const. \tag{2.16}$$

Choosing the scale factor this way, we have approximately a de Sitter universe ($H \equiv const$)

$$\mathrm{d}s^2 = \mathrm{d}t^2 - a^2(t)\mathrm{d}\mathbf{x}^2. \tag{2.17}$$

In conformal time $\tau$ with

$$\tau = -\int_t^\infty \frac{\mathrm{d}t'}{a(t')}, \quad -\infty < \tau < 0 \tag{2.18}$$

this becomes

$$\mathrm{d}s^2 = a^2(\tau)\left[\mathrm{d}\tau^2 - \mathrm{d}\mathbf{x}^2\right], \quad a(\tau) = -\frac{1}{H\tau}. \tag{2.19}$$

We will use this later in Chapter 4.

### Slow roll inflation

In slow roll inflation, we assume the potential to be very flat. This way, we can neglect $\ddot{\phi}$. We define the slow roll parameters

$$\epsilon_H = -\frac{\dot{H}}{H^2} \quad \text{and} \quad \eta_H = -\frac{\ddot{\phi}}{H\dot{\phi}} = -\frac{1}{2}\frac{\ddot{H}}{\dot{H}H}. \tag{2.20}$$

Neglecting $\ddot{\phi}$, Eq. (2.14) becomes

$$\dot{\phi} \approx -\frac{\partial_\phi V(\phi)}{3H} \approx 0. \tag{2.21}$$

From Eq. (2.13) we see that $H$ is almost constant now, thus $\epsilon_H \approx 0$. The criterion for successful inflation is $0 < \epsilon_H < 1$. This is equivalent to Eq. (2.15). In terms of the second slow roll parameter $\eta_H$ the condition for the $\ddot{\phi}$ term being negligible compared to the friction term is $\eta_H \ll 1$.

The simplest class of inflationary models are those with a monomial potential $V(\phi) = \lambda\phi^n$. In Chapter 4 we consider a model with $n = 4$. In Figure 2.1 we see that this model is not inside of the 95% CL region of the WMAP7+BAO+$H_0$ data. Being outside of the $2\sigma$ region in this plot does not at all mean exclusion. There are also several assumptions going into this plot that might be wrong. We study this potential, since it is the simplest model for investigating the two-loop contributions.

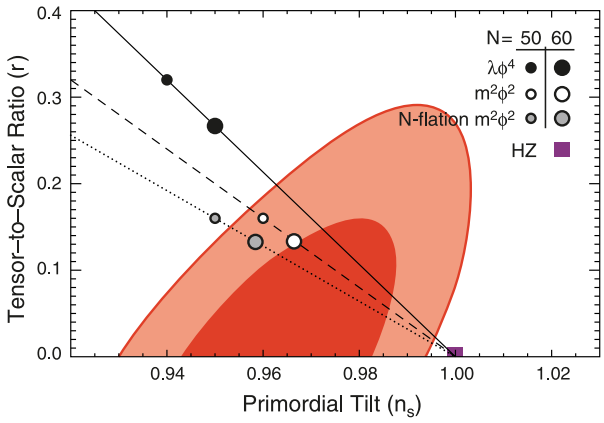


Figure 2.1.: *The 68% and 95% CL for the data derived from WMAP+BAO+$H_0$ [17]. $n_s$ is the scalar spectral index, $r$ is the tensor to scalar ratio.*

## 2.3. Tunneling universe

String theory is the leading candidate for a UV-complete theory describing our universe. Taking string theory for granted, we have to deal with vast amount of different vacua, the number usually quoted is $10^{500}$ [2, 3]. At the time of the big bang, the energy per

unit volume was very high, and the state of the universe was very far from any vacuum, true or false. As the universe expanded and cooled down, it might well have settled into a false vacuum instead of a true one.

From time to time, bubbles containing a vacuum of lower energy will form. A descriptive picture for this is boiling water with bubbles forming inside. These bubbles then either shrink to nothing or keep growing, depending on which case is energetically more favorable. These nucleations happens instantaneous. This process is described via instantons, which are classical solutions to the equation of motion of classical field theory on an euclidean spacetime. They can be used to calculate the transition probability for a quantum mechanical particle tunneling through a barrier (Figure 2.2: from vacuum A to vacuum B). Knowing the different tunneling probabilities, we can learn more about the local shape of the landscape.

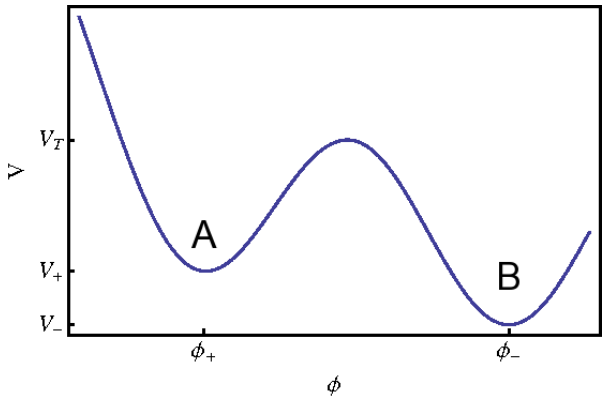


Figure 2.2.: *Schematic picture of true and false vacua. The field $\phi$ is at $\phi_+$ outside of the bubble and at $\phi_-$ on the inside.*

To start inflation, we assume the inflaton to tunnel from one vacuum to another. It will most likely not land at the minimum of the new vacuum, but slightly above it. The field then starts to slowly roll down the potential during a phase of inflation [21].

## 2.4. Cosmic Microwave Background

In 1964, Arno Penzias and Robert Wilson, two employees working at Bell Labs in Homdel, New Jesey, accidentally detected an isotropic and homogeneous radiation, while experimenting with a supersensitive horn antenna [22]. This radiation is today known as the cosmic microwave background (CMB) and became one of the strongest weapons for cosmologist trying to unveil the secrets of the universe.

This radiation was then interpreted by R. Dicke, P.J.E. Peebles, P.G. Roll and D.T. Wilkinson as a signature of the Big Bang. In 1978, Penzias and Wilson received the Nobel Prize for Physics for their discovery. This radiation consists of photons that travelled freely through space after decoupling of matter and radiation about 380 000 years after the Big Bang.

In 1990, the space-based COBE experiment [23] measured the spectrum of the photons [24]. It is an almost perfect blackbody spectrum of temperature $2.725K$ with a precision of 0.001% (see Figure 2.3).

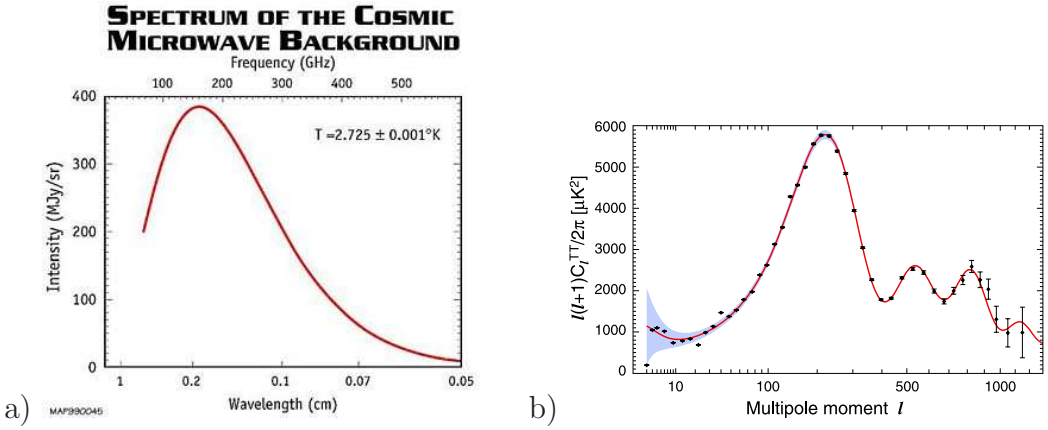


Figure 2.3.: *Blackbody Spectrum of the CMB measured by COBE (left), the TT-Power Spectrum derived from the 7-year WMAP data (right)*

Two years later, COBE observed the CMB anisotropies, which we will discuss in more detail. In 2006, John Mather and George Smoot were awarded the Nobel Prize in Physics for their work related to the CMB: John Mather for measuring the blackbody spectrum of the photons (1990) and George Smoot for measuring the anisotropies (1992).

WMAP, the successor of COBE, was launched in 2001. It improved the measurements of cosmological parameters enormously and collected data for 7 years. In 2009, PLANCK, the successor of WMAP, was launched. The release of the first data is expected for 2012. One main aim of PLANCK is to measure the polarization of the CMB. For more details on the mission see [25].

As mentioned in the beginning, the universe is only homogeneous and isotropic on large scales. In the CMB we find small anisotropies of the level of 0.001% (see Figure 2.5). CMB anisotropies can be expressed through spherical harmonics

$$\frac{\delta T(\phi,\theta)}{T} = \sum_{l,m} a_{lm} Y_{lm}(\phi,\theta). \tag{2.22}$$

The coefficients fulfill the following relation

$$\langle a_{lm} a_{l'm'} \rangle = C_l \, \delta_{ll'} \, \delta_{mm'}. \tag{2.23}$$

The inhomogeneities measured today in the CMB originate from vacuum quantum fluctuations. As the universe expands exponentially during inflation, the wavelength of the fluctuations grows. During the phase of inflation the fluctuations cross the Hubble

horizon at $aH = k$ (a: scale factor, H: Hubble constant, $k^{-1}$: comoving length scale). At this moment they become classical perturbations. After inflation, they re-enter. Those fluctuations which have crossed the horizon twice can be seen today as anisotropies in the CMB (see Figure 2.4).

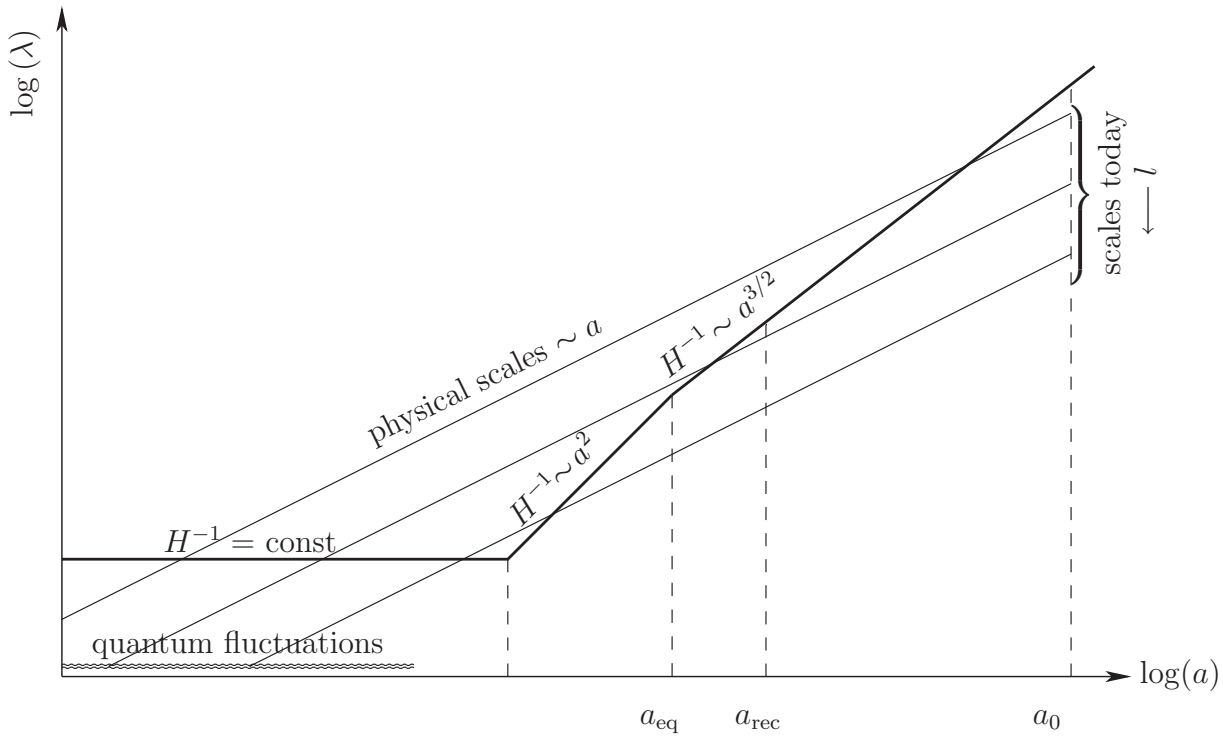


Figure 2.4.: *Behavior of the Hubble horizons $H^{-1}$ at the different epochs of the universe: Inflationary, radiation dominated and matter dominated phase. The thin straight lines represent physical scales. The scales that have entered the horizon until today correspond to the multipoles in the CMB measurement. The middle line of the three exemplary physical scales corresponds to a position somewhere around the first peak: It enters the horizon before recombination leaving just about enough time to collapse once. (Courtesy of Jan Heisig)*

These fluctuations have a gaussian distribution in first approximation. There are also deviations from this, the non-gaussianities. A quantity is gaussian, if all n-point correlation functions for n even are already determined by the two-point correlation function and all n-point correlation functions for n odd vanish. A quantity is non-gaussian otherwise. Figure 2.3 b) shows the measured temperature-temperature two-point function of the CMB

$$\left\langle \left(\frac{\delta T}{T}\right)^2 \right\rangle = \sum_l \frac{2l+1}{4\pi} C_l \approx \int \frac{l(l+1)}{2\pi} C_l \, \mathrm{d}\,(\ln l). \tag{2.24}$$

The three-point function, also knows as Bispectrum is the first test for non-gaussianities. If it is not zero, the fluctuations are not gaussian.

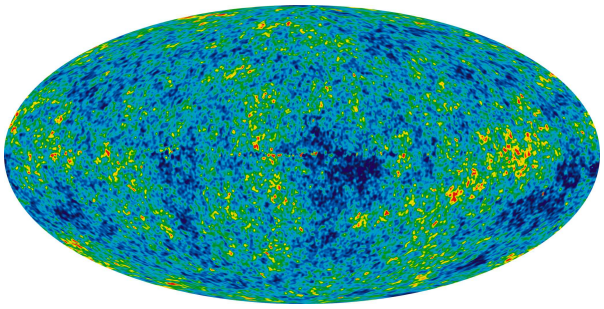

Figure 2.5.: *Temperature fluctuations of the CMB, 7 year WMAP data*

## 2.5. Density Fluctuations

Soon after introducing inflation to explain isotropy and homogeneity of the universe on large scales, it was realised that inflation can also produce fluctuations on small scales [26, 27]. Primordial inhomogeneities served as the seeds for structure formation. Primordial perturbations originated from quantum fluctuation. Their size is blown up from Planckian length to superhorizon scales during inflation. We will now describe these fluctuations of the CMB in more detail for single field inflation. In Chapter 4 we will calculate inflationary perturbations for a quartic potential.

In the following calculations, we assume a perturbed metric

$$\tilde{g}_{\mu\nu}(\mathbf{x}, t) = g_{\mu\nu}(t) + \delta g_{\mu\nu}(\mathbf{x}, t) \tag{2.25}$$

and a perturbed scalar field

$$\phi(\mathbf{x}, t) = \phi_{cl}(t) + \delta\phi(\mathbf{x}, t). \tag{2.26}$$

Of the inflaton field, only the perturbation $\delta\phi$ will be quantised. The field itself stays classical. The resulting scalar and tensor perturbations enable us to test inflation.

These perturbations split up into three different groups: scalar, vector and tensor perturbations.

- **Scalar perturbations** are induced by energy density inhomogeneities. These perturbations are most important because they exhibit gravitational instability and may lead to the formation of structure in the universe.
- **Vector perturbations** decay quickly and are not very interesting for us here.
- **Tensor perturbations** describe gravitational waves, which are the degrees of freedom of the gravitational field itself. In the linear approximation the gravitational waves do not induce any perturbations in the perfect fluid.

Scalar, vector and tensor perturbations are decoupled and thus can be studied separately. Important for the calculations is the ratio of the physical wavelength of the perturbations $\lambda_{ph}\ a/k$ and the Hubble horizon $1/H$. The Hubble scale does not change much during inflation, while $\lambda_{ph}$ grows strongly.

Standard results to first order in the slow roll approximation are

$$P_S^{\frac{1}{2}}(k) = \left(\frac{H^2}{2\pi\dot{\phi}}\right)\Bigg|_{aH=k} \tag{2.27}$$

for the scalar perturbation spectrum and

$$P_T^{\frac{1}{2}}(k) = \left(\frac{H}{\pi}\right)\Bigg|_{aH=k} \tag{2.28}$$

for the tensor perturbation spectrum. For more details see [28–30].

### 2.5.1. Scalar Perturbations

First, we will look at the scalar linear perturbations. The most general expression for this metric is

$$\mathrm{d}s^2 = a(\tau)^2\left\{(1+2A)\mathrm{d}\tau^2 - 2\partial_i B\mathrm{d}x^i\mathrm{d}\tau - [(1+2R)\delta_{ij} + 2\partial_i\partial_j E]\,\mathrm{d}x^i\mathrm{d}x^j\right\} \tag{2.29}$$

were $A, B, R, E$ are real scalars representing the four scalar degrees of freedom. After fixing the gauge, we insert the perturbed quantities into the action leading to

$$S_{\mathrm{pert}}^{\mathrm{scalar}} = \frac{1}{2}\int \mathrm{d}\tau\mathrm{d}^3\mathbf{x}\left[(u')^2 - (\partial_i u)^2 + \frac{z''}{z}u^2\right], \tag{2.30}$$

prime denoting the derivation with respect to conformal time, using also

$$u = -z\mathcal{R} = -z\left(R - \frac{H}{\dot{\phi}}\delta\phi\right), \quad z \equiv a\frac{\dot{\phi}}{H}. \tag{2.31}$$

$\mathcal{R}$ is the intrinsic curvature perturbation of comoving hypersurfaces

$$\mathcal{R} = \int \frac{\mathrm{d}^3\mathbf{k}}{(2\pi)^{\frac{3}{2}}}\mathcal{R}_{\mathbf{k}}(\tau)e^{i\mathbf{k}.\mathbf{x}}. \tag{2.32}$$

The two-point correlation function and the spectrum are defined by

$$\langle\mathcal{R}_{\mathbf{k}}\mathcal{R}_{\mathbf{l}}^*\rangle = \frac{2\pi^2}{k^3}P_S\delta^3(\mathbf{k}-\mathbf{l}). \tag{2.33}$$

Now we quantise the perturbations

$$\hat{u}(\tau,\vec{x}) = \int \frac{\mathrm{d}^3\mathbf{k}}{(2\pi)^{\frac{3}{2}}}\left\{u_k(\tau)\hat{a}_{\mathbf{k}}e^{i\mathbf{k}.\mathbf{x}} + u_k^*(\tau)\hat{a}_{\mathbf{k}}^\dagger e^{-i\mathbf{k}.\mathbf{x}}\right\}, \tag{2.34}$$

imposing the standard relations for the creation and annihilation operators

$$\left[\hat{a}_{\mathbf{k}}, \hat{a}_{\mathbf{l}}^{\dagger}\right] = \delta^3(\mathbf{k}-\mathbf{l}) \ , \quad \hat{a}_{\mathbf{k}}|0\rangle = 0, \ldots . \tag{2.35}$$

The Fourier components of momentum $k$ are decoupled from the other momenta and the equation of motion for $u_k$ is simply

$$u_k'' + \left(k^2 - \frac{z''}{z}\right) u_k = 0. \tag{2.36}$$

As $aH/k \to 0$ (wavelength of fluctuations much smaller than horizon), we can approximate the modes by the free field solution in flat space

$$u_k = \frac{1}{\sqrt{2k}} e^{-ik\tau}. \tag{2.37}$$

For $aH/k \gg 1$ (wavelength much larger than horizon), $u_k \propto z$. Now we can use the slow roll parameters to express the $z''/z$ term

$$\frac{z''}{z} = 2a^2H^2\left(1 + \frac{3}{2}\eta + \epsilon + \frac{1}{2}\eta^2 + \frac{1}{2}\epsilon\eta + \frac{1}{2H}\dot{\epsilon} + \frac{1}{2H}\dot{\eta}\right). \tag{2.38}$$

Assuming $\epsilon$ and $\eta$ are constant, (2.36) can be solved by

$$\frac{z''}{z} = \frac{1}{\tau^2}\left(\nu^2 - \frac{1}{4}\right), \quad \nu = \frac{1+\eta+\epsilon}{1-\epsilon} + \frac{1}{2} \tag{2.39}$$

with

$$\tau = \frac{-1}{aH}\left(\frac{1}{1-\epsilon}\right). \tag{2.40}$$

For a wavelength much larger than the horizon, $u_k$ will freeze out. Approximating $u_k$ in this regime

$$\begin{aligned} u_k &= \frac{1}{2}\sqrt{\pi} e^{i(\nu+\frac{1}{2})\frac{\pi}{2}} (-\tau)^{\frac{1}{2}} H_\nu^{(1)}(-k\tau) \\ &\to e^{i(\nu-\frac{1}{2})\frac{\pi}{2}} 2^{\nu-\frac{3}{2}} \frac{\Gamma(\nu)}{\Gamma(\frac{3}{2})} \frac{1}{\sqrt{2k}} (-k\tau)^{\frac{1}{2}-\nu} \ \text{ as } \ aH/k \to \infty, \end{aligned} \tag{2.41}$$

the scalar perturbation spectrum finally follows from Eq. (2.33)

$$\begin{aligned} P_S^{1/2}(k) =& \sqrt{\frac{k^3}{2\pi^2}} \left|\frac{u_k}{z}\right| \\ =& 2^{\nu-\frac{3}{2}} \frac{\Gamma(\nu)}{\Gamma(\frac{3}{2})} (1-\epsilon)^{\nu-\frac{1}{2}} \left.\frac{H^2}{2\pi|\dot{\phi}|}\right|_{aH=k}. \end{aligned} \tag{2.42}$$

### 2.5.2. Tensor perturbations

Now we turn to tensor perturbations, corresponding to gravity waves. Tensor linear perturbations can be most generally expressed as

$$\mathrm{d}s^2 = a(\tau)^2 \left[\mathrm{d}\tau^2 - (\delta_{ij} + 2h_{ij})\,\mathrm{d}x^i \mathrm{d}x^j\right]. \tag{2.43}$$

Notice that here we do not have gauge degrees of freedom as in the scalar case, since tensor perturbations are gauge invariant. The tensor $h_{ij}$ is symmetric $h_{ij} = h_{ji}$, traceless $\delta^{ij}h_{ij} = 0$ and transverse $\partial^i h_{ij} = 0$. Inserting the perturbed metric in the Einstein-Hilbert action yields the perturbed action

$$S^{\mathrm{tensor}}_{\mathrm{pert}} = \frac{1}{8}\int \mathrm{d}\tau \mathrm{d}^3\mathbf{x} a^2 \left[(h'_{ij})^2 - (\partial_l h_{ij})^2\right]. \tag{2.44}$$

Defining $v_{ij} \equiv \frac{a}{2}h_{ij}$ leads to

$$S^{\mathrm{tensor}}_{\mathrm{pert}} = \frac{1}{2}\int \mathrm{d}\tau \mathrm{d}^3\mathbf{x} \left[(v'_\lambda)^2 - \partial_l v^{ij}\partial^l v_{ij} - \frac{a''}{a}v_\lambda^2\right]. \tag{2.45}$$

The two point correlation function is

$$\sum_\lambda \left\langle h_{k,\lambda} h^*_{k',\lambda}\right\rangle = \frac{2\pi^2}{k^3}P_T(k)\delta^{(3)}(\mathbf{k}-\mathbf{k}'), \tag{2.46}$$

with $\lambda \in (+,\times)$ being the two polarisations. Quantizing $v_{ij}$ similar to the previous chapter gives

$$\hat{v}_{ij}(\tau,\mathbf{x}) = \int \frac{\mathrm{d}^3\mathbf{k}}{(2\pi)^{\frac{3}{2}}}\left\{(v_k)_{ij}(\tau)\hat{a}_\mathbf{k}e^{i\mathbf{k}.\mathbf{x}} + (v_k)^*_{ij}(\tau)\hat{a}^\dagger_\mathbf{k}e^{-i\mathbf{k}.\mathbf{x}}\right\}. \tag{2.47}$$

with

$$(v_k)_{ij} = v^+_k e^+_{ij}(\mathbf{k}) + v^\times_k e^\times_{ij}(\mathbf{k}), \tag{2.48}$$

and the polarisation tensors satisfying

$$\begin{aligned} &e_{ij} = e_{ji}, \quad k^i e_{ij} = 0, \quad e_{ii} = 0, \\ &e_{ij}(-\mathbf{k},\lambda) = e^*_{ij}(\mathbf{k},\lambda), \\ &e^*_{ij}(\mathbf{k},\lambda)e^{ij}(\mathbf{k},\lambda') = \delta^\lambda_{\lambda'}. \end{aligned} \tag{2.49}$$

Again we derive the equation of motion from the action

$$v''_k + \left(k^2 - \frac{a''}{a}\right)v_k = 0 \tag{2.50}$$

and make the approximations

$$\begin{aligned} v_k &= \frac{1}{\sqrt{2k}} e^{-ik\tau} \text{ as } aH/k \to 0 \\ v_k &\propto a \text{ for } aH/k \gg 1. \end{aligned} \tag{2.51}$$

One more time we express the mass term in terms of slow roll parameters (again assuming $\epsilon$ to be constant) to solve the equation of motion

$$\begin{aligned} \frac{a''}{a} =& 2a^2H^2\left(1-\frac{1}{2}\epsilon\right) \\ =& \frac{1}{\tau^2}\left(\mu^2-\frac{1}{4}\right), \quad \mu = \frac{1}{1-\epsilon}+\frac{1}{2}. \end{aligned} \tag{2.52}$$

Similar to the scalar spectrum we find

$$P_{\mathrm{T}}^{\frac{1}{2}}(k) = 2^{1+\mu-\frac{3}{2}}\frac{\Gamma(\mu)}{\Gamma(\frac{3}{2})}(1-\epsilon)^{\mu-\frac{1}{2}}\left.\frac{H}{2\pi}\right|_{aH=k}. \tag{2.53}$$

### 2.5.3. Useful relations

- **Tensor to Scalar ratio**
  A convenient parameter to encode the tensor power spectrum is the tensor to scalar ratio $r$

  $$r = \frac{P_{\mathrm{T}}(k_0)}{P_S(k_0)}. \tag{2.54}$$

  The scale dependence of the spectra is given by the spectral indices $n_S$ and $n_T$. Since probably $n_S \neq n_T$, $r$ will be scale dependent. $n_S$ is in most models expected to be slightly smaller than 1. For $\dot{H} = 0$, $P_s$ is independent of $k$ and is called Harrison-Zeldovich-spectrum.

  With (2.27), (2.28) and $\dot{\phi}^2 = -2\dot{H}$ we have

  $$r = 16\epsilon|_{k_0=aH}, \tag{2.55}$$

  so the tensor perturbations are expected to be much smaller than the scalar perturbations. $r$ could also be defined at a given multipole $l$ for a more observer-friendly approach. WMAP 7+BAO+SN data gives $r < 0.20$ (95% CL) [17].

- **Consistency relation**
  If gravitational waves were detected, a strong evidence for inflation could be given by the so called consistency relation. The spectral index for the tensor modes for single field inflation can be written as

  $$n_T = -2\epsilon. \tag{2.56}$$

Expressed through the spectra, we find

$$n_T = -\frac{P_T}{8P_S} = -\frac{r}{8}. \tag{2.57}$$

This means, if we manage to measure $P_T$ at least for two values good enough for a proper estimation of the slope, we can check the consistency relation. If it holds, it would strongly suggest inflation.

# 3. Tunneling

> We few, we happy few, we band of brothers;
> For he to-day that sheds his blood with me
> Shall be my brother; be he ne'er so vile,
> This day shall gentle his condition:
> And gentlemen in England now a-bed
> Shall think themselves accursed they were not here,
> And hold their manhoods cheap whiles any speaks
> That fought with us upon Saint Crispin's day.
>
> *(William Shakespeare — Henry V: Act IV, Scene III)*

In recent times, first order phase transitions have gained significant interest, for example as sources of gravitational waves [31] and in transversing the string theory landscape [4,5]. In the latter picture, the scalar field potential possesses a plethora of local minima. A field that is initially trapped in a higher energy vacuum jumps to a lower energy vacuum via a quantum tunneling process.

A semi-classical approach to quantum tunneling processes in field theory has been presented in a series of pioneering papers [32, 33]. The role of gravity in the process of tunneling was subsequently considered in [34]. The underlying microphysics of tunneling can be described by instantons, i.e. classical solutions of the Euclidean equations of motion of the system.

The authors presented a scheme for calculating tunneling amplitudes for transitions from false to true vacua. The calculation involves the evaluation of the Euclidean action of the bounce solution to the imaginary-time equations of motion.

Tunneling proceeds via the nucleation of bubbles of true (or rather lower energy) vacuum surrounded by the sea of false vacuum. If the curvature of the potential is large compared to the corresponding Hubble scale, this process can be described by Coleman de Luccia (CdL) instantons, i.e. bounce solutions to the Euclidean equations of motion [32, 34]. For relatively flat potentials, tunneling proceeds via Hawking-Moss instantons [35].

The existence of the bounce solution was proven in generality in [32]. For almost degenerate vacuum energy, the thin-wall approximation can be used to calculate the tunneling amplitude without having to compute the bounce solution.

In this Chapter, we will first give a short introduction to the tunneling procedure. We then present new exact tunneling solutions for a specific potential [7], ignoring the effects of gravity. We also give an application of these solutions in the context of landscape and comment on the existence of bounce solutions in general [8]. In Section 3.4 we briefly review the original arguments for the existence of bounce solutions. In Section 3.5, we

discuss the tunneling in a piecewise linear potential and explain how smoothing of the potential is important for certain parameter ranges of the potential. This subsequently leads us to a condition on the smooth potential for a meaningful approximation in terms of a piecewise linear potential in Section 3.6. We comment on the applicability of the shooting algorithm in the smooth potential and we conclude in Section 3.7.

## 3.1. Of bubbles and universes

In the CdL formalism, the tunneling amplitude for a transition from the false (or higher energy) vacuum at $\phi_+$ to the true (or lower energy) vacuum at $\phi_-$ per unit volume is given by

$$\Gamma/V = A\mathrm{e}^{-B} \tag{3.1}$$

[32]. The coefficient $A$ is typically ignored but in principle calculable, see [33]. The exponent

$$B = S_E(\phi_B) - S_E(\phi_+) \tag{3.2}$$

(sometimes also referred to as the bounce action) is the difference between the Euclidean action

$$S_E(\phi) = 2\pi^2 \int_0^\infty dr\, r^2 \left(\frac{1}{2}\phi'^2 + V(\phi)\right) \tag{3.3}$$

for the spherically symmetric bounce solution $\phi_B$ and for the false vacuum $\phi_+$. Since we ignore the effects of gravity here, we can always shift the potential such that $S_E(\phi_+) = 0$ and $B = S_E(\phi)$. The term "bounce" stems from the description of this process in QM, where the field sits in the false vacuum for $t \to -\infty$, reaches the true vacuum at some $-\infty < t_* < \infty$, and rolls back to the false vacuum for $t \to \infty$.

The bounce obeys the one-dimensional Euclidean equation of motion

$$\phi_B'' + \frac{3}{r}\phi_B' - \partial_\phi V(\phi_B) \;=\; 0\,, \tag{3.4}$$

where $\phi' \equiv \partial_r \phi$ and $r = \sqrt{t^2 - \vec{x}^2}$ is the radial coordinate of the spherical bubble. This configuration describes the bubble at the time of nucleation. In the following sections, we ignore its subsequent evolution, and focus on the computation of $B$.

In general, the CdL bounce solutions can be computed exactly only for very few potentials. However, if the potential difference between the two vacua is small compared to the typical potential scale, the tunneling amplitude can be computed using the thin wall approximation (see [32] for more details). We then have

$$B_{TW} \;\equiv\; \frac{27\pi^2}{2}\frac{S_1^4}{\epsilon^3}\,, \tag{3.5}$$

with

$$S_1 \equiv \int_{\phi_-}^{\phi_+} d\phi \sqrt{2\left(V(\phi) - V(\phi_+)\right)}. \tag{3.6}$$

If this approximation is not applicable, one needs to resort to either numerical computations (see [36] for an approach for a generic quartic potential) or approximate the potential by potentials for which the exact instanton solutions are known.

## 3.2. Exact tunneling solutions

To the best of our knowledge, only for very few potentials has the CdL tunneling process been solved analytically: a piecewise linear-linear potential [37], a piecewise linear-quadratic potentials [38–40] and a quartic-linear potential [41]. A different approach was taken in [42] who reconstruct fully analytically tractable potentials, including the effects of gravity, from analytically exact bubble geometries.

We present new exact solutions for tunneling within piecewise potentials where the true vacuum potential is a quartic, see Figures 3.1 and 3.2. The potential for $\phi > 0$ ('on the right') is given by

$$V_R(\phi) = V_T - \Delta V_- + \frac{\Delta V_-}{\phi_-^4}\left(\phi - \phi_-\right)^4 , \tag{3.7}$$

where $\Delta V_- \equiv V_T - V_-$. For simplicity, we choose $\phi = 0$ as the matching point and $V(\phi = 0) = V_T$. We will choose the potential for $\phi < 0$ ('on the left') as either linear or quartic and discuss the solutions in Section 3.2.1 and Section 3.2.2 respectively.

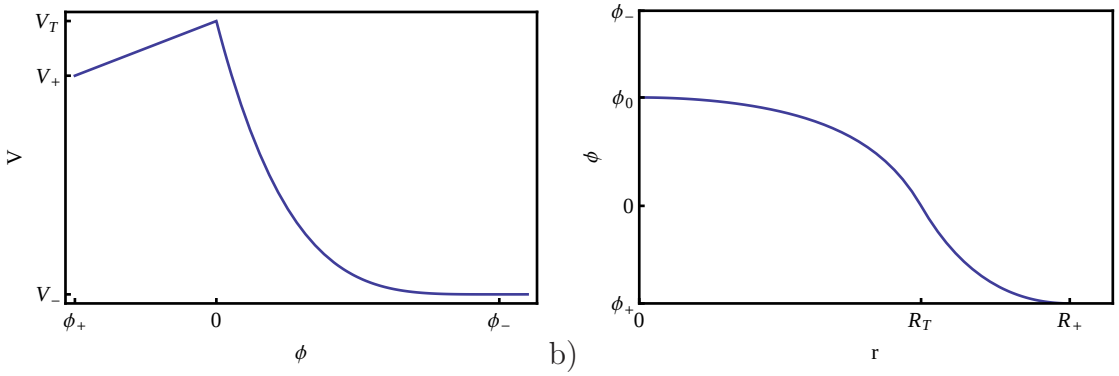


Figure 3.1.: *a) Schematic plot of the piecewise linear-quartic potential. The left part of the potential is a linear function of $\phi$, the right part a quartic function. The bounce describes tunneling from the field sitting in the false vacuum at $\phi_+$ towards the true vacuum located at $\phi_-$. b) Schematic view of the bounce solution for (a). Inside the bubble at $r = 0$, the field is at $\phi_0 > 0$. The bubble wall is located around $R_T$, but not necessarily thin. Outside of the bubble at $r = R_+$, the field is still in the false vacuum.*

For each piecewise potential, we proceed analogously to [37, 40]: First we solve the equation of motion for the scalar field in $V_R(\phi)$, subject to the boundary condition at the center of the bubble $\phi_R(0) = \phi_0$, $\phi_R'(0) = 0$. We assume that the bubble nucleation point is located at $\phi_0 > 0$, i.e. it is in the valley of the true vacuum. Then, we solve the equation of motion for the field in $V_L$, subject to $\phi_L(R_+) = \phi_+$, $\phi_L'(R_+) = 0$. In other words, we assume that at some radius $R_+$ (which can be $\infty$) outside of the bubble of true vacuum, the field sits in the false vacuum. Then, we match the solutions at some radius $R_T$ by enforcing $\phi_L(R_T) = \phi_R(R_T) = 0$ and $\phi_L'(R_T) = \phi_R'(R_T)$. This allows us to determine the constants $R_T$, $R_+$, and $\phi_0$. Here, $R_T$ is roughly the radius of the bubble when it materializes at $\phi = \phi_0$, whereas the value comparing $R_+$ to $R_T$ gives us an idea about the width of the bubble wall.

It is then straightforward to integrate the action for $\phi_L$ and $\phi_R$, obtaining $B$. We compare the tunneling bounce action $B$ for the piecewise linear-quartic potential with the results of both the thin-wall approximation and the piecewise linear-linear potential solved in [37]. Finally, we compute the tunneling amplitude for the piecewise quartic-quartic potential and compare it with the results obtained using the thin-wall approximation, as well as with the tunneling amplitude in a piecewise linear-quartic potential.

### 3.2.1. Linear-quartic potential

We compute the tunneling rate for a piecewise potential of the form

$$V(\phi) = \begin{cases} V_T - \frac{\Delta V_+}{\phi_+}\phi\,, & \phi \leq 0\,, \\ V_T - \Delta V_- + \frac{\Delta V_-}{\phi_-^4}\left(\phi - \phi_-\right)^4 & \phi > 0\,, \end{cases} \tag{3.8}$$

where $\Delta V_- \equiv V_T - V_- = \frac{\lambda_4}{4}\phi_-^4$ and $\Delta V_+ \equiv V_T - V_+ = -\lambda_1\phi_+$ are the depths of the true and false minimum, see Figure 3.1.

Subject to the boundary conditions $\phi_R(0) = \phi_0$ and $\phi_R'(0) = 0$, solving the equation of motion of the bounce, i.e. Eq. (3.4) on the right side of the potential, we have [21]

$$\phi_R(r) = \phi_- + \frac{2(\phi_0 - \phi_-)}{2 - \frac{\Delta V_-(\phi_0 - \phi_-)^2}{\phi_-^4} r^2}\,. \tag{3.9}$$

Similarly on the left side of the potential, subject to $\phi_L(R_+) = \phi_+$ and $\phi_L'(R_+) = 0$, we have the bounce solution

$$\phi_L(r) = \phi_+ - \frac{\Delta V_+}{8\phi_+}\frac{(r^2 - R_+^2)^2}{r^2}\,. \tag{3.10}$$

A schematic view of the bounce is shown in Figure 3.1 b).

We now determine the constants $R_+$ and $\phi_0$ by solving the matching equations for the two solutions $\phi_R(R_T) = 0$, $\phi_L(R_T) = 0$. Using the first condition, we get $\phi_0$ in terms of $R_T$

$$\phi_0 = \frac{\phi_-^3}{\Delta V_- R_T^2}\left[\frac{\Delta V_- R_T^2}{\phi_-^2} + \left(1 - \sqrt{\frac{2\Delta V_- R_T^2}{\phi_-^2} + 1}\right)\right]\,, \tag{3.11}$$

while the second condition gives

$$R_+ \;=\; \sqrt{R_T\left(R_T+\frac{2\sqrt{2}\alpha\phi_-}{\sqrt{\Delta\Delta V_-}}\right)}\,. \tag{3.12}$$

Here, we have introduced $\Delta = \Delta V_+/\Delta V_-$ and $\alpha = -\phi_+/\phi_-$. Similarly, using the smoothness of the solution at $R_T$, i.e. $\phi'_R(R_T) = \phi'_L(R_T)$, we find

$$R_T = \frac{\phi_-\left(\sqrt{\Delta}(1+2\alpha)+\sqrt{4\alpha(1+\alpha)+\Delta}\right)}{(1-\Delta)\sqrt{2\Delta V_-}}\,. \tag{3.13}$$

Computing the exponent of the tunneling amplitude in terms of $R_T$ gives

$$\begin{aligned} B \;=\; & \frac{\pi^2}{6\Delta V_-}\left\{2R_T^2\Delta V_-\phi_-^2\left[(6\alpha^2-3)+2\sqrt{1+\frac{2R_T^2\Delta V_-}{\phi_-^2}}\right]+3R_T^4\,(\Delta-1)\,\Delta V_-^2\right. \\ & \left.+8\sqrt{2}R_T^3\alpha\Delta V_-\sqrt{\Delta\Delta V_-}\phi_-+2\phi_-^4\left[-1+\sqrt{1+\frac{2R_T^2\Delta V_-}{\phi_-^2}}\right]\right\}\,. \end{aligned} \tag{3.14}$$

With $R_T$ from Eq. (3.13), we obtain a rather monstrous expression

$$\begin{aligned} B \;=\; & \frac{\pi^2\phi_-^4}{6\Delta V_-}\left\{4\alpha\sqrt{\Delta}\left[\frac{(1+2\alpha)\sqrt{\Delta}+\sqrt{4\alpha(1+\alpha)+\Delta}}{1-\Delta}\right]^3\right. \\ & -\frac{3}{4}\left[\frac{(1+2\alpha)\sqrt{\Delta}+\sqrt{4\alpha(1+\alpha)+\Delta}}{(1-\Delta)^{3/4}}\right]^4 \\ & +2\left[-1+\sqrt{1+\left[\frac{(1+2\alpha)\sqrt{\Delta}+\sqrt{4\alpha(1+\alpha)+\Delta}}{1-\Delta}\right]^2}\right] \\ & +\left[\frac{(1+2\alpha)\sqrt{\Delta}+\sqrt{4\alpha(1+\alpha)+\Delta}}{1-\Delta}\right]^2 \\ & \left.\times\left[-3+6\alpha^2+2\sqrt{1+\left[\frac{(1+2\alpha)\sqrt{\Delta}+\sqrt{4\alpha(1+\alpha)+\Delta}}{1-\Delta}\right]^2}\right]\right\}. \end{aligned} \tag{3.15}$$

To cross check our result, we take the thin-wall limit of Eq. (3.15) by replacing $\Delta = 1-\frac{\epsilon}{\Delta V_-}$, where $\epsilon$ is the energy difference between the true and false vacua. In the thin-wall limit $\epsilon \ll V_T$. Performing a series expansion around $\epsilon = 0$, the lowest order term in $\epsilon$ is

$$\lim_{\epsilon\to 0} B = \frac{2\pi^2}{3}\frac{(1+2\alpha)^4\phi_-^4\Delta V_-^2}{\epsilon^3}\,. \tag{3.16}$$

We compare this with the results obtained using the thin wall approximation [32]

$$B_{TW} \equiv \frac{27\pi^2}{2}\frac{S_1^4}{\epsilon^3}\,, \tag{3.17}$$

where

$$\begin{aligned} S_1 &\equiv \int_{\phi_-}^{\phi_+} d\phi\sqrt{2\left(V(\phi)-V(\phi_+)\right)} \\ &= -\frac{\sqrt{2\Delta V_-}\phi_-}{3}\left[(1+2\alpha)\sqrt{\Delta}+2\sqrt{\Delta-1}\,{}_2F_1\left(\frac{1}{4},\frac{1}{2},\frac{5}{4},\frac{1}{1-\Delta}\right)\right], \end{aligned} \tag{3.18}$$

with hypergeometric function ${}_2F_1$. Again, replacing $\Delta = 1 - \frac{\epsilon}{\Delta V_-}$ gives to the lowest order in $\epsilon$

$$B_{TW} \approx \frac{2\pi^2}{3}\frac{(1+2\alpha)^4\phi_-^4\Delta V_-^2}{\epsilon^3}\,, \tag{3.19}$$

in agreement with Eq. (3.16).

Comparing our results with [41], we find that the tunneling rate is quite different. This can be traced back to the fact that tunneling from a quartic into a linear potential should reduce to the $\alpha < 1$ solution of [37] in the appropriate limit. We observe that for fixed $\Delta$ and $\phi_+$, sending $|\phi_-| \ll |\phi_+|$, the potential on the right appears more and more like a linear potential. In other words, in the limit of $\alpha \gg 1$, the tunneling bounce solution in Eq. (3.15) must agree with the tunneling bounce action in a piecewise linear-linear potential. The exact tunneling amplitude for a piecewise linear-linear potential has been calculated in [37]. In our notation, their result for $\alpha > 1$ is given by

$$B_{DJ} = \frac{2\pi^2}{3}\left(\frac{1+\alpha}{\sqrt{\Delta}-1}\right)^3\frac{\phi_-^4}{\Delta V_-}\left[(\alpha-3)\sqrt{\Delta}+1-3\alpha\right]. \tag{3.20}$$

In the limit of large $\alpha \gg 1$, i.e. for $|\phi_-| \ll |\phi_+|$, this becomes

$$\lim_{\alpha\to\infty} B_{DJ} = \frac{2\pi^2}{3}\frac{\alpha^4(\sqrt{\Delta}-3)}{(\sqrt{\Delta}-1)^3}\frac{\phi_-^4}{\Delta V_-}\,, \tag{3.21}$$

which indeed agrees with the corresponding limit of Eq. (3.15). Note that this is independent of the thin-wall limit.

As an aside, we observe some curious systematic behavior: the radius of the bubble in the thin-wall limit for a piecewise linear-quartic potential is given by

$$R_T = \frac{3S_1}{\epsilon} = (1+2\alpha)\frac{\sqrt{2\Delta V_-}\phi_-}{\epsilon}\,. \tag{3.22}$$

For a cubic potential for $V_R(\phi)$ on the right, the thin-wall approximation gives

$$R_T = \left(\frac{6}{5}+2\alpha\right)\frac{\sqrt{2\Delta V_-}\phi_-}{\epsilon}\,. \tag{3.23}$$

Finally, for $V_R(\phi)$ a quadratic potential, the bubble radius is given by [40]

$$R_T = \left(\frac{3}{2} + 2\alpha\right) \frac{\sqrt{2\Delta V_-}\phi_-}{\epsilon}. \tag{3.24}$$

Thus we find that in the thin wall approximation, the nucleated bubble size shrinks mildly as the power of the monomials for potential in the exiting part (near the true vacuum) becomes larger.

### 3.2.2. Quartic-quartic potential

We now compute the bounce solution for tunneling from the false vacuum in a quartic potential to the true minimum in another quartic potential, see Figure 3.2a).

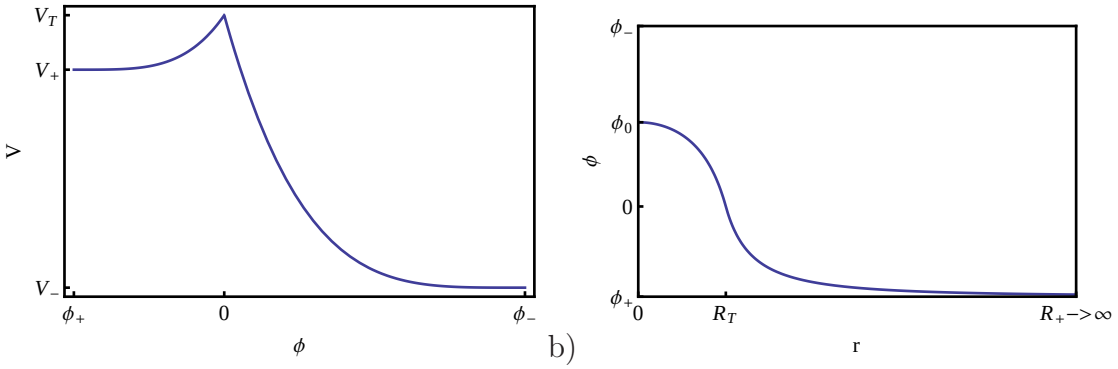


Figure 3.2.: *a) Schematic view of a piecewise quartic-quartic potential. b) Schematic view of the bounce solution for a). Note that the position where the field is still in the false vacuum goes to infinity, $R_+ \to \infty$.*

We can reuse parts of the previous calculation, in particular the solution inside the bubble from Eq. (3.9) and Eq. (3.11). Outside of the bubble, the field sits in the false vacuum

$$\phi_L(R_+) = \phi_+, \quad \phi_L'(R_+) = 0\,. \tag{3.25}$$

Note that, if we are not interested in knowing the width of the bubble, the boundary conditions above can also be set at $r \to \infty$. It turns out that this is what we need to do. The solution $\phi_L(r)$ has the form

$$\phi_L(r) \;=\; \phi_+ + \frac{8A}{8 - \frac{4\Delta\Delta V_- A^2 r^2}{\phi_+^4}}\,, \tag{3.26}$$

with $A$ to be fixed by the condition that $\phi_L(R_T) = 0$. Thus we find

$$\phi_L(r) \;=\; \frac{(r^2 - R_T^2)\,\alpha\phi_- \left(\frac{\Delta R_T^2 \Delta V_-}{\alpha^2\phi_-^2} + \left(1 + \sqrt{\frac{2\Delta R_T^2 \Delta V_-}{\alpha^2\phi_-^2} + 1}\right)\right)}{\Delta R_T^2 \alpha^2 \frac{\Delta R_T^2 \Delta V_-}{\alpha^2\phi_-^2} - r^2\left(\frac{\Delta R_T^2 \Delta V_-}{\alpha^2\phi_-^2} + \left(1 + \sqrt{\frac{2\Delta R_T^2 \Delta V_-}{\alpha^2\phi_-^2} + 1}\right)\right)}\,. \tag{3.27}$$

a)

| | $B_{\rm ll}$ | $B_{\rm lq}$ | $B_{\rm qq}$ |
|---|---|---|---|
| $\alpha = 0.01$ | 0.0072 | 0.00024 | 0.00010 |
| $\alpha = 0.1$ | 0.4 | 0.058 | 0.033 |
| $\alpha = 0.5$ | 24 | 6.7 | 4.8 |

b)

| | $B_{\rm qq}$ | $B_{\rm qq,\ thin\text{-}wall}$ |
|---|---|---|
| $\Delta = 0.99$ | $3.3 \times 10^7$ | $3.3 \times 10^7$ |
| $\Delta = 0.9$ | $2.8 \times 10^4$ | $3.3 \times 10^4$ |
| $\Delta = 0.7$ | $7.2 \times 10^2$ | $1.2 \times 10^3$ |

Table 3.1.: *a) Tunneling bounce actions for different values of $\alpha$ with $\Delta = 0.01$ fixed. Tunneling in a linear-linear potential is consistently suppressed compared to tunneling in linear-quartic and quartic-quartic potentials – keeping in mind that a larger $B$ corresponds to smaller tunneling rates. b) Comparison with the thin-wall approximation for tunneling in a quartic-quartic potential for fixed $\alpha = 0.5$. Decreasing $\Delta$ away from unity (i.e. exact equality between false and true vacuum energy), it is clear that the thin-wall approximation eventually fails.*

From the smoothness of the solution $\phi'_L(R_T) = \phi'_R(R_T)$ we obtain

$$R_T = \frac{\sqrt{2(1+\alpha)(\alpha+\Delta)}}{1-\Delta}\frac{\phi_-}{\sqrt{V_-}}\,. \tag{3.28}$$

Integrating the Euclidean action gives

$$B = \frac{2\pi^2}{3}\frac{4\alpha^3 + 6\alpha^2\Delta + 4\alpha\Delta^2 + \Delta^3 + \alpha^4(3+\Delta(\Delta-3))}{(1-\Delta)^3}\frac{\phi_-^4}{\Delta V_-}\,, \tag{3.29}$$

which in the thin-wall limit reduces to

$$B \approx \frac{2\pi^2}{3}\frac{(1+\alpha)^4\Delta V_-^2\phi_-^4}{\epsilon^3}\,. \tag{3.30}$$

Using the thin wall formula we find

$$S_1 = -\frac{\sqrt{2\Delta V_-}}{3}\left[(1+\alpha)\sqrt{\Delta} + 2\sqrt{(\Delta-1)}\,{}_2F_1\left(\frac{1}{4},\frac{1}{2},\frac{5}{4},\frac{1}{1-\Delta}\right)\right]\,, \tag{3.31}$$

and in the small $\epsilon$ limit $B$ agrees with Eq. (3.30).

We note that in the thin-wall limit, the tunneling bounce action $B$ for tunneling in a piecewise linear-quartic potential differs from the one in a piecewise quartic-quartic potential by the substitution $\alpha \to 2\alpha$. In particular, this means that for $\alpha \gg 1$, tunneling in a piecewise linear-quartic potential is much more suppressed than tunneling in a piecewise quartic-quartic potential: the respective values of $B$ differ by a factor of 16, suppressing the relative amplitude by the $16^{\rm th}$ power.

To further explore the differences in tunneling rates for different potential shapes, we tabulate the values for $B$ for different values of $\alpha$, keeping $\Delta = 0.01$ fixed for tunneling in a linear-linear (ll), linear-quartic (lq), and quartic-quartic (qq) potential, see Table 3.1. For all values of $\alpha$, the width of the wall of the nucleated bubble is non-negligible, $(R_+ - R_T)/R_T = \mathcal{O}(1)$, so we are dealing with tunneling in the thick-wall regime. As can be seen, the action $B$ for tunneling in a linear-linear potential are always significantly larger than for tunneling in linear-quartic and quartic-quartic potentials. As the tunneling rate is proportional to $e^{-B}$, even $\mathcal{O}(1)$ factors lead to significant differences of the tunneling rates. In the thick-wall regime tunneling seems to depend crucially on the exact shape of the potential, making the search for more exact tunneling solutions even more pressing.

### 3.2.3. Local shape of the landscape

It may be appropriate at this point to outline, that our exact results here for tunneling in a piecewise linear-quartic or quartic-quartic potential can be used to describe analytically models of open inflation in a toy landscape constructed from piecewise linear and quartic potentials. The toy inflationary landscape is constructed from a piecewise linear-quartic or quartic-quartic potential, to which a slow-roll inflationary region is attached with matching $V'$ at $\phi \simeq \phi_-$. The crucial point here is that the quartic potential which dominates field evolution after tunneling and before entering the slow-roll region, completely suppresses a would-be fast-roll overshoot problem in the slow-roll region. This happens because the negative spatial curvature inside the CdL bubble (once gravity is to be included [34], which we – but for the negative curvature inside the bubble – do not discuss here) formed during tunneling provides a very strong friction term. This Hubble friction is sufficient for damping the downhill motion enough to start slow-roll subsequently [21] for any potential

$$V(\phi) = V_0 + (\phi - \phi_-)^p, \qquad p \geq 4. \tag{3.32}$$

In such potentials the field will reach slow-roll already at some $\phi < \phi_-$ without overshoot, if the field starts its evolution inside a negatively curved CdL bubble following tunneling. Because of this fact, it does not matter whether the slow-roll inflationary region in the scalar potential at $\phi \gtrsim \phi_-$ will describe a small-field or large-field inflation model, as all models are treated equally in this toy landscape. We can now take a look at the situation where the barrier parameters $\alpha$, $\Delta$ take values in a dense discretuum specified in terms of a dense discretuum of microscopic parameters of a landscape of isolated vacua, such as the landscape of string theory vacua. For the moment, we will keep $\alpha$ fixed, as at $\alpha = 0$ the scalar potential becomes discontinuous and the bounce ceases to exist. We may now assign $\Delta$, which controls the aspect of the barrier shape crossing over between the thin-wall and thick-wall limit, a prior probability distribution $p(\Delta)$. This distribution contains the unknown microscopic landscape data. As explained before, all values of $\Delta$ are treated equally when it comes to the slow-roll inflationary regime attached at $\phi \gtrsim \phi_-$ in our toy landscape. Therefore, the expectation value of $\Delta$ is given by

$$\langle \Delta \rangle = \frac{\int d\Delta\, p(\Delta)\, e^{-B(\Delta)}}{\int d\Delta\, p(\Delta)}. \tag{3.33}$$

This does not depend on the post-tunneling inflationary dynamics due to the absence of overshoot. Therefore, in such a toy landscape the question whether the tunneling dynamics succeeds in pushing $\langle \Delta \rangle \to 0$, or whether it is overwhelmed by the prior $p(\Delta)$, is directly determined by the choice of the measure on eternal inflation entering $p(\Delta)$, and decouples from the phase space problem of post-tunneling inflation.

## 3.3. On the existence of bounce solutions

Given the fact that a bounce exists, a necessary and sufficient condition in this scheme for the false vacuum to be unstable and tunneling to occur is the existence of a single negative eigenvalue of the operator $\delta^2 S$, the second variational derivative of the Euclidean action evaluated at the bounce, [43]. Various authors examined systems where the tunneling rate may become zero, either through the appearance of singularities in multi-field setups including gravity [44–46], or through the appearance of intermediate vacua in single field setups [47,48]. Therefore, the decay process of false vacua via tunneling in the semi-classical picture firstly depends on the existence of a bounce under consistent approximations, and secondly on having only one negative eigenvalue of $\delta^2 S$.

We address the issue of the existence of a bounce solution in piecewise linear potentials that act as approximations to locally smooth potentials. It is obvious that violating the conditions set out (implicitly) in the proof of [32] is difficult in any physically realistic setup. Still this does not guarantee that the two pictures lead to quantitatively similar actions.

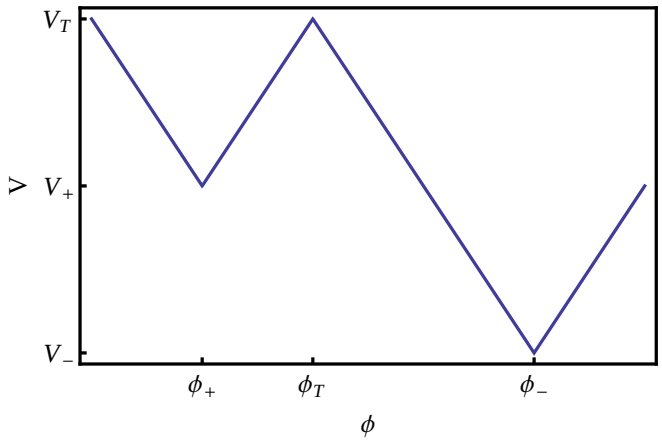


Figure 3.3.: *The piecewise linear potential first analyzed by [37]. For $|\phi_+ - \phi_T| < |\phi_- - \phi_T|$, the bounce solution does not always exist.*

Consider an effective potential that has sharp minima and maxima ('kinks'), see Figure 3.3. Tunneling in this setup was first discussed analytically in [37]. In this case, for certain ranges of parameters, a consistent bounce solution exists if we allow the field to rest for some amount of Euclidean time at the true minimum. With this field profile, it is possible for the relevant friction term to die off sufficiently so that the field can roll back up to the false vacuum. Having the field 'wait' in such a manner is only an approximation to the physical situation of replacing the tip of the potential by a smooth cap.

However, within the context of the 4D effective field theory approximation to a theory of quantum gravity such as string theory, the situation can become somewhat more involved. If the cap smoothing the potential has a curvature $\partial^2 V/\partial\phi^2$ that is larger

than $M_P^2$, effective field theory cannot be trusted. In particular, it cannot be guaranteed that the cap is strictly concave, i.e. large corrections may induce local saddle points or minima within the highly curved region of the cap. Thus the whole semi-classical approximation for the calculations of the bubble nucleation also breaks down and we can no longer talk about tunneling in the usual picture of [32] and [34]. In this case, full quantum gravity effects must be incorporated to calculate the tunneling amplitude.

If the curvature of the smooth cap is smaller than $M_P^2$, approximating this setup by keeping the field fixed should not introduce too much of an error. We analyze under which circumstances this expectation holds true.

## 3.4. Coleman's proof

In his pioneering paper [32], Coleman offered an existence proof for the bounce solution. We briefly sketch this proof before we specialize to piecewise linear potentials in the next Section.

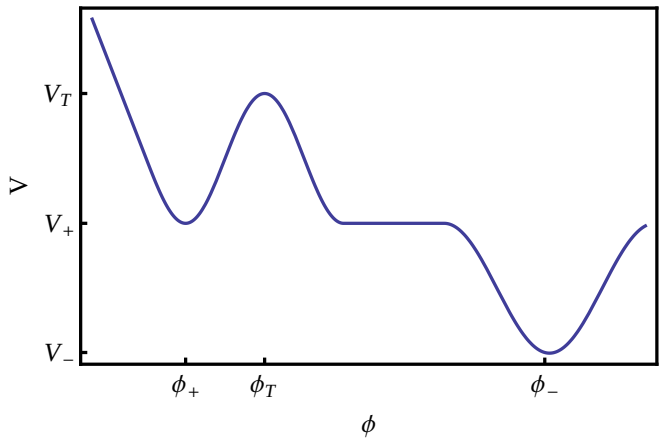


Figure 3.4.: *Schematic view of a potential with an existing bounce solution. The crucial part is that the true minimum is a smooth function of $\phi$, i.e. $\partial_\phi V$ is continuous.*

In the inverted potential (see Figure 3.4), the bounce solution $\phi_B$ is the solution to the equation of motion (in $3+1$ dimensional Euclidean space time)

$$\phi'' + \frac{3}{r}\phi' - \partial_\phi V(\phi) \;=\; 0\,, \tag{3.34}$$

where $\phi' \equiv \partial_r \phi$ with the following properties. At the center of the bubble, at $r = 0$, the field sits with zero velocity at position $\phi_0$ somewhere between $\phi_T$, the location of the top of the potential barrier, and $\phi_-$, the location of the true vacuum. For $r > 0$, the field moves towards the false vacuum $\phi_+$, reaching it with zero speed for $r \to \infty$. Owing to the friction term in Eq. (3.34), it is not immediately clear that the field can ever reach $\phi_+$.

Inside of the bubble, starting ever closer to $\phi_-$, the field can sit almost fixed at that position for a longer and longer time – until friction dies off. Then, energy conservation makes the field roll past $\phi_+$ as long as $\Delta V_- \geq \Delta V_+$ ($\phi_\pm$ being the location of the false and true vacuum respectively, and $\Delta V_\pm = V_T - V_\pm$). To show that overshooting past $\phi_+$ occurs for starting values $\phi_0$ close enough to $\phi_-$, we need to be somewhat quantitative: For analytic potentials it is possible to linearize the equation of motion close to the true vacuum $\phi_-$, giving

$$\left(\partial_r^2 + \frac{3}{r}\partial_r - \mu^2\right)(\phi - \phi_-) \;=\; 0\,, \tag{3.35}$$

with $\mu^2 = V''(\phi_-)$. It is solved by

$$\phi(r) - \phi_- \;=\; 2(\phi_0 - \phi_-)\frac{I_1(\mu r)}{\mu r}\,, \tag{3.36}$$

where $I_1$ is the Bessel function of the first kind, see [32]. Hence for $\phi_0$ ever closer to $\phi_-$, the field can sit near $\phi_-$ for larger and larger $r$. Making the initial displacement from $\phi_-$ sufficiently small, $r$ becomes large enough such that the friction term effectively disappears. Thus by energy conservation, $\phi$ can rush past $\phi_+$.

On the other hand, starting far away from the top of the inverted potential, the field does not have enough energy to climb up to $\phi_+$. Thus, by continuity, there must be an initial value $\phi_0$ being $\phi_T < \phi_0 < \phi_-$ such that the field reaches $\phi_+$ with zero velocity.

## 3.5. Failure of the existence proof

The existence of the bounce crucially depends on the possibility of the field to spend arbitrarily long times arbitrarily close to the true vacuum. In other words, if the equation of motion (3.35) takes on a different form, it is not guaranteed that the field can spend enough time near the true minimum for the friction term to die out. In particular, it is intuitively clear that this is the case for piecewise linear potentials, see Figure 3.3. In the following, we discuss the tunneling solutions in detail for a piecewise linear potential, pointing out several subtleties before we analyze the transition to the smooth and regular potential where the kinks are resolved by caps.

Tunneling in a piecewise linear potential

$$V(\phi) \;=\; \begin{cases} V_T + \lambda_+(\phi - \phi_T)\,, & \phi < \phi_T \\ V_T - \lambda_-(\phi - \phi_T)\,, & \phi \geq \phi_T \end{cases}\,, \tag{3.37}$$

has been analyzed by [37]. We present their analysis in a slightly different form.

First of all, we set $\phi_T = V_T = 0$ as shifts in the field and in the zero point energy do not change the physics – ignoring the effects of gravity. Solving the equation of motion inside of the bubble

$$\phi_i'' + \frac{3}{r}\phi_i' + \lambda_- \;=\; 0\,, \tag{3.38}$$

subject to $\phi(0) = \phi_0$, $\phi'(0) = 0$, we find

$$\phi_i \;=\; \phi_0 - \frac{\lambda_-}{8} r^2 \,. \tag{3.39}$$

Enforcing the matching condition $\phi_i(R_T) = 0$ gives

$$R_T \;=\; 2\sqrt{\frac{2\phi_0}{\lambda_-}} \,. \tag{3.40}$$

Solving the equation of motion on the outside of the bubble

$$\phi_o'' + \frac{3}{r}\phi_o' - \lambda_+ \;=\; 0 \,, \tag{3.41}$$

subject to $\phi_o(R_T) = 0$, $\phi_o'(R_T) = \phi_i'(R_T)$, we find

$$\phi_o \;=\; \frac{(R_T^2 - r^2)(R_T^2(\lambda_- + \lambda_+) - r^2\lambda_+)}{8r^2} \,. \tag{3.42}$$

On the outside, the field settles in the false vacuum at radius $R_+ > R_T$, for which $\phi_o'(R_+) = 0$

$$R_+ \;=\; \left(1 + \frac{\lambda_-}{\lambda_+}\right)^{1/4} R_T \,. \tag{3.43}$$

At this position, the field has the value

$$\phi_o(R_+) \;\equiv\; \phi_+ = -\phi_0 \frac{\sqrt{1+c} - 1}{\sqrt{1+c} + 1} \,, \tag{3.44}$$

where $c = \lambda_-/\lambda_+$. As $\phi_0 < \phi_-$, this gives a restriction on the shape of the potential

$$\alpha \equiv \frac{-\phi_+}{\phi_-} \leq \frac{-\phi_+}{\phi_0} = \frac{\sqrt{1+c} - 1}{\sqrt{1+c} + 1} < 1 \,. \tag{3.45}$$

This is equivalent to

$$\frac{\Delta V_+}{\Delta V_-} \;\leq\; \frac{1}{2 + c + 2\sqrt{1+c}} \leq \frac{1}{4} \,. \tag{3.46}$$

In other words, the bounce solutions given by Eq. (3.39) and Eq. (3.42) with initial condition $\phi(0) = \phi_0$, $\phi'(0) = 0$ are only valid for the parameter range $\alpha < 1$ and $\Delta < \frac{1}{4}$.

Before proceeding, let us take a look at the physical meaning of this condition. It corresponds to a potential profile where the energy difference between the false and the true vacuum is large (i.e. *not* thin-wall) and $|\phi_+| < |\phi_-|$. In this case, it is always possible to find a field position $\phi_0 < \phi_-$ with zero initial velocity such that the field can roll up the hill to $\phi_+$.

On the other hand, if either $\Delta > 1/4$ for any value of $\alpha$, or $\Delta < 1/4$ and $\alpha > 1$, it is not immediately clear that a bounce solution exists for $\phi_0 \leq \phi_-$. The physical picture is as follows:

For $\Delta > 1/4$ (and any value of $\alpha$), there is a smaller energy difference between the true and the false minimum – in the extreme case, making the energy difference infinitesimally small for $\Delta \to 1$, the thin-wall limit. For almost degenerate minima, the field would need to wait near the true minimum for the friction term to fall off. But the linear potential makes it impossible for the field to stay longer at that initial position. Therefore, with a small energy difference between the true and the false vacuum, the field can not roll up the hill due to friction, and no solution exists that reaches $\phi_+$.

For $\Delta < 1/4$ and $\alpha > 1$, although the field has a large potential energy to start with, the non-vanishing friction term still prevents it from climbing up the long shallow part to reach $\phi_+$.

Another example in which a large difference in potential energy does not guarantee a bounce solution are scalar potentials with local $\phi^4$ (or higher power) behavior

$$V(\phi) \;=\; -\frac{c_4}{4}(\phi - \phi_*)^4 + \text{higher order}\,, \quad c_4 > 0\,. \tag{3.47}$$

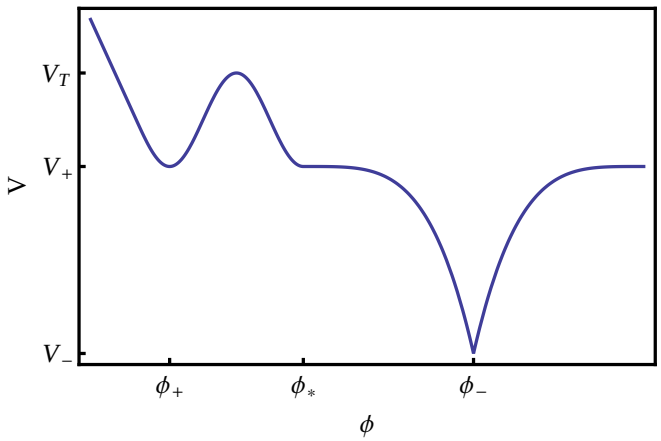


Figure 3.5.: *Shape of a true minimum for which no bounce exists. If the wings of the trough at $\phi_-$ are polynomials of at least order 4, the bounce solution in the inverted potential cannot roll past the point $\phi_*$ on the left.*

For solutions to the equation of motion

$$\phi'' + \frac{3}{r}\phi' + c_4(\phi - \phi_*)^3 \;=\; 0\,, \tag{3.48}$$

with initial conditions $\phi(0) = \phi_0$ and $\phi'(0) = 0$, the field reaches $\phi = \phi_*$ with zero speed [21] independent from the release point $\phi_0$. If the $\phi^4$ behavior ends with a kink (as depicted in Figure 3.5) no bounce solution exists.

It is important to note that the arguments illustrated in Section 3.4 do not immediately hold here: there is no quadratic approximation of the potential around the true minimum

to get Eq. (3.35). In a linear potential, putting the initial position ever closer to the true minimum $\phi_-$ does not force the field to spend an ever longer time there.

As [37] pointed out, we thus need to modify the initial conditions. Inside the bubble, the field should be artificially fixed at the true minimum $\phi_-$ until radius $R_0$. This should be understood as an approximation. In particular, this can be interpreted as mimicking the effect of removing the kink and replacing it with a smooth cap. In this suitably capped potential, the field can sit arbitrarily close to the true minimum and spend ever longer time there. The original argument of the existence of bounce solution as outlined in Section 3.4 immediately holds.

This waiting period can be realized by a change in the boundary conditions as first done by [37] for a piecewise linear potential. The modified initial conditions become $\phi_i(r) = \phi_-$, $\phi_i'(r) = 0$ for $0 \leq r \leq R_0$, giving

$$\phi_i(r) \;=\; \phi_- - \frac{(r^2 - R_0^2)^2}{8r^2}\lambda_- \tag{3.49}$$

for $R_0 \leq r < R_T$. Outside of the bubble at $R_+ > R_T$, the field comes to rest in the false vacuum $\phi_o'(R_+) = 0$, $\phi_o'(R_+) = 0$, giving

$$\phi_o(r) \;=\; \phi_+ + \frac{(r^2 - R_+^2)^2}{8r^2}\lambda_+ \,. \tag{3.50}$$

Now matching the two solutions $\phi_i(R_T) = 0 = \phi_o(R_T)$, $\phi_i'(R_T) = \phi_o'(R_T)$ gives

$$\begin{aligned}
R_0 &= \frac{\phi_-}{1-\sqrt{\Delta}}\sqrt{\frac{2}{V_-}}\sqrt{(1+\alpha)\left[\alpha - 1 + 2\sqrt{\Delta}\right]}\,,\\
R_T &= \frac{\phi_-}{1-\sqrt{\Delta}}\sqrt{\frac{2}{V_-}}(1+\alpha)\,,\\
R_+ &= \frac{\phi_-}{1-\sqrt{\Delta}}\sqrt{\frac{2}{V_-}}\sqrt{(1+\alpha)\left[1+\alpha\left(\frac{2}{\sqrt{\Delta}}-1\right)\right]}\,,
\end{aligned} \tag{3.51}$$

with $R_0 < R_T < R_+$, $\alpha = -\frac{\phi_+}{\phi_-}$, $\Delta V_\pm = V_T - V_\pm$ and $\Delta = \frac{\Delta V_+}{\Delta V_-}$. Note that the condition that $R_0$ is real implies that $\alpha > 1 - 2\sqrt{\Delta}$.

The tunneling amplitude can then be computed as

$$B \;=\; B_a + B_b + B_c\,, \tag{3.52}$$

with

$$B_a \;=\; 2\pi^2 \int_0^{R_0} dr\, r^3 \left(-\lambda_-\phi_- - \lambda_+\phi_+\right)\,, \tag{3.53}$$

$$B_b \;=\; 2\pi^2 \int_{R_0}^{R_T} dr\, r^3 \left(\frac{1}{2}\phi_L'^2 - \lambda_-\phi_L - \lambda_+\phi_+\right)\,, \tag{3.54}$$

$$B_c = 2\pi^2 \int_{R_T}^{R_+} dr\, r^3 \left( \frac{1}{2}\phi_R'^2 + \lambda_+ \phi_R - \lambda_+ \phi_+ \right) , \tag{3.55}$$

giving

$$B = \frac{2\pi^2}{3} \frac{\phi_-^4}{\Delta V_-} \frac{(1+\alpha)^3 \left( (\alpha-3)\sqrt{\Delta} + 1 - 3\alpha \right)}{(\sqrt{\Delta}-1)^3} . \tag{3.56}$$

For certain choices of parameters of a piecewise linear potential, we just saw that the bounce solutions exist only when we keep the field artificially fixed at the true minimum. Holding it there for a sufficiently long time, the damping term becomes small enough such that the field can reach the false vacuum with zero velocity. Of course, holding the field fixed at the tip of a piecewise linear potential is all but impossible. This should be thought of as an approximation to the physical situation of smoothing the tip with a cap.

## 3.6. Caps vs. Kinks

In this Section, we discuss in which cases replacing the tip of a piecewise linear potential with a smooth cap can be well approximated by keeping the field artificially fixed at the minimum as outlined in the previous Section.

Suppose that a piecewise linear potential is obtained as the limit of a regular smooth potential. The scale $\delta\phi$ on which the kink is resolved in the regular potential serves as expansion parameter $\delta\phi \ll |\phi_T - \phi_-|$. Apparently, the bounce actions can be very different, if the smooth potential varies strongly in the cap region. For example, if the potential has a large positive spike, the bounce solution can leave the cap region with a sizable velocity that can alter the bounce action significantly. Hence we demand that the potential in the cap does not differ too much from the corresponding value $V_-$ in the kink potential at least up to the first local minimum in the regularized potential

$$|V_-^{\text{cap}} - V_-^{\text{kink}}| \lesssim \lambda_- \, \delta\phi. \tag{3.57}$$

Still, the potential can vary strongly in the cap region in the sense that its derivative does not need to be small. Some examples are given in Figure 3.6.

Now, consider the bounce solutions for the kink potential and the cap potential outside the cap region. Even for large $r$ these two solutions only coincide approximately. It might well be that one of the two solutions passes a given point in the potential a little bit later but compensates by a slightly smaller velocity. The former effect leads to a reduced friction that is compensated by the latter effect.

Even a small difference between the two bounces can have a large effect on the action. To see this, consider a piecewise linear potential with two slightly different kink positions $\phi_-$ but same slope $\lambda_-$. Suppose that we would arrange this shift in $\phi_-$ such that the bounce solution of this modified kink potential and the bounce of the regular

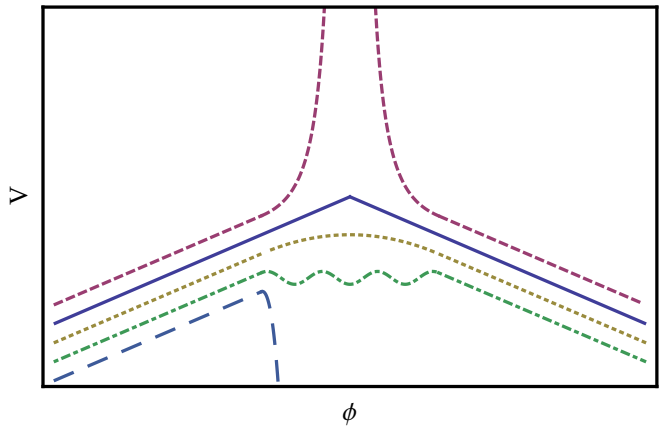


Figure 3.6.: *The piecewise linear potential and different regular potentials in the cap region. The three potentials on the bottom pass the criterion (3.57) while the potential on top can lead to large deviations in the bounce action.*

potential coincide. The potential with the more remote kink position $\phi_-$ has a smaller $R_0$. According to (3.56), a shift $\Delta\phi_-$ leads generically to a change in the bounce action of order $\delta B/B \sim \Delta\phi_-/\phi_-$ and hence be small. Only in the thin wall regime where $\Delta \simeq 1$ this change can be large and of order

$$\frac{\delta B}{B} \simeq \frac{3}{2}\frac{1}{\sqrt{\Delta}-1}\frac{\Delta\phi_-}{\phi_-}. \tag{3.58}$$

Fortunately, $\Delta\phi_-$ cannot be larger than $\delta\phi$. We prove this by contradiction. The solution to the field equations of motion are (see Eq. (3.49))

$$\phi_i(r) \;=\; \phi_- + \Delta\phi_- - \frac{(r^2-(R_0+\delta R_0)^2)^2}{8r^2}\lambda_- \;. \tag{3.59}$$

Now assume $\delta\phi \ll \Delta\phi_- \ll \phi_-$: the field leaves the cap at

$$r^2-(R_0+\delta R_0)^2 \simeq \sqrt{8\Delta\phi_-(R_0+\delta R_0)^2/\lambda_-} \tag{3.60}$$

with velocity

$$\phi_i' \simeq \sqrt{2\Delta\phi_-\lambda_-}. \tag{3.61}$$

However, due to energy conservation and the condition (3.57), the energy at the border of the cap cannot exceed the potential energy. This implies

$$\phi_i' \lesssim \sqrt{2\lambda_-\delta\phi}, \tag{3.62}$$

and hence $\Delta\phi_- \lesssim \delta\phi$ such that

$$\frac{\delta B}{B} \lesssim \frac{3}{2}\frac{1}{\sqrt{\Delta}-1}\frac{\delta\phi}{\phi_-}\,. \tag{3.63}$$

Thus we demand

$$\sqrt{\Delta}-1 \gg \frac{\delta\phi}{\phi_-}, \tag{3.64}$$

in order to obtain accurate results for the bounce action in the kink approximation.

Even though our reasoning above seems very conservative, no better upper bound on the variation of the action exists in the thin-wall regime. The boundary of the relation (3.64) is equivalent to

$$|V_+ - V_-| \simeq \lambda_- \delta\phi \,, \tag{3.65}$$

but in this case the potential difference between the true and false vacua in the regular capped potential can be very different from that in the kink potential. This can lead to grossly different bounce actions. For this special situation, the constraint in (3.63) is saturated.

Combining the criteria (3.57) and (3.64), our two conditions on the kink approximation read

$$|V_-^{\rm cap} - V_-^{\rm kink}| \lesssim \lambda_- \delta\phi \ll |V_+^{\rm kink} - V_-^{\rm kink}| \,. \tag{3.66}$$

In the preceding Sections, we demonstrated that under most circumstances, smoothing the kink in a piecewise linear potential is equivalent to holding the field fixed at some radius $R_0$. This statement depends crucially on the choice of cap that replaces the kink. The shape of the cap must be such that the field can spend an arbitrarily long time $R$ close to the true vacuum to allow the friction term to get sufficiently small. This time $R$ is approximately (assuming that friction dominates over acceleration in the equation of motion)

$$\frac{3}{r}\frac{d\phi}{dr} \approx V'(\phi) \quad \Rightarrow \quad \int_{\phi_0}^{\phi(R)} \frac{d\phi}{V'(\phi)} = \frac{1}{6}R^2 \,. \tag{3.67}$$

To spend an arbitrary and potentially infinite amount of time near the cap, the integral must diverge in the limit $\phi_0 \to \phi_-$. Certainly this is true for analytic potentials with a finite mass $|V''(\phi_-)| < \infty$. For example, taking $V(\phi) = \frac{1}{2}m^2\phi^2$, it is clear that the integrand becomes $1/V'(\phi) = 1/m^2\phi$ which is logarithmically divergent.

However, potentials such that the integral is finite in the limit $\phi_0 \to \phi_-$ do also exist. One class of examples are potentials of the form $V \propto |\phi - \phi_-|^\alpha$, with $1 < \alpha < 2$, which we shall now analyze in more detail. The derivative of the potential at the minimum is $V'(\phi_*) = 0$ in the limit $\phi_* \to \phi_-$ both from the left and from the right.

To set up the full picture, let us assume a piecewise potential, where we examine the area around the cap. We assume that the other piecewise parts of the potential contain at least one other local minimum. The complete bounce is given by matching the solutions in each part of the potential. We solve the equations of motion for the bounce in the part of the potential describing the cap where $V(\phi) = \lambda|\phi - \phi_-|^\alpha$, $1 < \alpha < 2$. The equation of motion reads

$$\phi'' + \frac{3}{r}\phi' - \lambda\alpha\,\mathrm{sgn}(\phi - \phi_-)|\phi - \phi_-|^{\alpha-1} \;=\; 0 \,, \tag{3.68}$$

subject to the boundary conditions $\phi(0) = \phi_0$, $\phi'(0) = 0$. Even in the limit $\phi_0 \to \phi_-$,

the solution spends only a finite amount of time in the cap region and is given by

$$\phi(r) \;=\; \phi_- + \left(\frac{4\alpha\lambda(\alpha-2)^2}{3-\alpha}\right)^{\frac{1}{2-\alpha}} r^{\frac{2}{2-\alpha}}\,. \tag{3.69}$$

Hence, even though the field starts off from the extremum where there is no force ($V'(\phi_-) = 0$), it begins rolling away in finite time. However, this does not imply that there is no bounce. The field can wait for some time at $\phi_-$ and then still leave the cap in finite time (friction is even less important than in the previous case). This solution can be obtained by using the boundary conditions $\phi(R_0) = \phi_0$ and $\phi'(R_0) = 0$, and sending the release point subsequently to $\phi_-$. If the waiting period $R_0$ is chosen appropriately, the field reaches the false vacuum, thus constituting a bounce solution.

Numerically, the bounce solution is often determined using the shooting algorithm [32]. In this case, a release position for the field is chosen and the corresponding initial value problem using the equation of motion is solved. The release point is then varied until the correct boundary conditions of the bounce solution in the false vacuum are fulfilled. Obviously, a bounce of the kind described above cannot be found with the conventional shooting algorithm.

This situation might be rather surprising, since the potential is smooth and even differentiable everywhere. This special situation arises because the equation of motion for the bounce in the potential (3.68) with $\alpha < 2$ does not fulfill the Lipschitz condition. Hence the Picard-Lindelöf theorem does not hold and a solution to the initial value problem is not necessarily unique. This kind of situation is well known in the philosophy of science community [49] in the context of classical mechanics. Fortunately, here we need not concern ourselves with the initial value problem. We are interested in computing the tunneling amplitude, and the bounce solution with the usual boundary conditions is indeed unique. So for this kind of potential, one can be in the situation that the kink approximation describes the tunneling process quite well, while the common shooting algorithm in the smooth and regular potential fails.

## 3.7. Conclusions

We first discussed a quantum tunneling event in a piecewise potential where the false vacuum part is either linear or quartic and the true vacuum is described by a quartic potential. Often, the analysis of quantum tunneling in field theory is performed in the thin wall approximation [32]. This does not necessarily capture all realistic scenarios. In particular, cosmological phase transitions usually involve a large change of the energy scale. For example, the relative energy difference between neighboring vacua in the landscape of string theory is typically large. Although any specific realistic scenario can be solved by numerical methods, this makes it rather difficult to get a good qualitative understanding of the process under a change of potential parameters. As shown in Section 3.2, the exact shape of the potential plays a non-negligible role when considering tunneling in the thick-wall regime. Together with previous exact tunneling solutions

[37–40], this work contributes to bridging the gap in qualitative understanding. As a consistency check, we have shown that the tunneling rates always reduce to the thin-wall result in the appropriate limit. We also explain how the exact tunneling solutions can give information about the local shape of the landscape.

We have also addressed the issue of the existence of a bounce solution in an effective potential that has sharp minima and maxima ('kinks'). Tunneling in this setup was first discussed analytically in [37]. For certain ranges of parameters, a consistent bounce solution exists only if the field can rest for some amount of Euclidean time at the true vacuum. With this field profile, it is possible for the relevant friction term to die off sufficiently so that the field can roll back up to the false vacuum. Having the field 'wait' in such a manner is only an approximation to the full bounce solution where the tip represents a smooth cap of a regular potential.

We found that replacing a regular smooth potential by its piecewise linear approximation is a very robust procedure. A sufficient criterion for the bounce action of the kink potential to yield accurate results is given by

$$|V_-^{\text{cap}} - V_-^{\text{kink}}| \lesssim \lambda_- \delta\phi \ll |V_+^{\text{kink}} - V_-^{\text{kink}}| \,. \tag{3.70}$$

Here, $\delta\phi$ is the scale on which the kink is resolved in the smooth and regular potential, $\lambda_-$ denotes the slope in the kink potential close to the true minimum and $V_\mp$ denote values of the potential in the true (false) vacuum, respectively.

The first inequality reflects the fact that the bounce action varies strongly if the field can accumulate a sizable kinetic energy in the cap; the second inequality results from the fact that the bounce action is very sensitive to the potential difference between the true and the false vacuum in the thin-wall regime.

For example, this includes potentials that fluctuate strongly or that do not have a finite second derivative in the true vacuum, as for potentials that behave close to the true vacuum as $V \simeq (\phi - \phi_-)^\alpha$ with $1 < \alpha < 2$. In particular, for the latter class of potentials, the kink approximation yields accurate results even though the bounce solutions cannot be obtained from the regular potential using the conventional shooting algorithm.

Violations of the condition Eq. (3.70) can appear for instance within the context of the 4D effective field theory approximation to a theory of quantum gravity such as string theory. It is not clear how to self-consistently describe caps with curvature larger than $M_p^2$ within this framework. In particular, in such a high curvature cap, steep local maxima acting as large positive spikes as discussed before cannot be excluded. In a situation where the cap is confined to such a region of strong quantum gravity effects, we can no longer guarantee that condition (3.70) is satisfied from a calculation of the cap from effective field theory. Thus, a description of the tunneling using the description of [32] and [34] entirely within the realm of effective field theory is not possible for a high curvature cap. In this case, full quantum gravity effects must be incorporated to calculate the tunneling amplitude.

Possible examples in string theory are e.g. warped compactifications with D3-branes. In such compactifications, the warp factor contributes to the 4D effective scalar potential.

To leading order, the warp factor, and in turn its contribution to the 4D scalar potential, may develop 'kinks' at the position of a D3-brane, similar to the case of 5D warped Randall-Sundrum compactifications [50]. String theory effects can smooth such 'kinks', but the curvature of the smoothing cap may then be too large, as mentioned above, for a treatment within effective field theory alone.

# 4. Inflationary Perturbations

If you're going through hell, keep going.

*(Winston Churchill)*

Since COBE twenty years ago first detected anisotropies in the cosmic microwave background, this data became better and better with every subsequent experiment, most important WMAP and PLANCK. The more precise data now allows us to make stronger tests on theoretical models [51–57], for example testing different models of inflation. Here, calculating these fluctuations on de Sitter background brings up some new properties [58, 59].

The anisotropies in the CMB go back to quantum fluctuations, which are stretched to classical fluctuations during inflation. Investigations of these perturbations are normally done by solving classical equations of motion, although it is not clear if this is a valid approximation. In [6] this was tested up to one-loop for a cubic inflaton potential. They calculated the two-point function for a scalar field. In the context of the CMB this corresponds to the temperature power spectrum [60]. For tree-level and one-loop the approximation turned out to be valid, but it was not expected to be valid for two-loop.

As an extension of this work we study a model with quartic inflaton potential up to two-loop corrections [9]. The highly improved quality of CMB data from PLANCK demands the extension of the analysis to the next loop-level. We use the Closed Time Path formalism [61–63]. We calculate the cosmological correlation functions after horizon exit for $\phi^4$ theory on de Sitter background for a massless minimally coupled scalar field $\phi$. The calculation of the two-loop corrections is much more complicated than the one-loop corrections. One peculiarity here is that IR $\times$ UV-divergent terms can appear. Another important point is the time dependence of the contributions. For a $\lambda\phi^4$ theory with $\lambda$ small, the terms of $\mathcal{O}(\lambda)$ are dominating the terms of $\mathcal{O}(\lambda^2)$. In this case here, one might get terms like $\lambda^2\tau$ with $\tau$ very large, so called late time contributions. These contributions can become dominant.

We will first give a short introduction to the Closed Time Path formalism and derive the Feynman rules on de Sitter background for a scalar field with quartic potential. In Section 4.3 we calculate the one-loop contributions to the two-point function, in Section 4.4 we extend our analysis to two-loop. We conclude in Section 4.5.

## 4.1. Closed Time Path Formalism

The Closed Time Path formalism (CTP) we are using here comes originally from condensed matter theory, known as Schwinger-Keldysh formalism. It was then refined for cosmology by Calzetta and Hu [61]. Another common name for this formalism is 'in-in' formalism, which also gives a nice intuitive idea of it. Instead of calculating 'in-out' reactions like in particle physics ($e^+e^- \to \mu^+\mu^-$), we now look twice at the same 'in' state, having a time dependent Hamiltonian $H(t)$. The integration is done over a closed time path $\mathcal{C}$

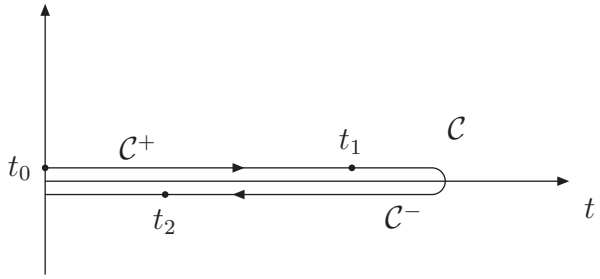


Figure 4.1.: *CTP contour*

starting and finishing at $t_0$, looking at the expectation value at time $t$ (see Figure 4.1). The expectation value of the operator $\mathcal{O}$ at time $t > t_0$ is given by

$$\langle \mathcal{O}(t) \rangle = \left\langle \text{in} \left| \left[ \bar{\text{T}} \exp\left( i \int_{t_0}^{t} \mathrm{d}t' H(t') \right) \right] \mathcal{O}(t) \left[ \text{T} \exp\left( -i \int_{t_0}^{t} \mathrm{d}t' H(t') \right) \right] \right| \text{in} \right\rangle . \quad (4.1)$$

Here $T$ is the time ordered product for the upper path $\mathcal{C}_+$ and $\bar{T}$ is the anti time ordered product for the lower path $\mathcal{C}_-$. We also split the field $\phi$ up into $\phi^+$ on $\mathcal{C}_+$ and $\phi^-$ on $\mathcal{C}_-$ with $\phi^+(t) = \phi^-(t)$ for all $t$. This gives us four different two-point functions $G^{++}$, $G^{--}$, $G^{+-}$, $G^{-+}$, where for example $G^{++}$ represents the case when both $t_1$ and $t_2$ are on $\mathcal{C}_+$. $G^{-+}$ means $t_2$ is on $\mathcal{C}_+$ and $t_1$ is on $\mathcal{C}_-$, ....
Written out we have

$$\begin{aligned}
G^{-+}(x,y) &= i \left\langle \phi(x)\phi(y) \right\rangle^{(0)}, \\
G^{+-}(x,y) &= i \left\langle \phi(y)\phi(x) \right\rangle^{(0)}, \\
G^{++}(x,y) &= i \left\langle \text{T}\phi(y)\phi(x) \right\rangle^{(0)} = \theta(x_0 - y_0) G^{-+}(x,y) + \theta(y_0 - x_0) G^{+-}(x,y), \\
G^{--}(x,y) &= i \left\langle \bar{\text{T}}\phi(y)\phi(x) \right\rangle^{(0)} = \theta(x_0 - y_0) G^{+-}(x,y) + \theta(y_0 - x_0) G^{-+}(x,y).
\end{aligned} \quad (4.2)$$

Only two of them are independent. They fulfill the identity

$$G^{++}(x,y) + G^{--}(x,y) = G^{-+}(x,y) + G^{+-}(x,y). \quad (4.3)$$

and can be arranged in a matrix

$$\mathbf{G}(x,y) = \begin{pmatrix} G^{++}(x,y) & G^{+-}(x,y) \\ G^{-+}(x,y) & G^{--}(x,y) \end{pmatrix}. \tag{4.4}$$

We now perform a basis transformation from $\phi^+$ and $\phi^-$ to $\phi^{(1)}$ and $\phi^{(2)}$ for convenience

$$\begin{pmatrix} \phi^{(1)} \\ \phi^{(2)} \end{pmatrix} = \begin{pmatrix} (\phi^+ + \phi^-)/2 \\ \phi^+ - \phi^- \end{pmatrix} = \mathbf{R} \begin{pmatrix} \phi^+ \\ \phi^- \end{pmatrix} \tag{4.5}$$

using

$$\mathbf{R} = \begin{pmatrix} 1/2 & 1/2 \\ 1 & -1 \end{pmatrix}. \tag{4.6}$$

Later, $\phi^{(1)}$ will be indicated by the solid line, $\phi^{(2)}$ by the dashed line. This is a variation of the Keldysh basis also used in [64]. In this basis, the matrix of two-point functions becomes

$$\mathbf{G}_K(x,y) = \mathbf{R}\mathbf{G}(x,y)\mathbf{R}^T = \begin{pmatrix} \mathrm{i}F(x,y) & G^R(x,y) \\ G^A(x,y) & 0 \end{pmatrix}. \tag{4.7}$$

Our propagators are

$$\begin{aligned} F(x,y) &= -\frac{\mathrm{i}}{2}\left(G^{-+}(x,y) + G^{+-}(x,y)\right) \\ G^R(x,y) &= G^{++}(x,y) - G^{+-} = \Theta(x_0 - y_0)\left(G^{-+}(x,y) - G^{+-}(x,y)\right) \\ G^A(x,y) &= G^{++}(x,y) - G^{-+} = \Theta(y_0 - x_0)\left(G^{+-}(x,y) - G^{-+}(x,y)\right). \end{aligned} \tag{4.8}$$

$G^R$ is the retarded propagator, $G^A$ is the advanced propagator with $G^R(x,y) = G^A(y,x)$.

## 4.2. Feynman Rules on de Sitter background

We will consider the flat de Sitter metric in conformal time to be

$$ds^2 = g_{\mu\nu}dx^\mu dx^\nu = a^2(\tau)\left(d\tau^2 - dr^2 - r^2 d\Omega\right). \tag{4.9}$$

The de Sitter scale factor is $a(\tau) = -\frac{1}{H\tau}$, with constant Hubble parameter $H$ and the conformal time $\tau$ given by

$$\tau = \int_t^\infty \frac{dt}{a(t)} = \int_t^\infty dt\; e^{-Ht} = -\frac{1}{H\; e^{Ht}}. \tag{4.10}$$

$\tau$ varies between $-\infty$ and zero.

For our calculation, the Lagrangian density is given by

$$\mathcal{L}[\phi] = \sqrt{-g}\left(-\frac{1}{2}\partial_\mu\phi\partial^\mu\phi - \frac{1}{2}m^2\phi^2 - \frac{1}{2}\xi R\phi^2 - \frac{\lambda}{4!}\phi^4\right) + \delta\mathcal{L}. \tag{4.11}$$

The signature of the metric $g_{\mu\nu}$ is diag$(+,-,-,-)$. $m = 0$ if not needed as IR regulator. Set $\xi = 0$ for a minimally coupled scalar field.
The counterterms are

$$\delta\mathcal{L} = \sqrt{-g}\left(-\frac{1}{2}\delta_Z\partial_\mu\phi\partial^\mu\phi - \frac{1}{2}\delta_m\phi^2 - \frac{\delta_\lambda}{4!}\phi^4\right). \tag{4.12}$$

Note the symmetry of Lagrangian under $\phi^+ \to \phi^-$

$$\begin{aligned}\mathcal{L}[\phi] = \mathcal{L}[\phi^+] - \mathcal{L}[\phi^-] =& \sqrt{-g}\left(-\frac{1}{2}\partial_\mu[\phi^+]\partial^\mu[\phi^+] + \frac{1}{2}\partial_\mu[\phi^-]\partial^\mu[\phi^-] - \frac{1}{2}m^2[(\phi^+)^2 - (\phi^-)^2]\right.\\ &\left. - \frac{\lambda}{4!}[(\phi^+)^4 - (\phi^-)^4]\right) + \delta\mathcal{L}.\end{aligned} \tag{4.13}$$

Replacing $\phi_+$ and $\phi_-$ with our new basis $\phi^{(1)}$ and $\phi^{(2)}$ gives

$$\begin{aligned}\mathcal{L}[\phi^{(1)},\phi^{(2)}] =& \sqrt{-g}\left(-\partial_\mu\phi^{(1)}\partial^\mu\phi^{(2)} - m^2\phi^{(1)}\phi^{(2)}\right.\\ &\left. - \frac{\lambda}{4!}(4(\phi^{(1)})^3\phi^{(2)} + \phi^{(1)}(\phi^{(2)})^3)\right) + \delta\mathcal{L}.\end{aligned} \tag{4.14}$$

The propagators, vertices and counterterms are


$$= F(k,\tau_1,\tau_2) \tag{4.15}$$


$$= -\mathrm{i}G^R(k,\tau_1,\tau_2) = -\mathrm{i}G^A(k,\tau_2,\tau_1) \tag{4.16}$$

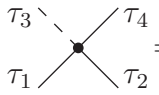
$$= -\mathrm{i}a^4\frac{\lambda}{3!}\delta(\tau_1-\tau_2)\,\delta(\tau_2-\tau_3)\,\delta(\tau_3-\tau_4) \tag{4.17}$$

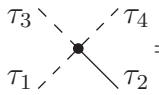
$$= -\mathrm{i}a^4\frac{\lambda}{4!}\delta(\tau_1-\tau_2)\,\delta(\tau_2-\tau_3)\,\delta(\tau_3-\tau_4) \tag{4.18}$$

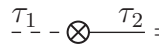
$$= -\mathrm{i}a^4\delta_m\delta(\tau_1-\tau_2) \tag{4.19}$$

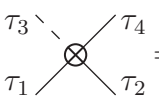
$$= -\mathrm{i}a^4\frac{\delta_\lambda}{3!}\delta(\tau_1-\tau_2)\,\delta(\tau_2-\tau_3)\,\delta(\tau_3-\tau_4) \tag{4.20}$$

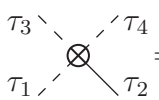
$$= -\mathrm{i}a^4\frac{\delta_\lambda}{4!}\delta(\tau_1-\tau_2)\,\delta(\tau_2-\tau_3)\,\delta(\tau_3-\tau_4)\,. \tag{4.21}$$

In the following we will give the expressions for the diagrams after evaluating the $\delta$-functions.

## Propagators

We start with the equation of motion for a free scalar field on a de Sitter background, here $x = (\tau, \vec{x})$:

$$\partial_\tau^2 \phi(x) + 2Ha(\tau)\partial_\tau \phi(x) - \nabla^2 \phi(x) + a^2(\tau) m \phi(x) = 0. \tag{4.22}$$

Choosing the Bunch-Davies vacuum, this equation is solved by

$$\phi_{k,\alpha}(\tau) = -\frac{\sqrt{-\pi\tau}}{2a(\tau)} H_\nu^{(\alpha)}(-k\tau) \tag{4.23}$$

with $H_\nu^{(\alpha)}(-k\tau)$ [65] being the Hankel functions with $\nu^2 = \frac{9}{4} - \frac{m^2}{H^2}$ and $\alpha = 1, 2$

$$\begin{aligned} H_\nu^{(1)}(-k\tau) =& J_\nu(-k\tau) + \mathrm{i} Y_\nu(-k\tau) \\ H_\nu^{(2)}(-k\tau) =& J_\nu(-k\tau) - \mathrm{i} Y_\nu(-k\tau), \end{aligned} \tag{4.24}$$

and the Bessel function of first kind $J_\nu$ and of second kind $Y_\nu$

$$\begin{aligned} J_\nu(-k\tau) =& \frac{1}{\Gamma(\nu+1)} \left(-\frac{1}{2} k\tau\right)^\nu (1 + \mathcal{O}(k^2\tau^2)) \\ Y_\nu(-k\tau) =& \frac{\cos\nu\pi J_\nu(-k\tau) - J_{-\nu}(-k\tau)}{\sin\nu\pi}. \end{aligned} \tag{4.25}$$

We will now derive three pairs of propagators. First, the exact propagators which we will use for large momenta. Second, a pair of approximated propagators for small momenta using a IR-regulating small mass. Third, a pair of approximated propagators for small momenta without a regulator mass.

### Exact propagators

For $m = 0, \xi = 0$, $\nu = \frac{3}{2}$ Eq. (4.23) simplifies to

$$\phi_{k,1}(\tau) = \mathrm{i} \frac{H}{\sqrt{2k^3}} (1 + \mathrm{i}k\tau) e^{-\mathrm{i}k\tau}. \tag{4.26}$$

Following from Eq. (4.8) the propagators are

$$\begin{aligned} F(x,y) =& -\frac{\mathrm{i}}{2} \left( G^{-+}(x,y) + G^{+-}(x,y) \right) \\ =& -\frac{\mathrm{i}}{2} \left( \mathrm{i} \langle \phi(x)\phi(y) \rangle^{(0)} + \mathrm{i} \langle \phi(y)\phi(x) \rangle^{(0)} \right), \end{aligned} \tag{4.27}$$

$$F(k, \tau_1, \tau_2) = \frac{H^2}{2k^3} \left[ \left(1 + k^2\tau_1\tau_2\right) \cos k(\tau_1 - \tau_2) + k(\tau_1 - \tau_2) \sin k(\tau_1 - \tau_2) \right],$$

and

$$\begin{aligned} G^R(x,y) =& \Theta(x_0-y_0)\left(G^{-+}(x,y)-G^{+-}(x,y)\right) \\ =& \Theta(x_0-y_0)\left(\mathrm{i}\left\langle\phi(x)\phi(y)\right\rangle^{(0)}-\mathrm{i}\left\langle\phi(y)\phi(x)\right\rangle^{(0)}\right), \end{aligned}$$

$$G^R(k,\tau_1,\tau_2) = \frac{H^2}{k^3}\Theta(\tau_1-\tau_2)\left[(1+k^2\tau_1\tau_2)\sin k(\tau_1-\tau_2)-k(\tau_1-\tau_2)\cos k(\tau_1-\tau_2)\right]. \tag{4.28}$$

### Small momenta with mass

For small momenta, we need $m \neq 0$ to regulate the IR divergences. We use Eq. (4.23) and choose $m \ll H$ and $\nu = \frac{3}{2}-\epsilon$ with $\epsilon = m^2/3H^2$. From Eq. (4.23) and Eq. (4.8) we find

$$\begin{aligned} F(k,\tau_1,\tau_2) =& \frac{\pi\sqrt{\tau_1\tau_2}}{4a(\tau_1)a(\tau_2)}\mathrm{Re}\left[H_\nu^{(1)}(-k\tau_1)H_\nu^{(1)*}(-k\tau_2)\right], \\ G^R(k,\tau_1,\tau_2) =& -\frac{\pi\sqrt{\tau_1\tau_2}}{2a(\tau_1)a(\tau_2)}\Theta(\tau_1-\tau_2)\mathrm{Im}\left[H_\nu^{(1)}(-k\tau_1)H_\nu^{(1)*}(-k\tau_2)\right]. \end{aligned} \tag{4.29}$$

The propagators are then

$$\begin{aligned} F(k,\tau_1,\tau_2) =& \frac{\pi\sqrt{\tau_1\tau_2}}{4a(\tau_1)a(\tau_2)}\mathrm{Re}\left[H_\nu^{(1)}(-k\tau_1)H_\nu^{(1)*}(-k\tau_2)\right] \\ =& \frac{H^2}{2k^3}\left(k^2\tau_1\tau_2\right)^\epsilon, \\ G^R(k,\tau_1,\tau_2) =& -\frac{\pi\sqrt{\tau_1\tau_2}}{2a(\tau_1)a(\tau_2)}\Theta(\tau_1-\tau_2)\mathrm{Im}\left[H_\nu^{(1)}(-k\tau_1)H_\nu^{(1)*}(-k\tau_2)\right] \\ =& \frac{H^2}{3}\Theta(\tau_1-\tau_2)\left(\tau_1^3\left(\frac{\tau_2}{\tau_1}\right)^\epsilon-\left(\frac{\tau_1}{\tau_2}\right)^\epsilon\tau_2^3\right). \end{aligned} \tag{4.30}$$

### Small momenta without mass

For the external propagators we do not need a regulating mass. Either the momentum is not zero, thus not IR divergent, or it is zero and the whole contributions is zero. Without regulating mass the propagators can also be approximated using

$$\sin x = x-\mathcal{O}(x^3), \quad \cos x = 1-\frac{x^2}{2}+\mathcal{O}(x^4). \tag{4.31}$$

This gives

$$F(k,\tau_1,\tau_2) = \frac{H^2}{2k^3}\left[1+\frac{1}{2}k^2(\tau_1^2+\tau_2^2)+\mathcal{O}(\tau_{i,j}^3)\right] \tag{4.32}$$

and

$$G^R(k,\tau_1,\tau_2) = \Theta(\tau_1-\tau_2)\frac{H^2}{3k^3}\left[k^3(\tau_1^3-\tau_2^3)+\mathcal{O}(\tau_{i,j}^5)\right]. \tag{4.33}$$

For the special case of $\tau_1 = \tau_2$ the expressions simplify to

$$F(k,\tau_1,\tau_1) = \frac{H^2}{2k^3}\left[1+k^2\tau_1^2+\mathcal{O}(\tau_1^3)\right], \quad G^R(k,\tau_1,\tau_1) = 0. \tag{4.34}$$

being in this special case equal to Eq. (4.27) and Eq. (4.28).

## 4.3. One-Loop Contributions

We will now first calculate the one-loop contributions for the two-point function including the counterterm. Then we will calculate the four-point contributions to determine the counterterms for the vertices.

### 4.3.1. 2-point function

We first discuss which diagrams contribute on one loop level to the two point function. We begin with the five diagrams below.

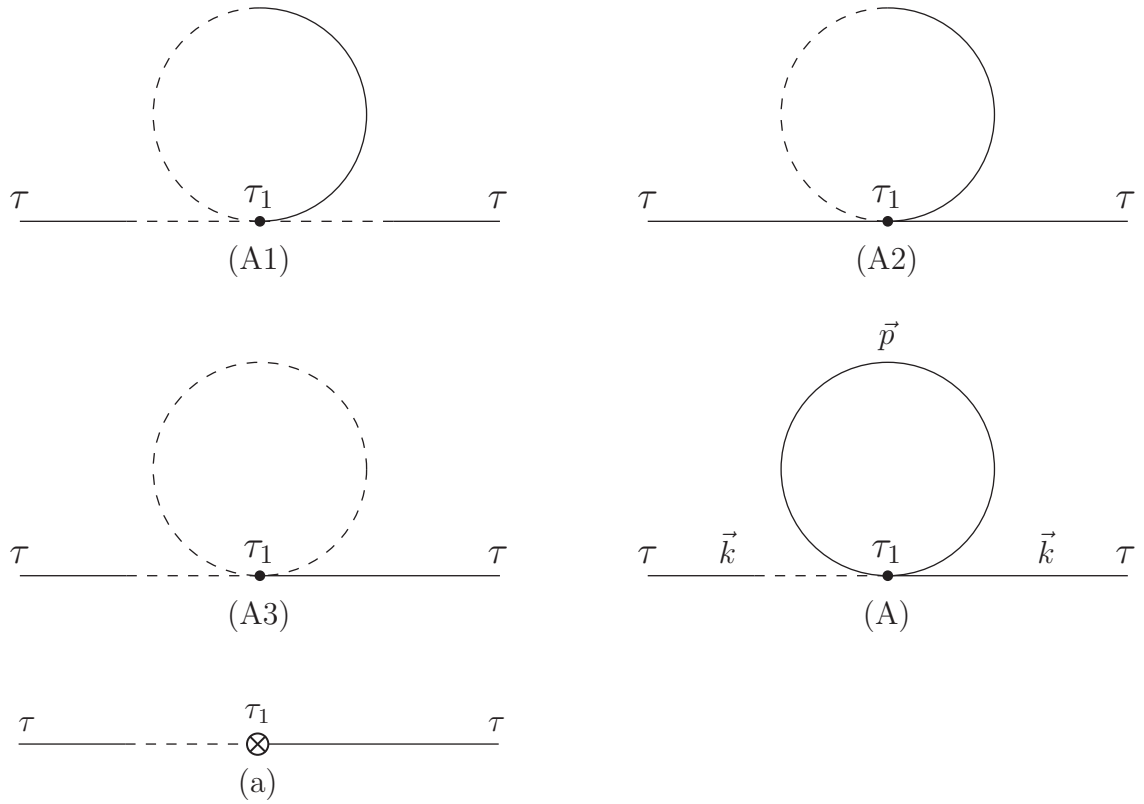


Note that we already applied the $\delta$-functions on the $\tau_i$-parameters. Diagram (A1) vanishes, since the $G^R(k,x,x) = 0$ for all $x$. There is also a mirror version of this diagram,

replacing $G^R$ with $G^A$, which vanishes for the same reason. Diagram (A2) does not contribute for the same reason, as well as its mirror version. Diagram (A3) does not exist, since the Feynman rules do not include a completely dashed propagator. The only loop diagram that exists and contributes is diagram (A) with a symmetry factor of 3. There is one counterterm diagram (a). The UV-divergences on this level will be absorbed by the counterterm. We expect IR-divergences, since $F$ is IR-divergent.
The complete expression for diagram (A) is

$$(A) =(-i)^2\frac{\lambda}{2}\int_{\tau_{in}}^{\tau} \mathrm{d}\tau_1 a^4(\tau_1)\int \frac{\mathrm{d}^3p}{(2\pi)^3}G^R(k,\tau,\tau_1)F(k,\tau_1,\tau)F(p,\tau_1,\tau_1) \tag{4.35}$$

We first compute the loop integral and then attach the external legs.

$$A_{\rm amp} = -\frac{i\lambda}{2}a^4(\tau_1)\int \frac{d^3p}{(2\pi)^3}F(p,\tau_1,\tau_1) \tag{4.36}$$

We split the integral into a piece with small internal momentum (up to $p = M_{\rm cm}$) and a piece with momentum larger than $M_{\rm cm}$. Small internal momenta using Eq. (4.30):

$$\begin{aligned} A^{\rm small}_{\rm amp} &= -\frac{i\lambda}{2}\,a^4(\tau_1)\int_0^{M_{\rm cm}} \frac{\mathrm{d}^3p}{(2\pi)^3}\,F(p,\tau_1,\tau_1) = -\frac{i\lambda}{2}\frac{1}{H^4\tau_1^4}\int_0^{M_{\rm cm}} \frac{\mathrm{d}^3p}{(2\pi)^3}\frac{H^2}{2p^3}\,(p^2\tau_1^2)^\epsilon \\ &= -\frac{i\lambda\tau_1^{2\epsilon}}{8\pi^2H^2\tau_1^4}\int_0^{M_{\rm cm}} \mathrm{d}p\; p^{2\epsilon-1} = -\frac{i\lambda}{8\pi^2H^2\tau_1^4}\frac{(|\tau_1|M_{\rm cm})^{2\epsilon}}{2\epsilon} \\ &= -\frac{i\lambda}{16\pi^2H^2\tau_1^4}\left(\frac{1}{\epsilon}+2\ln(|\tau_1|M_{\rm cm})+\mathcal{O}(\epsilon)\right). \end{aligned} \tag{4.37}$$

For large internal momenta, up to a time-dependent UV cut-off $\Lambda\, a(\tau_1)$, we have

$$\begin{aligned} A^{\rm large}_{\rm amp} &= -\frac{i\lambda}{2}\,a^4(\tau_1)\int_{M_{\rm cm}}^{\Lambda a(\tau_1)} \frac{\mathrm{d}^3p}{(2\pi)^3}\,F(p,\tau_1,\tau_1) = -\frac{i\lambda}{2H^4\tau_1^4}\int_{M_{\rm cm}}^{\Lambda a(\tau_1)} \frac{d^3p}{(2\pi)^3}\frac{H^2}{2p^3}\,(1+p^2\tau_1^2) \\ &= -\frac{i\lambda}{8\pi^2H^2\tau_1^4}\left(\int_{M_{\rm cm}}^{\Lambda a(\tau_1)}\frac{dp}{p}+\tau_1^2\int_0^{\Lambda a(\tau_1)} dp\; p\right) \\ &= -\frac{i\lambda}{16\pi^2H^2\tau_1^4}\left(2\ln\left(\frac{\Lambda a(\tau_1)}{M_{\rm cm}}\right)+\tau_1^2(\Lambda a(\tau_1))^2\right). \end{aligned} \tag{4.38}$$

In the last expression the logarithmic term in $M_{\rm cm}$ corresponds to the IR-divergence of the small momentum integral. Note that in the second integral, we can directly take the limit $M_{\rm cm} = 0$ since such term is finite in the IR and corresponds to IR-finite term of the propagator in the small momentum limit.

Combining the two expressions we obtain:

$$A_{\text{amp}} = -\frac{\mathrm{i}\lambda}{16\pi^2 H^2 \tau_1^4}\left(\frac{1}{\epsilon} + 2\ln\left(\frac{\Lambda}{H}\right) + \left(\frac{\Lambda}{H}\right)^2\right). \tag{4.39}$$

We can then use the counterterm diagram $(a)$ to cancel the UV-divergence as

$$a_{amp}(k,\tau_1,\tau_1) = -\frac{\mathrm{i}}{H^4\tau_1^4}\delta_m = -\frac{\mathrm{i}\lambda}{16\pi^2 H^2\tau_1^4}\left(2\ln\left(\frac{\Lambda}{\mu}\right) + \left(\frac{\Lambda}{H}\right)^2\right). \tag{4.40}$$

So the mass counterterm becomes

$$\delta_m = -\frac{\lambda H^2}{16\pi^2}\left(2\ln\left(\frac{\Lambda}{\mu}\right) + \frac{\Lambda^2}{H^2}\right) \tag{4.41}$$

and it is time-independent for constant $H$.
Hence the complete amplitude is UV finite and reads

$$A_{amp} + a_{amp} = -\frac{\mathrm{i}\lambda}{16\pi^2 H^2\tau_1^4}\left(\frac{1}{\epsilon} + 2\ln\left(\frac{\mu}{H}\right)\right) \tag{4.42}$$

where the $\frac{1}{\epsilon}$ term is due to the IR-divergence of the diagram.
Now we attach the external legs using the regime where $k\tau \ll 1$ with the propagators Eq. (4.32) and Eq. (4.33). This gives

$$\begin{aligned}
(A) &= -\int_{\tau_{in}}^{\tau} d\tau_1 G^R(k,\tau,\tau_1)F(k,\tau_1,\tau)\frac{-i\lambda}{16\pi^2H^2\tau_1^4}\left(\frac{1}{\epsilon} + 2\ln\left(\frac{\mu}{H}\right)\right) \\
&= -\frac{\lambda H^2}{8\pi^2 12k^3}\int_{\tau_{in}}^{\tau}\mathrm{d}\tau_1\frac{\tau^3-\tau_1^3}{\tau_1^4}\left(\frac{1}{\epsilon} + 2\ln\left(\frac{\mu}{H}\right)\right) \\
&= \frac{\lambda H^2}{8\pi^2 12k^3}\left[\left(\frac{1}{\epsilon} + 2\ln\left(\frac{\mu}{H}\right)\right)\left(\ln\left(\frac{\tau}{\tau_{in}}\right) + \frac{1}{3} - \frac{\tau^3}{3\tau_{in}^3}\right)\right].
\end{aligned} \tag{4.43}$$

This is the total contribution to the correlation function at one-loop level. We see that the correction is time-dependent and contains an IR-divergent part. Our results agree with [66, 67]. Using the equality $\tau = -\frac{1}{aH}$, one obtains for the time-dependent factor:

$$\ln\left(\frac{\tau}{\tau_{in}}\right) + \frac{1}{3} - \frac{\tau^3}{3\tau_{in}^3} = \ln\left(\frac{a_{in}}{a}\right) + \frac{1}{3} - \frac{a_{in}^3}{3a^3} \sim \ N_{in} - N. \tag{4.44}$$

This is the only contribution to the two-point function at one loop. In [6], $\phi^3$ theory was discussed. The two point function there has contributions coming from three one loop diagrams and one counterterm. For large internal momenta they find contributions proportional to $\lambda^2\ln^3(\tau/\tau_{in})$, for small internal momenta they find contributions proportional to $\lambda^2\ln^3(\tau/\tau_{in})$ and $\lambda^2\ln^2(\tau/\tau_{in})/\epsilon$. The UV-divergences cancel. In the Minkowski case, both theories are UV-finite and logarithmic diverent in the infrared.

### 4.3.2. 4-point function

There are four more one-loop diagrams with four external legs and two more counterterms to calculate for $\delta_\lambda$. All other diagrams of this kind are either not allowed due to the two given vertices or vanish having two $G^R/G^A$-propagators on the inside. For the detailed calculation see Appendix B. The diagrams of interest are shown below.

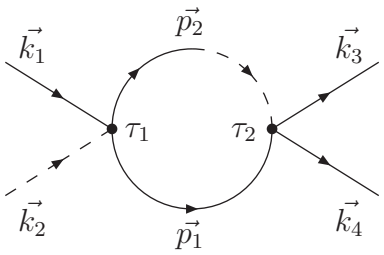


$(BN^{(1)})$


$(bn^{(1)})$

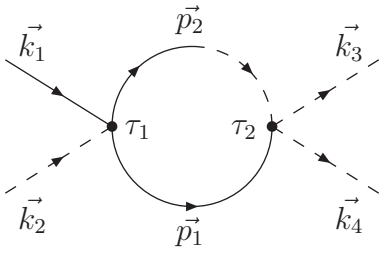


$(BN^{(2)})$


$(bn^{(2)})$

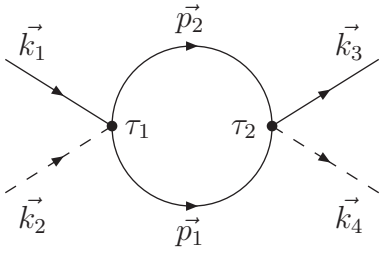


$(BN^{(3)})$

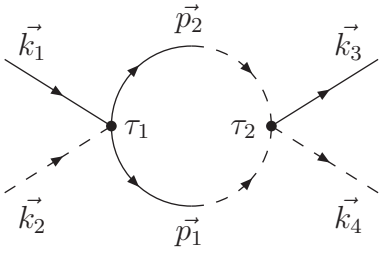


$(BN^{(4)})$

The amputated expressions for them are

$$
\begin{aligned}
(BN^{(1)}_{amp}) = (3!)^2(-i)^3 \left(\frac{\lambda}{3!}\right)^2 a^4(\tau_1)a^4(\tau_2)\,\delta(\vec{k_1}+\vec{k_2}-\vec{k_3}-\vec{k_4}) \\
\times \int \frac{d^3p_1}{(2\pi)^3}\int \frac{d^3p_2}{(2\pi)^3}\,F(p_1,\tau_1,\tau_2)G^R(p_2,\tau_1,\tau_2)\,\delta(\vec{k_1}+\vec{k_2}-\vec{p_1}-\vec{p_2})
\end{aligned}
\tag{4.45}
$$

$$
\begin{aligned}
(BN^{(2)}_{amp}) = (3!)^2(-i)^3\frac{\lambda^2}{3!4!}a^4(\tau_1)a^4(\tau_2)\,\delta(\vec{k_1}+\vec{k_2}-\vec{k_3}-\vec{k_4}) \\
\times\int\frac{d^3p_1}{(2\pi)^3}\int\frac{d^3p_2}{(2\pi)^3}\,F(p_1,\tau_1,\tau_2)G^R(p_2,\tau_1,\tau_2)\,\delta(\vec{k_1}+\vec{k_2}-\vec{p_1}-\vec{p_2})
\end{aligned}
\tag{4.46}
$$

$$
\begin{aligned}
(BN^{(3)}_{amp}) = 2\cdot 3!(-i)^3\frac{\lambda^2}{3!4!}a^4(\tau_1)a^4(\tau_2)\,\delta(\vec{k_1}+\vec{k_2}-\vec{k_3}-\vec{k_4}) \\
\times\int\frac{d^3p_1}{(2\pi)^3}\int\frac{d^3p_2}{(2\pi)^3}\,F(p_1,\tau_1,\tau_2)F(p_2,\tau_1,\tau_2)\,\delta(\vec{k_1}+\vec{k_2}-\vec{p_1}-\vec{p_2})
\end{aligned}
\tag{4.47}
$$

$$
\begin{aligned}
(BN^{(4)}_{amp}) = 2\cdot 3!(-i)^3\frac{\lambda^2}{3!4!}a^4(\tau_1)a^4(\tau_2)\,\delta(\vec{k_1}+\vec{k_2}-\vec{k_3}-\vec{k_4}) \\
\times\int\frac{d^3p_1}{(2\pi)^3}\int\frac{d^3p_2}{(2\pi)^3}\,G^R(p_1,\tau_1,\tau_2)G^R(p_2,\tau_1,\tau_2)\,\delta(\vec{k_1}+\vec{k_2}-\vec{p_1}-\vec{p_2})
\end{aligned}
\tag{4.48}
$$

For the counterterm diagrams the amputated contributions are:

$$
(bn^{(1)}_{amp}) = -\,3\cdot 2i\,\frac{\delta_\lambda}{3!}\,a^4(\tau_1)\,\delta(\vec{k_1}+\vec{k_2}-\vec{k_3}-\vec{k_4}) \tag{4.49}
$$

$$
(bn^{(2)}_{amp}) = -\,3\cdot 2i\,\frac{\delta_\lambda}{4!}\,a^4(\tau_1)\,\delta(\vec{k_1}+\vec{k_2}-\vec{k_3}-\vec{k_4}) \tag{4.50}
$$

Now if we compare the expressions $(BN^{(1)}_{amp})+(bn^{(1)}_{amp})$ and $(BN^{(2)}_{amp})+(bn^{(2)}_{amp})$ to the ones given in Appendix B we immediately see, that

$$
\delta_\lambda = \frac{3\lambda^2}{16\pi^2}\ln\frac{\Lambda}{\mu}. \tag{4.51}
$$

The 3 in the nominator results from the three different channels (s,t,u) that we have to consider.

## 4.4. Two-Loop Contributions

Now we move on to two-loop. Here, it is a lot more complicated and we split the diagrams into two groups for the calculation. First, we have the sunset diagrams in Section 4.4.1 followed by double-bubble diagrams and the counterterms in Section 4.4.2.

### 4.4.1. Sunset-diagrams

Let us start with the sunset diagrams, which are the more involved. They differ in the number of internal retarded propagators and we therefore expect them to have different IR divergencies. There are three different kinds of divergences that might appear: pure IR- or UV-divergences, but also mixed IR $\times$ UV ones. $\vec{k}$ is always small, for the three internal momenta we can have the three different cases

- all three internal momenta are small, thus we can only have IR-divergences,
- all three internal momenta are large, thus we can only have UV-divergences,
- one momenta is small, two are large, this would allow IR $\times$ UV-divergences.

The four sunset diagrams are:

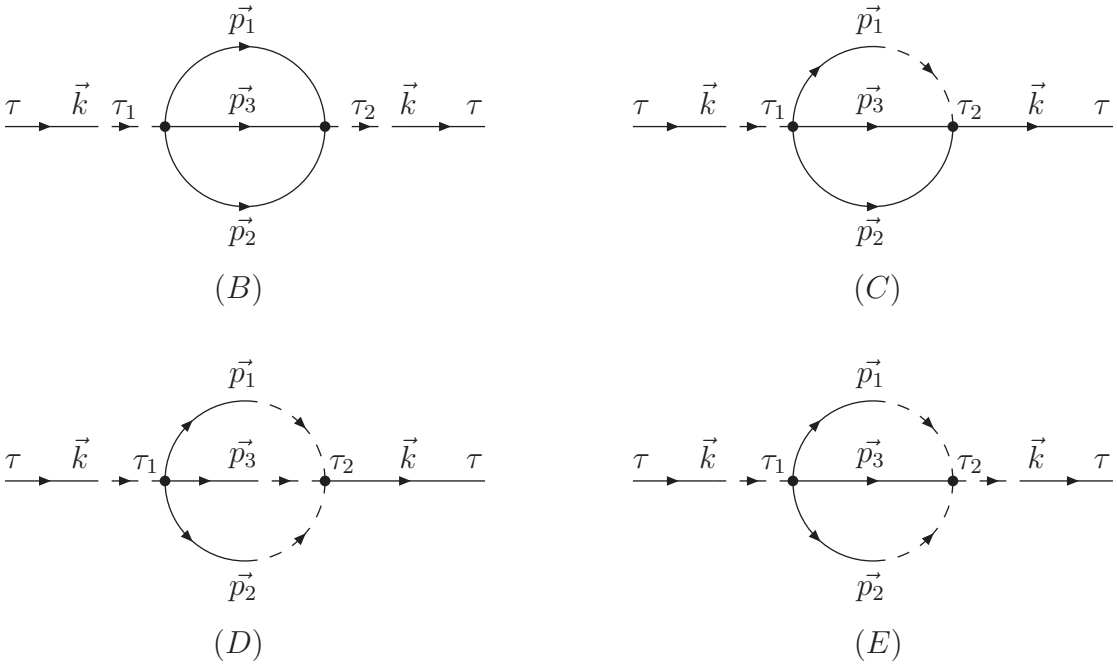


and using the Feynman rules we get the following expressions for them:

$$
\begin{aligned}
(B) = &(-i)^4 \frac{\lambda^2}{3} \int_{\tau_{in}}^{\tau} d\tau_1 \int_{\tau_{in}}^{\tau} d\tau_2 \int \frac{\mathrm{d}^3 p_1}{(2\pi)^3} \int \frac{\mathrm{d}^3 p_2}{(2\pi)^3} \int \frac{\mathrm{d}^3 p_3}{(2\pi)^3}\, \delta(\vec{k} - \vec{p_1} - \vec{p_2} - \vec{p_3}) \\
&\times a^4(\tau_1) a^4(\tau_2) G^R(k, \tau, \tau_1) G^R(k, \tau, \tau_2) F(p_1, \tau_1, \tau_2) F(p_3, \tau_1, \tau_2) F(p_2, \tau_1, \tau_2) \quad (4.52) \\
= &(-i)^2 \int_{\tau_{in}}^{\tau} d\tau_1 \int_{\tau_{in}}^{\tau} d\tau_2\, G^R(k, \tau, \tau_1) G^R(k, \tau, \tau_2) B_{amp}
\end{aligned}
$$

$$
\begin{aligned}
(C) =& (-i)^4\lambda^2 \int\limits_{\tau_{in}}^{\tau} d\tau_1 \int\limits_{\tau_{in}}^{\tau} d\tau_2 \int \frac{\mathrm{d}^3p_1}{(2\pi)^3}\int \frac{\mathrm{d}^3p_2}{(2\pi)^3}\int \frac{\mathrm{d}^3p_3}{(2\pi)^3}\delta(\vec{k}-\vec{p_1}-\vec{p_2}-\vec{p_3}) \\
&\times a^4(\tau_1)a^4(\tau_2)G^R(k,\tau,\tau_1)F(k,\tau_2,\tau)G^R(p_1,\tau_1,\tau_2)F(p_3,\tau_1,\tau_2)F(p_2,\tau_1,\tau_2) \\
=& -i\int\limits_{\tau_{in}}^{\tau} d\tau_1 \int\limits_{\tau_{in}}^{\tau} d\tau_2\, G^R(k,\tau,\tau_1)F(k,\tau_2,\tau)C_{amp}
\end{aligned}
\tag{4.53}
$$

$$
\begin{aligned}
(D) =& (-i)^6 2\frac{\lambda^2}{4!} \int\limits_{\tau_{in}}^{\tau} d\tau_1 \int\limits_{\tau_{in}}^{\tau} d\tau_2 \int \frac{\mathrm{d}^3p_1}{(2\pi)^3}\int \frac{\mathrm{d}^3p_2}{(2\pi)^3}\int \frac{\mathrm{d}^3p_3}{(2\pi)^3}\delta(\vec{k}-\vec{p_1}-\vec{p_2}-\vec{p_3}) \\
&\times a^4(\tau_1)a^4(\tau_2)G^R(k,\tau,\tau_1)F(k,\tau_2,\tau)G^R(p_1,\tau_1,\tau_2)G^R(p_3,\tau_1,\tau_2)G^R(p_2,\tau_1,\tau_2) \\
=& -i\int\limits_{\tau_{in}}^{\tau} d\tau_1 \int\limits_{\tau_{in}}^{\tau} d\tau_2\, G^R(k,\tau,\tau_1)F(k,\tau_2,\tau)D_{amp}
\end{aligned}
\tag{4.54}
$$

$$
\begin{aligned}
(E) =& (-i)^6 \frac{\lambda^2}{4} \int\limits_{\tau_{in}}^{\tau} d\tau_1 \int\limits_{\tau_{in}}^{\tau} d\tau_2 \int \frac{\mathrm{d}^3p_1}{(2\pi)^3}\int \frac{\mathrm{d}^3p_2}{(2\pi)^3}\int \frac{\mathrm{d}^3p_3}{(2\pi)^3}\delta(\vec{k}-\vec{p_1}-\vec{p_2}-\vec{p_3}) \\
&\times a^4(\tau_1)a^4(\tau_2)G^R(k,\tau,\tau_1)G^R(k,\tau,\tau_2)G^R(p_1,\tau_1,\tau_2)F(p_3,\tau_1,\tau_2)G^R(p_2,\tau_1,\tau_2) \\
=& (-i)^2\int\limits_{\tau_{in}}^{\tau} d\tau_1 \int\limits_{\tau_{in}}^{\tau} d\tau_2\, G^R(k,\tau,\tau_1)G^R(k,\tau,\tau_2)E_{amp}
\end{aligned}
\tag{4.55}
$$

We start our analysis with the pure IR-divergences.

### IR-divergences

The computation of the $(C)$, $(D)$ and $(E)$ diagrams is straightforward and can be performed splitting the integrals with an intermediate cut-off as discribed for the one-loop

case. We begin with diagram $(B)$ which needs some special treatment.

$$\begin{aligned}(B)^{small}_{amp} &= (-i)^2\,\frac{\lambda^2}{3}\frac{1}{H^8\tau_1^4\tau_2^4}\int\frac{\mathrm{d}^3p_1}{(2\pi)^3}\int\frac{\mathrm{d}^3p_2}{(2\pi)^3}\int\frac{\mathrm{d}^3p_3}{(2\pi)^3}\,\delta(\vec{k}-\vec{p_1}-\vec{p_2}-\vec{p_3})\\ &\qquad\qquad\times\frac{H^6}{8}(\tau_1\tau_2)^{3\epsilon}\,p_1^{2\epsilon-3}\,p_2^{2\epsilon-3}\,p_3^{2\epsilon-3}\\ &= (-i)^2\frac{\lambda^2}{3}\frac{(\tau_1\tau_2)^{3\epsilon}}{8H^2\tau_1^4\tau_2^4}\int\frac{\mathrm{d}^3p_1}{(2\pi)^3}\,p_1^{2\epsilon-3}\int\frac{\mathrm{d}^3p_2}{(2\pi)^3}\,p_2^{2\epsilon-3}\int\frac{\mathrm{d}^3p_3}{(2\pi)^3}\,p_3^{2\epsilon-3}\int\mathrm{d}^3x e^{i(\vec{p_1}+\vec{p_2}+\vec{p_3})\vec{x}-i\vec{k}\vec{x}}\\ &= -\,(-i)^2\frac{\lambda^2}{48\pi^5}\frac{k^{6\epsilon-3}}{H^2\tau_1^{4-3\epsilon}\tau_2^{4-3\epsilon}}\Gamma^3(2\epsilon-1)\sin(3\pi\epsilon)\cos^3(\pi\epsilon)\end{aligned} \tag{4.56}$$

where we have replaced the $\delta$-function by its integral representation and then used the results of computation in Appendix A. Now we can attach the external legs and perform the time integration

$$(B)^{small} = \frac{\lambda^2}{48\pi^5}\frac{H^2}{9}k^{6\epsilon-3}\Gamma^3(2\epsilon-1)\sin(3\pi\epsilon)\cos^3(\pi\epsilon)\left[\frac{\tau^{3\epsilon}}{4\epsilon-3}-\frac{\tau^{3-\epsilon}\tau_{in}^{4\epsilon-3}}{4\epsilon-3}-\frac{\tau^{3\epsilon}}{2\epsilon}+\frac{\tau^{\epsilon}\tau_{in}^{2\epsilon}}{2\epsilon}\right]^2. \tag{4.57}$$

After expansion we obtain

$$\begin{aligned}(B)^{small} = \frac{\lambda^2H^2}{27k^3}\frac{1}{16\pi^4}\Bigg\{&-\frac{3}{8\epsilon^2}X_1^2-\frac{1}{4\epsilon}X_1\left[9\ln^2\left(\frac{\tau}{\tau_{in}}\right)\right.\\ &\left.+X_1\left(13-9\gamma+9\ln(k\tau_{in})-3\ln\left(\frac{\tau}{\tau_{in}}\right)\right)\right]\\ &+\frac{11}{8}\pi\ln^4\left(\frac{\tau}{\tau_{in}}\right)-2X_1^2+2X_1^2\ln\left(\frac{\tau}{\tau_{in}}\right)-\frac{3}{4}X_1^2\ln\left(\frac{\tau}{\tau_{in}}\right)\\ &-X_1\ln\left(\frac{\tau}{\tau_{in}}\right)^2\left(5-\ln\left(\frac{\tau}{\tau_{in}}\right)\right)\\ &+X_1^2\left[\frac{3}{4}\pi^2-\frac{9}{4}-\frac{27}{4}(\ln(k\tau_{in})-\gamma+1)^2\right]\\ &-\frac{3}{2}X_1(\ln(k\tau_{in})-\gamma+1)\left(4X_1-3X_1\ln\frac{\tau}{\tau_{in}}+9\ln^2\frac{\tau}{\tau_{in}}\right)+O(\epsilon)\Bigg\},\end{aligned} \tag{4.58}$$

where to make the expressions somewhat shorter we have introduced the notation

$$X_1 = \frac{1}{3}\left(1-\left(\frac{\tau}{\tau_{in}}\right)^3+3\ln\frac{\tau}{\tau_{in}}\right). \tag{4.59}$$

The amplitude of diagram (C) reads

$$(C)^{small}_{amp} = i\frac{\lambda^2}{48\pi^4}\frac{\theta(\tau_1-\tau_2)}{H^2\tau_1^{4-2\epsilon}\tau_2^{4-2\epsilon}}\frac{M_{cm}^{4\epsilon}}{4\epsilon^2}\left[\tau_1^3\left(\frac{\tau_2}{\tau_1}\right)^{\epsilon}-\left(\frac{\tau_1}{\tau_2}\right)^{\epsilon}\tau_2^3\right]. \tag{4.60}$$

Now attaching the external legs we get

$$(C)^{small} = \frac{\lambda^2}{(2\pi)^4}\frac{H^2}{72k^3}\frac{k^{2\epsilon}M_{cm}^{4\epsilon}}{24\epsilon^2(1-2\epsilon)(3-4\epsilon)}\left[(3-2\epsilon)^2\tau^{6\epsilon} - 4\epsilon(3-2\epsilon)\frac{\tau^3}{\tau_{in}^3}\tau_{in}^{6\epsilon}\right.$$
$$\left. -6(3-8\epsilon+4\epsilon^2)\tau^{4\epsilon}\tau_{in}^{2\epsilon} + (3-8\epsilon+4\epsilon^2)\left(4\epsilon\frac{\tau^3}{\tau_{in}^3} - 4\epsilon + 3\right)\tau^{2\epsilon}\tau_{in}^{4\epsilon}\right]. \tag{4.61}$$

After expansion we obtain

$$(C)^{small} = \frac{\lambda^2H^2}{(2\pi)^4 72k^3}\left\{\frac{1}{6\epsilon^2}X_2 + \frac{1}{3\epsilon}\left[\left(\ln k\tau_{in} + 2\ln M_{cm}\tau_{in} + \frac{4}{3} + \ln\frac{\tau}{\tau_{in}}\right)X_2 + X_1\ln^2\frac{\tau}{\tau_{in}}\right]\right.$$
$$+2\left(\frac{4X_2}{9} + \frac{X_2}{3}\ln\frac{\tau}{\tau_{in}} + X_1\ln^2\frac{\tau}{\tau_{in}}\right)(\ln(k\tau_{in}) + 2\ln(M_{cm}\tau_{in}))$$
$$+\frac{X_2}{3}(\ln(k\tau_{in}) + 2\ln(M_{cm}\tau_{in}))^2 + \frac{2}{9}\left(\frac{\tau}{\tau_{in}}\right)^3\ln\frac{\tau}{\tau_{in}}\left(2 - 4\ln\frac{\tau}{\tau_{in}} + \ln^2\frac{\tau}{\tau_{in}}\right)$$
$$+\frac{25}{6}\ln^4\frac{\tau}{\tau_{in}} + \frac{4}{9}\ln\frac{\tau}{\tau_{in}}\left(\ln^2\frac{\tau}{\tau_{in}} - \ln\frac{\tau}{\tau_{in}} - 1\right) + \frac{10}{3}X_1\ln^2\frac{\tau}{\tau_{in}}$$
$$\left.+\frac{10}{9}X_2\ln\frac{\tau}{\tau_{in}} + \frac{28}{27}X_2 + O(\epsilon)\right\}, \tag{4.62}$$

where we again introduced a new notation

$$X_2 = -2\left(\frac{\tau}{\tau_{in}}\right)^3 + 2\left(\frac{\tau}{\tau_{in}}\right)^3\ln\left(\frac{\tau}{\tau_{in}}\right) + 2 + 4\ln\left(\frac{\tau}{\tau_{in}}\right) + 3\ln^2\left(\frac{\tau}{\tau_{in}}\right). \tag{4.63}$$

The amplitude of diagram (D) is

$$(D)_{amp}^{small} = -i\frac{\lambda^2}{(2\pi)^4}\frac{M_{cm}^6\theta(\tau_1-\tau_2)}{27\cdot 27H^2\tau_1^4\tau_2^4}\left[\tau_1^3\left(\frac{\tau_2}{\tau_1}\right)^\epsilon - \left(\frac{\tau_1}{\tau_2}\right)^\epsilon\tau_2^3\right]^3. \tag{4.64}$$

After time integration and expansion in powers of $\epsilon$ we get the following expression:

$$(D)^{small} = -\frac{\lambda^2}{(2\pi)^4}\frac{H^2(M_{cm}\tau_{in})^6}{27^2\cdot 18k^3}\left[\frac{1}{54}\left(\frac{\tau}{\tau_{in}}\right)^9 + \frac{1}{3}\left(\frac{\tau}{\tau_{in}}\right)^6 - \frac{1}{6}\left(\frac{\tau}{\tau_{in}}\right)^3 - \frac{5}{27}\right.$$
$$\left. -\frac{1}{6}\ln\frac{\tau}{\tau_{in}}\left(3\left(\frac{\tau}{\tau_{in}}\right)^6 + 6\left(\frac{\tau}{\tau_{in}}\right)^3 + 1\right)\right], \tag{4.65}$$

which is not divergent and depends on the upper limit of the integration.
The amplitude of the diagram (E) is then

$$(E)_{amp}^{small} = \frac{\lambda^2}{(2\pi)^4}\frac{\theta(\tau_1-\tau_2)M_{cm}^3}{54H^2}\frac{M_{cm}^{2\epsilon}}{2\epsilon\tau_1^{4-\epsilon}\tau_2^{4-\epsilon}}\left[\tau_1^3\left(\frac{\tau_2}{\tau_1}\right)^\epsilon - \left(\frac{\tau_1}{\tau_2}\right)^\epsilon\tau_2^3\right]^2. \tag{4.66}$$

After attaching the external legs we get

$$\begin{aligned}(E)^{small} = &-\frac{\lambda^2}{(2\pi)^4}\frac{H^2 M_{cm}^3}{54\cdot 9}\frac{M_{cm}^{2\epsilon}}{2\epsilon}\left[\left(\frac{\tau^{6-\epsilon}}{3}-\frac{\tau^{3-\epsilon}\tau_{in}^3}{3}-\frac{\tau^{6-\epsilon}}{6-2\epsilon}+\frac{\tau^{\epsilon}\tau_{in}^{6-2\epsilon}}{6-2\epsilon}\right)\right.\\ &\times\left(\frac{\tau^{3\epsilon}}{4\epsilon-3}-\frac{\tau^{3-\epsilon}\tau_{in}^{4\epsilon-3}}{4\epsilon-3}-\frac{\tau^{3\epsilon}}{2\epsilon}+\frac{\tau^{\epsilon}\tau_{in}^{2\epsilon}}{2\epsilon}\right)\\ &\left.-\left(\frac{\tau^{3+\epsilon}}{2\epsilon}-\frac{\tau^{3-\epsilon}\tau_{in}^{2\epsilon}}{2\epsilon}-\frac{\tau^{3+\epsilon}}{3}+\frac{\tau^{\epsilon}\tau_{in}^3}{3}\right)^2\right].\end{aligned} \tag{4.67}$$

Expansion in powers of $\epsilon$ gives

$$\begin{aligned}(E)^{small} = &-\frac{\lambda^2}{(2\pi)^4}\frac{H^2(M_{cm}\tau_{in})^3\tau_{in}^3}{54\cdot 18}\left\{-\frac{1}{\epsilon}\left[\frac{1}{2}X_1^2\left(3-\left(\frac{\tau}{\tau_{in}}\right)^3\right)\right.\right.\\ &\left.-\ln\frac{\tau}{\tau_{in}}\left(1-\left(\frac{\tau}{\tau_{in}}\right)^3\right)\left(\frac{X_1}{2}-\ln\frac{\tau}{\tau_{in}}+\ln\frac{\tau}{\tau_{in}}\left(\frac{\tau}{\tau_{in}}\right)^3\right)\right]\\ &-\frac{X_1}{3}\ln\frac{\tau}{\tau_{in}}-\frac{X_1}{18}\left[1-\left(\frac{\tau}{\tau_{in}}\right)^3\right]\left[11+3\left(\frac{\tau}{\tau_{in}}\right)^3\right]\\ &\left.+\frac{1}{6}\left[1-\left(\frac{\tau}{\tau_{in}}\right)^3\right]^2\ln^2\frac{\tau}{\tau_{in}}+O(\epsilon)\right\}.\end{aligned} \tag{4.68}$$

Now we sum up the $\epsilon$ terms. For $\frac{1}{\epsilon^2}$ we have the following contributions

$$\begin{aligned}(B) &= \frac{\lambda^2 H^2}{27k^3}\frac{1}{16\pi^4}(-\frac{3}{8\epsilon^2})X_1^2,\\ (C) &= \frac{\lambda^2 H^2}{(2\pi)^4 72k^3}\frac{1}{6\epsilon^2}X_2,\end{aligned} \tag{4.69}$$

summing up to

$$\begin{aligned}(B)+(C) &= \frac{\lambda^2 H^2}{(2\pi)^4 k^3 2^4 3^3\,\epsilon^2}\left(X_2-6X_1^2\right)\\ &= \frac{\lambda^2 H^2}{(2\pi)^4 k^3 2^4 3^3}\left(6\frac{\tau^3}{\tau_{in}^3}\ln\left(\frac{\tau}{\tau_{in}}\right)-\frac{2}{3}\left(\frac{\tau^6}{{\tau_{in}}^6}+\frac{\tau^3}{{\tau_{in}}^3}-2\right)-3\ln^2\left(\frac{\tau}{\tau_{in}}\right)\right).\end{aligned} \tag{4.70}$$

For $\frac{1}{\epsilon}$ we have the following contributions

$$
\begin{aligned}
(B) &= \frac{\lambda^2 H^2}{27k^3}\frac{1}{16\pi^4}\left(-\frac{1}{4\epsilon}X_1\left[9\ln^2\left(\frac{\tau}{\tau_{in}}\right)+X_1\left(13-9\gamma+9\ln(k\tau_{in})-3\ln\left(\frac{\tau}{\tau_{in}}\right)\right)\right]\right),\\
(C) &= \frac{\lambda^2 H^2}{(2\pi)^4 72k^3}\frac{1}{3\epsilon}\left[\left(\ln k\tau_{in}+2\ln M_{cm}\tau_{in}+\frac{4}{3}+\ln\frac{\tau}{\tau_{in}}\right)X_2+X_1\ln^2\frac{\tau}{\tau_{in}}\right],\\
(E) &= -\frac{\lambda^2}{(2\pi)^4}\frac{H^2(M\tau_{in})^3\tau_{in}^3}{54\cdot 18}\left(-\frac{1}{\epsilon}\left[\frac{1}{2}X_1^2\left(3-\left(\frac{\tau}{\tau_{in}}\right)^3\right)-\ln\frac{\tau}{\tau_{in}}\left(1-\left(\frac{\tau}{\tau_{in}}\right)^3\right)\right.\right.\\
&\quad\left.\left.\times\left(\frac{X_1}{2}-\ln\frac{\tau}{\tau_{in}}+\ln\frac{\tau}{\tau_{in}}\left(\frac{\tau}{\tau_{in}}\right)^3\right)\right]\right),
\end{aligned}
\tag{4.71}
$$

sorting them by powers of $\ln^n$, summing up to

$$
\begin{aligned}
(B)+(C)+(E) &= \frac{\lambda^2 H^2}{(2\pi)^4\cdot 2^2\cdot 3^3\,\epsilon}\left[-\frac{4}{k^3}\ln^3\left(\frac{\tau}{\tau_{in}}\right)+\ln^2\left(\frac{\tau}{\tau_{in}}\right)\left(\frac{3\ln(M_{cm}\tau)}{k^3}-\frac{15\ln(k\tau)}{2k^3}+\frac{11}{6k^3}\right.\right.\\
&\left(\frac{\tau}{\tau_{in}}\right)^3+\frac{9\gamma}{k^3}-\frac{59}{6k^3}-\frac{1}{9}M_{cm}^3\tau^6\left(\left(\frac{\tau}{\tau_{in}}\right)^6+2\left(\frac{\tau}{\tau_{in}}\right)^3-2\right)\Bigg)\\
&+\ln\left(\frac{\tau}{\tau_{in}}\right)\left(\frac{2\left(\frac{\tau}{\tau_{in}}\right)^3\ln(M_{cm}\tau)}{k^3}+\frac{4\ln(M_{cm}\tau)}{k^3}+\frac{7\left(\frac{\tau}{\tau_{in}}\right)^3\ln(k\tau)}{k^3}-\frac{4\ln(k\tau)}{k^3}+\frac{\left(\frac{\tau}{\tau_{in}}\right)^6}{3k^3}\right.\\
&-\frac{6\left(\frac{\tau}{\tau_{in}}\right)^3\gamma}{k^3}+\frac{25\left(\frac{\tau}{\tau_{in}}\right)^3}{3k^3}+\frac{6\gamma}{k^3}-\frac{14}{3k^3}-\frac{1}{54}\left(\left(\frac{\tau}{\tau_{in}}\right)^3-5\right)\left(\left(\frac{\tau}{\tau_{in}}\right)^3-1\right)\Bigg)\\
&-\frac{2\left(\frac{\tau}{\tau_{in}}\right)^3\ln(M_{cm}\tau)}{k^3}+\frac{2\ln(M_{cm}\tau)}{k^3}-\frac{\left(\frac{\tau}{\tau_{in}}\right)^6\ln(k\tau)}{k^3}+\frac{\left(\frac{\tau}{\tau_{in}}\right)^3\ln(k\tau)}{k^3}+\frac{\left(\frac{\tau}{\tau_{in}}\right)^6\gamma}{k^3}\\
&-\frac{13\left(\frac{\tau}{\tau_{in}}\right)^6}{9k^3}-\frac{2\left(\frac{\tau}{\tau_{in}}\right)^3\gamma}{k^3}+\frac{14\left(\frac{\tau}{\tau_{in}}\right)^3}{9k^3}+\frac{\gamma}{k^3}-\frac{1}{9k^3}+\frac{1}{162}M_{cm}^3\tau^6\left(\frac{\tau}{\tau_{in}}\right)^9\\
&\left.-\frac{5}{162}M_{cm}^3\tau^6\left(\frac{\tau}{\tau_{in}}\right)^6+\frac{7}{162}M_{cm}^3\tau^6\left(\frac{\tau}{\tau_{in}}\right)^3-\frac{M_{cm}^3\tau^6}{54}\right].
\end{aligned}
\tag{4.72}
$$

Diagram (D) has no IR-divergences. In $\lambda^2$ and $\mathcal{O}(\epsilon^2)$ we have contibutions proportional to $\ln^2\left(\frac{\tau}{\tau_{in}}\right)$ and $\ln\left(\frac{\tau}{\tau_{in}}\right)$, for $\mathcal{O}(\epsilon)$ we even have contributions proportional to $\ln^3\left(\frac{\tau}{\tau_{in}}\right)$. This concludes the computations of the sunset diagrams for small internal momenta.

### IR×UV-divergences

To calculate the mixed IR×UV-divergences, we consider the diagrams (B)+(E) as a unit. Here the contribution consists of two pieces

$$\begin{aligned}
&-3\frac{\lambda^2}{3}\int\limits_l \frac{d^3p_1}{(2\pi)^3}\int\limits_l \frac{d^3p_2}{(2\pi)^3}\int\limits_s \frac{d^3p_3}{(2\pi)^3}\, F(p_1,\tau_1,\tau_2)\, F(p_2,\tau_1,\tau_2)\, F(p_3,\tau_1,\tau_2)\\
&\qquad\qquad \times \delta^3(\vec{k}-\vec{p_1}-\vec{p_2}-\vec{p_3})\\
&+\frac{\lambda^2}{4}\int \frac{d^3p_1}{(2\pi)^3}\int \frac{d^3p_2}{(2\pi)^3}\int\limits_s \frac{d^3p_3}{(2\pi)^3}\, G^R(p_1,\tau_1,\tau_2)\, G^R(p_2,\tau_1,\tau_2)\, F(p_3,\tau_1,\tau_2)\\
&\qquad\qquad \times \delta^3(\vec{k}-\vec{p_1}-\vec{p_2}-\vec{p_3}).
\end{aligned} \tag{4.73}$$

As $\vec{p_3}$ momenta is $\epsilon$-small we redefine it in $\vec{k}$, so that we can write

$$\begin{aligned}
\int\limits_s \frac{d^3p_3}{(2\pi)^3}\, F(p_3,\tau_1,\tau_2) \Bigg[ &-\lambda^2 \int\limits_l \frac{d^3p_1}{(2\pi)^3}\int\limits_l \frac{d^3p_2}{(2\pi)^3}\, F(p_1,\tau_1,\tau_2)\, F(p_2,\tau_1,\tau_2)\, \delta(\vec{k}-\vec{p_1}-\vec{p_2})\\
&+\frac{\lambda^2}{4}\int \frac{d^3p_1}{(2\pi)^3}\int \frac{d^3p_2}{(2\pi)^3}\, G^R(p_1,\tau_1,\tau_2)\, G^R(p_2,\tau_1,\tau_2)\, \delta(\vec{k}-\vec{p_1}-\vec{p_2})\Bigg].
\end{aligned} \tag{4.74}$$

The expression in bracket was computed in [6]. We repeat the results in Appendix B. For us it is most important that the expression in brackets is UV-finite. The integration of the $p_3$ integrals will give us the finite terms and terms of $\frac{1}{2\epsilon}$ subleading in IR.
For the diagrams (C) and (D), it works in a similar way, but this time, we put the $G^R$-propagator in front of the bracket:

$$\begin{aligned}
\int\limits_s \frac{d^3p_3}{(2\pi)^3}\, G^R(p_3,\tau_1,\tau_2) \Bigg[ &-\lambda^2 \int\limits_l \frac{d^3p_1}{(2\pi)^3}\int\limits_l \frac{d^3p_2}{(2\pi)^3}\, F(p_1,\tau_1,\tau_2)\, F(p_2,\tau_1,\tau_2)\, \delta(\vec{k}-\vec{p_1}-\vec{p_2})\\
&+\frac{\lambda^2}{4}\int \frac{d^3p_1}{(2\pi)^3}\int \frac{d^3p_2}{(2\pi)^3}\, G^R(p_1,\tau_1,\tau_2)\, G^R(p_2,\tau_1,\tau_2)\, \delta(\vec{k}-\vec{p_1}-\vec{p_2})\Bigg].
\end{aligned} \tag{4.75}$$

Summarising, we do not have mixed IR×UV-divergences.

### UV-divergences

Again, we evaluate the diagrams (B) and (E) together. Now let us prove that the sum of these diagrams is not UV-divergent. For this we have to consider the last two

contributions

$$\begin{aligned}
&-\frac{\lambda^2}{3}\int_l \frac{d^3p_1}{(2\pi)^3}\int_l \frac{d^3p_2}{(2\pi)^3}\int_l \frac{d^3p_3}{(2\pi)^3}\, F(p_1,\tau_1,\tau_2)\, F(p_2,\tau_1,\tau_2)\, F(p_3,\tau_1,\tau_2) \\
&\qquad\qquad \times \delta^3(\vec{k}-\vec{p_1}-\vec{p_2}-\vec{p_3}) \\
&+\frac{\lambda^2}{4}\int \frac{d^3p_1}{(2\pi)^3}\int \frac{d^3p_2}{(2\pi)^3}\int_l \frac{d^3p_3}{(2\pi)^3}\, G^R(p_1,\tau_1,\tau_2)\, G^R(p_2,\tau_1,\tau_2)\, F(p_3,\tau_1,\tau_2) \\
&\qquad\qquad \times \delta^3(\vec{k}-\vec{p_1}-\vec{p_2}-\vec{p_3}).
\end{aligned} \tag{4.76}$$

Here the momentum $\vec{p_3}$ is large, therefore we can redefine $\vec{k}$ in it. So we write

$$\begin{aligned}
\int_l \frac{d^3p_3}{(2\pi)^3}\, F(p_3,\tau_1,\tau_2) \Bigg[ &-3\frac{\lambda^2}{3}\int_l \frac{d^3p_1}{(2\pi)^3}\int_l \frac{d^3p_2}{(2\pi)^3}\, F(p_1,\tau_1,\tau_2)\, F(p_2,\tau_1,\tau_2)\, \delta(-\vec{p_1}-\vec{p_2}-\vec{p_3}) \\
&+\frac{\lambda^2}{4}\int \frac{d^3p_1}{(2\pi)^3}\int \frac{d^3p_2}{(2\pi)^3}\, G^R(p_1,\tau_1,\tau_2)\, G^R(p_2,\tau_1,\tau_2)\, \delta(-\vec{p_1}-\vec{p_2}-\vec{p_3}) \Bigg].
\end{aligned} \tag{4.77}$$

where 3 in the first term stays for the possible choices of momentum for integral outside of brackets. The expression inside the brackets consists of two terms

$$\begin{aligned}
-\frac{\lambda^2}{4(2\pi)^2 p_3^3 H^4(\tau_1\tau_2)^4} &\left(-\frac{p_3}{M}+\frac{1}{2}\ln\frac{M+p_3}{M-p_3}\right) \\
&+\left[-\frac{\lambda^2 \sin p_3\Delta\tau}{8(2\pi)^2 p_3 H^4(\tau_1\tau_2)^2\Delta\tau}\frac{\sin 2p_1\Delta\tau}{\Delta\tau}\right]_M^\Lambda .
\end{aligned} \tag{4.78}$$

Both terms are UV-finite. Now we have to replace $\vec{p_3}$ by $\vec{p_3}-\vec{k}$ and integrate. After some tedious integrations one sees that the sum of diagram (B) and (E) is UV-finite. The analysis for diagram (C) and (D) is still in progress.

## 4.4.2. Bubbles and Counterterms

Let us now come to the second class of two-loop diagrams. We can calculate the following diagrams without splitting them up into small and large contributions. We can organize these diagrams into three groups.

### Two retarded external propagators

First of all let us consider the one-particle reducible one-bubble diagrams, which are renormalized directly by considering the one-loop mass counterterm. We have two types of such diagrams, depending on the external legs and the internal propagator. The bubble and counterterm diagrams with two external retarded propagators are

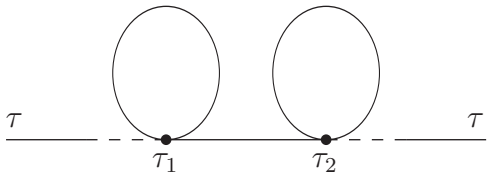


(Db1)


(b)

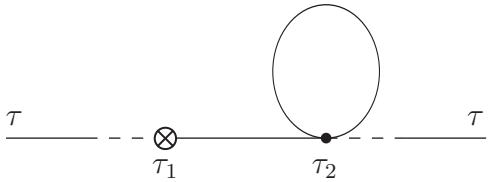


(e)

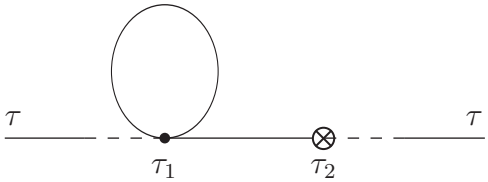


(e)

So the total amplitude is given by

$$
\begin{aligned}
&(Db1)+(b)+(e)\\
&\quad=(-i)^4\int_{\tau_{in}}^{\tau}d\tau_1\int_{\tau_{in}}^{\tau}d\tau_2\,G^R(k,\tau,\tau_1)\,G^R(k,\tau,\tau_2)\,F(k,\tau_1,\tau_2)\,a^4(\tau_1)\,a^4(\tau_2)\\
&\qquad\times\left[3\cdot 3\,\frac{\lambda^2}{3!^2}\int\frac{d^3p_1}{(2\pi)^3}\int\frac{d^3p_2}{(2\pi)^3}\,F(p_1,\tau_1,\tau_1)\,F(p_2,\tau_2,\tau_2)+\delta_m^2\right.\\
&\qquad\left.+3\,\frac{\lambda}{3!}\,\delta_m\int\frac{d^3p_2}{(2\pi)^3}\,F(p_2,\tau_2,\tau_2)+3\,\frac{\lambda}{3!}\,\delta_m\int\frac{d^3p_1}{(2\pi)^3}\,F(p_1,\tau_1,\tau_1)\right]\\
&\quad=\int_{\tau_{in}}^{\tau}d\tau_1\int_{\tau_{in}}^{\tau}d\tau_2\,a^4(\tau_1)\,a^4(\tau_2)\,G^R(k,\tau,\tau_1)\,G^R(k,\tau,\tau_2)\,F(k,\tau_1,\tau_2)\\
&\qquad\times\left[\frac{\lambda}{2}\int\frac{d^3p_1}{(2\pi)^3}\,F(p_1,\tau_1,\tau_1)+\delta_m\right]\left[\frac{\lambda}{2}\int\frac{d^3p_2}{(2\pi)^3}\,F(p_2,\tau_2,\tau_2)+\delta_m\right]\\
&\quad=\int_{\tau_{in}}^{\tau}d\tau_1\int_{\tau_{in}}^{\tau}d\tau_2\,a^4(\tau_1)\,a^4(\tau_2)\,G^R(k,\tau,\tau_1)\,G^R(k,\tau,\tau_2)\,F(k,\tau_1,\tau_2)\\
&\qquad\times\left(\frac{\lambda H^2}{16\pi^2}\right)^2\left[\frac{1}{\epsilon}+2\ln\left(\frac{\mu}{H}\right)\right]^2.
\end{aligned}
\tag{4.79}
$$

In the last step we have used the result of one-loop computation, which allows us to compute the internal integration for any internal momentum and cancel the UV-divergence with the counterterms. After adding the external propagators and integrating in time, we obtain

$$
(Db1)+(b)+(e)=\frac{\lambda^2H^2}{64\pi^4}\frac{X_1^2}{18k^3}\left[\frac{1}{2\epsilon}+\ln\left(\frac{\mu}{H}\right)\right]^2. \tag{4.80}
$$

### One retarded external propagator

Very similarly we can compute the analogous diagrams with only one external retarded propagator, given here

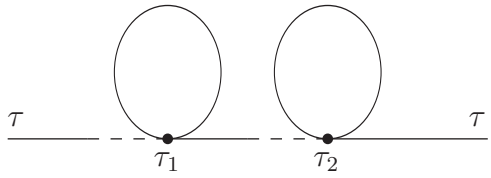


(Db2)


(a2)

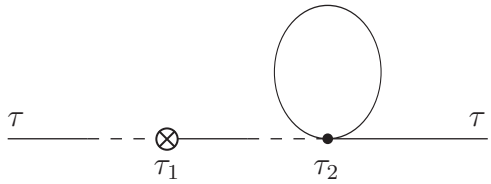


(d)

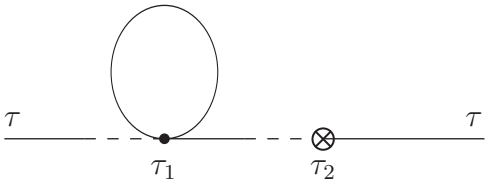


(d)

The total amplitude reads

$$
\begin{aligned}
&(Db2)+(a2)+(d)\\
&\quad=(-i)^4\int_{\tau_{in}}^{\tau}d\tau_1\int_{\tau_{in}}^{\tau}d\tau_2\,G^R(k,\tau,\tau_1)\,F(k,\tau_2,\tau)\,G^R(k,\tau_1,\tau_2)\,a^4(\tau_1)\,a^4(\tau_2)\\
&\qquad\times\left[3\cdot 3\,\frac{\lambda^2}{3!^2}\int\frac{d^3p_1}{(2\pi)^3}\int\frac{d^3p_2}{(2\pi)^3}\,F(p_1,\tau_1,\tau_1)\,F(p_2,\tau_2,\tau_2)+\delta_m^2\right.\\
&\qquad\left.+3\,\frac{\lambda}{3!}\,\delta_m\int\frac{d^3p_1}{(2\pi)^3}\,F(p_1,\tau_1,\tau_1)+3\frac{\lambda}{3!}\delta_m\int\frac{d^3p_2}{(2\pi)^3}\,F(p_2,\tau_2,\tau_2)\right]\\
&\quad=\int_{\tau_{in}}^{\tau}d\tau_1\int_{\tau_{in}}^{\tau}d\tau_2\,G^R(k,\tau,\tau_1)\,F(k,\tau_2,\tau)\,G^R(k,\tau_1,\tau_2)\,a^4(\tau_1)\,a^4(\tau_2)\\
&\qquad\times\left[\frac{\lambda}{2}\int\frac{d^3p_1}{(2\pi)^3}\,F(p_1,\tau_1,\tau_1)+\delta_m\right]\left[\frac{\lambda}{2}\int\frac{d^3p_2}{(2\pi)^3}\,F(p_2,\tau_2,\tau_2)+\delta_m\right]\\
&\quad=\int_{\tau_{in}}^{\tau}d\tau_1\int_{\tau_{in}}^{\tau}d\tau_2\,G^R(k,\tau,\tau_1)\,F(k,\tau_2,\tau)\,G^R(k,\tau_1,\tau_2)\,a^4(\tau_1)\,a^4(\tau_2)\\
&\qquad\times\left(\frac{\lambda H^2}{16\pi^2}\right)^2\left[\frac{1}{\epsilon}+2\ln\left(\frac{\mu}{H}\right)\right]^2.
\end{aligned}
\tag{4.81}
$$

After the time integrations we obtain in a similar way

$$(Db2) + (a2) + (d) = \frac{\lambda^2 H^2}{64\pi^4} \frac{X_2}{3 \cdot 36 k^3} \left[ \frac{1}{2\epsilon} + \ln\left(\frac{\mu}{H}\right) \right]^2 . \tag{4.82}$$

Note that the two diagrams display the same time-structure found in the IR-divergent sunset diagrams (B) and (C). In this case though the amplitudes are automatically finite in the UV.

### Bubble-on-bubble and one more counterterm

Finally, we have to consider the double-bubble diagram with the mass insertion in the one-loop diagram given by

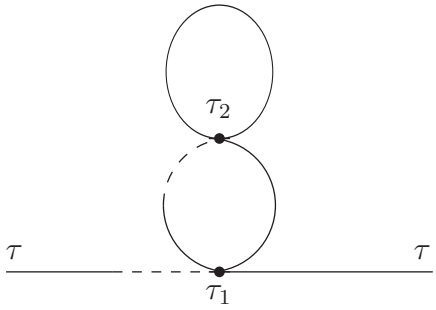


(Db3)

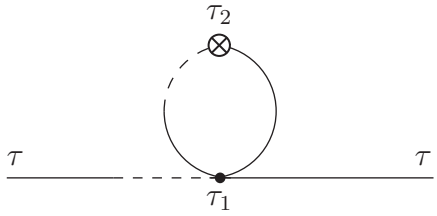


(c)

So the amplitude is

$$\begin{aligned}
(Db3) + (c) = & (-i)^4 \int_{\tau_{in}}^{\tau} d\tau_1 \int_{\tau_{in}}^{\tau} d\tau_2 \, G^R(k,\tau,\tau_1) \, F(k,\tau_2,\tau) \, a^4(\tau_1) \, a^4(\tau_2) \\
& \times 3 \cdot 2 \, \frac{\lambda}{3!} \int \frac{d^3 p_1}{(2\pi)^3} \, G^R(p_1,\tau_1,\tau_2) \, F(p_1,\tau_2,\tau_1) \\
& \times \left[ 3 \, \frac{\lambda}{3!} \int \frac{d^3 p_2}{(2\pi)^3} \, F(p_2,\tau_2,\tau_2) + \delta_m \right] \\
= & \frac{\lambda^2 H^2}{16\pi^2} \left[ \frac{1}{\epsilon} + 2 \ln\left(\frac{\mu}{H}\right) \right] \int_{\tau_{in}}^{\tau} d\tau_1 \int_{\tau_{in}}^{\tau} d\tau_2 \, G^R(k,\tau,\tau_1) \, F(k,\tau_2,\tau) \, a^4(\tau_1) \, a^4(\tau_2) \\
& \times \int \frac{d^3 p_1}{(2\pi)^3} \, G^R(p_1,\tau_1,\tau_2) \, F(p_1,\tau_2,\tau_1).
\end{aligned} \tag{4.83}$$

The first momentum integration is identical to the one-loop case and again only IR-divergent. We are then left with a second momentum integration which is more complex.

Let us consider this integral only for the start and split the internal momentum up into an IR- and an UV-part:

$$\int \frac{d^3p_1}{(2\pi)^3}\, G^R(p_1,\tau_1,\tau_2)\, F(p_1,\tau_2,\tau_1) = \frac{1}{2\pi^2}\int_0^M dp_1\, p_1^2\, G^R(p_1,\tau_1,\tau_2)\, F(p_1,\tau_2,\tau_1) + \frac{1}{2\pi^2}\int_M^\infty dp_1\, p_1^2\, G^R(p_1,\tau_1,\tau_2)\, F(p_1,\tau_2,\tau_1). \tag{4.84}$$

After integration the IR-integral becomes

$$\int_0^M dp_1\, p_1^2\, G^R(p_1,\tau_1,\tau_2)\, F(p_1,\tau_2,\tau_1) = \theta(\tau_1-\tau_2)\,\frac{H^4}{6}\left[\tau_1^3\tau_2^{2\epsilon}-\tau_1^{2\epsilon}\tau_2^3\right]\frac{M^{2\epsilon}}{2\epsilon} = \theta(\tau_1-\tau_2)\,\frac{H^4}{6}\left[\frac{\tau_1^3-\tau_2^3}{2\epsilon}+\tau_1^3\ln(M\tau_2)-\tau_2^3\ln(M\tau_1)\right]. \tag{4.85}$$

We see that this integration brings another factor of $\frac{1}{\epsilon}$ and a different time-dependence. The UV-integral is somewhat more involved. Here we insert the full expressions for the propagators

$$\int_M^\infty dp_1\, p_1^2\, G^R(p_1,\tau_1,\tau_2)\, F(p_1,\tau_2,\tau_1) = \theta(\tau_1-\tau_2)\,\frac{H^4}{2}\int_M^\Lambda dp_1\left[\frac{\sin 2p_1(\tau_1-\tau_2)}{2p_1^4}\right.$$
$$-(\tau_1-\tau_2)\,\frac{\cos 2p_1(\tau_1-\tau_2)}{p_1^3}+\left(\tau_1\tau_2-\frac{(\tau_1-\tau_2)^2}{2}\right)\frac{\sin 2p_1(\tau_1-\tau_2)}{p_1^2} \tag{4.86}$$
$$\left.-\tau_1\tau_2\,(\tau_1-\tau_2)\,\frac{\cos 2p_1(\tau_1-\tau_2)}{p_1}+\frac{\tau_1^2\tau_2^2}{2}\,\sin 2\,p_1(\tau_1-\tau_2)\right].$$

Now considering each term separately we have

$$\int_M^\Lambda dp_1\,\sin 2\,p_1\,(\tau_1-\tau_2) = \frac{\cos 2M(\tau_1-\tau_2)}{2(\tau_1-\tau_2)}-\frac{\cos 2\Lambda(\tau_1-\tau_2)}{2(\tau_1-\tau_2)}, \tag{4.87}$$

$$\int_M^\Lambda dp_1\frac{\cos 2p_1(\tau_1-\tau_2)}{p_1} = -\mathrm{Ci}(2M(\tau_1-\tau_2)), \tag{4.88}$$

$$\int_M^\Lambda dp_1\,\frac{\sin 2p_1(\tau_1-\tau_2)}{p_1^2} = -\frac{\sin 2\Lambda(\tau_1-\tau_2)}{\Lambda}+\frac{\sin 2M(\tau_1-\tau_2)}{M} +2(\tau_1-\tau_2)\,\mathrm{Ci}(2\Lambda(\tau_1-\tau_2))-2(\tau_1-\tau_2)\,\mathrm{Ci}(2M(\tau_1-\tau_2)), \tag{4.89}$$

$$\int_M^\Lambda dp_1 \frac{\cos 2p_1(\tau_1-\tau_2)}{p_1^3} = -\frac{\cos 2\Lambda(\tau_1-\tau_2)}{2\Lambda^2} + \frac{\cos 2M(\tau_1-\tau_2)}{2M^2} - (\tau_1-\tau_2)\int_M^\Lambda dp_1 \frac{\sin 2p_1(\tau_1-\tau_2)}{p_1^2}, \tag{4.90}$$

and

$$\int_M^\Lambda dp_1 \frac{\sin 2p_1(\tau_1-\tau_2)}{p_1^4} = -\frac{\sin 2\Lambda(\tau_1-\tau_2)}{3\Lambda^3} + \frac{\sin 2M(\tau_1-\tau_2)}{3M^3} + \frac{2}{3}(\tau_1-\tau_2)\int_M^\Lambda dp_1 \frac{\cos 2p_1(\tau_1-\tau_2)}{p_1^3}. \tag{4.91}$$

Analyzing these terms we can easily see that the integral is UV-finite. The only term which survives is

$$-\frac{\tau_1^2\tau_2^2}{2}\frac{\cos 2\Lambda(\tau_1-\tau_2)}{2(\tau_1-\tau_2)} \tag{4.92}$$

and it is finite. Now we collect all the $M_{cm}$-terms. Here we have two sorts of terms, those containing cosine-integrals and those who do not. The terms without cosine-integral cancel in the limit $|M_{cm}\tau_i| \ll 1$ and we remain with the following expression

$$-\theta(\tau_1-\tau_2)\frac{H^4}{6}\left(\tau_1^3-\tau_2^3\right)\left[\gamma+\ln(2M(\tau_1-\tau_2))\right], \tag{4.93}$$

where the logarithmic part exactly matches the $M_{cm}$-dependence that we found in the IR-integration.
So the full momenta integral becomes

$$\int \frac{d^3p_1}{(2\pi)^3} G^R(p_1,\tau_1,\tau_2)\,F(p_1,\tau_2,\tau_1) = \theta(\tau_1-\tau_2)\frac{H^4}{12\pi^2}\left[\frac{\tau_1^3-\tau_2^3}{2\epsilon} - \frac{\tau_1^2\tau_2^2}{4}\frac{\cos 2\Lambda(\tau_1-\tau_2)}{\tau_1-\tau_2} - \gamma(\tau_1^3-\tau_2^3) + \tau_1^3\ln\frac{\tau_2}{2(\tau_1-\tau_2)} - \tau_2^3\ln\frac{\tau_1}{2(\tau_1-\tau_2)}\right]. \tag{4.94}$$

Attaching the external legs

$$(Db3) = \frac{\lambda^2H^2}{32\pi^4}\frac{1}{18k^3}\left[\frac{1}{2\epsilon}+\ln\left(\frac{\mu}{H}\right)\right]\int_{\tau_{in}}^{\tau} d\tau_1 \frac{\tau^3-\tau_1^3}{\tau_1^4}\int_{\tau_{in}}^{\tau_1} d\tau_2 \frac{1}{\tau_2^4}\left[\left(\tau_1^3-\tau_2^3\right)\left(\frac{1}{2\epsilon}-\gamma\right) + \tau_1^3\ln\tau_2 - \tau_2^3\ln\tau_1 - (\tau_1^3-\tau_2^3)\ln 2(\tau_1-\tau_2) - \frac{\tau_1^2\tau_2^2}{4}\frac{\cos 2\Lambda(\tau_1-\tau_2)}{\tau_1-\tau_2}\right] \tag{4.95}$$

and executing the time integrations leads to a very lengthly, complicated and not very illuminating expression. So let us just stay with the expression above that already shows that these diagrams are again IR divergent, but UV finite.

## 4.5. Conclusions

In this Chapter we examined the two-point correlation function for a $\phi^4$-theory on de Sitter background. We completed the analysis for one-loop, for two-loop we analyzed the IR- and the IR×UV contributions. The work on the UV-part is still in progress.

For one-loop, our results agree with [66, 67]. We find IR-divergent terms, but it is finite in the UV-limit. We also found a logarithmic time dependence.

The calculation for two-loop is far more complex, thus we split the calculation up in different parts. For the IR-part we find cubic, quadratic and linear logarithmic contributions. Although IR×UV terms are possible in general, we find that they all cancel each other. The UV-calculation for two-loop is still in progress.

# 5. Conclusions and Outlook

> Good judgment comes from experience,
> and experience comes from bad judgment.
>
> *(Rita Mae Brown)*

We derived exact tunneling solutions for piecewise linear and quartic potentials and discussed what this teaches us about the local shape of the landscape. We then analyzed the situation of general existence of such solutions and showed in which cases we can approximate potentials with kinks by those with smooth caps. We also analyzed quantum corrections for a $\phi^4$ scalar field theory on de Sitter background.

Taking string theory serious, we have to deal with a large number of vacua. Since it is the leading candidate for a UV-complete theory describing the universe, we take this as motivation for our work. In this context, it is obviously of great interest to study tunneling mechanics. Tunneling amplitudes are very sensitive to the shape of the potential and the commonly used thin-wall approximation only gives usable results in very small parameter ranges. The relative energy difference between neigboring vacua in the string landscape is usually too large for the thin-wall approximation. It is therefore crucial to know the exact tunneling solutions for many different potentials. With these solutions we can learn more about the local shape of the landscape around us.

The calculation of the two-point function to the next loop-level is motivated by the fastly improving data that is coming from the new cosmological experiments, here especially PLANCK. With the new data, we will hopefully be able to distinguish more inflationary models for example.

We analyze the situation of tunneling for piecewise potentials with the false vacuum being described by a linear or a quartic potential towards the true vacuum described by a quartic potential. We find exact tunneling solutions for these two cases and show that the tunneling amplitude is very sensitive to the shape of the potential. Having exact solutions also allows a better qualitative understanding of these processes. The solutions give also information about the local shape of the landscape.

Another important point is of course the existence of these solutions in general. In previous papers [32, 37] the problems caused by kinks were simply ignored, the justification for this was missing. We presented an explanation for the validity in this work. In case of non-smooth potentials it is possible to save the situation in certain cases by replacing the kink by a smooth cap.

We also partly derived the two-point correlation function for a $\phi^4$-theory on de Sitter background for a massless minimally coupled scalar field $\phi$. For one-loop, our results agree with [66, 67]. We find IR-divergent terms, but it is finite in the UV-limit. We also found a logarithmic time dependence.

The calculation for two-loop is far more complex, thus we split the calculation up in different parts. For the IR-part we find cubic, quadratic and linear logarithmic contributions. Although IR×UV terms are possible in general, we find that they all cancel each other. Parts of the UV-calculation for two-loop are still in progress.

Projects of interest for the future include analyzing the tunneling mechanics of more complicated potentials. So far, only monomials have been studied. A first step would be to look at polynomials. The obvious next step for the analysis of inflationary perturbations of Chapter 4 is to complete the UV-calculation for two-loop.

# A. Useful relations for loop calculations

## A.1. Diagram B — small momenta

For the computation of diagram $(B)$ in the small internal momenta limit we need the following two integrals:

$$
\begin{aligned}
I_1 &= \int \frac{\mathrm{d}^3 p}{(2\pi)^3}\, e^{i\vec{p}\vec{x}}\, p^{2\epsilon-3} = \frac{2\pi}{(2\pi)^3} \int_0^\infty p^2\, \mathrm{d}p \int_{-1}^{1} \mathrm{d}\cos\theta\, p^{2\epsilon-3}\, e^{ipr\cos\theta} \\
&= \frac{1}{4\pi^2} \int_0^\infty p^2\, \mathrm{d}p\, p^{2\epsilon-3}\, \frac{e^{ipr} - e^{-ipr}}{ipr} = \frac{1}{2\pi^2 r} \int_0^\infty \mathrm{d}p\, p^{2\epsilon-2}\, \sin(pr) \\
&= \frac{1}{2\pi^2}\, r^{-2\epsilon+2-1-1} \int_0^\infty \mathrm{d}(pr)\, (pr)^{2\epsilon-2}\, \sin(pr) = \frac{1}{2\pi^2}\, r^{-2\epsilon}\, \Gamma(2\epsilon-1)\, \sin\frac{\pi(2\epsilon-1)}{2}
\end{aligned}
$$

$$
\begin{aligned}
I_2 &= \int \mathrm{d}^3 x\, r^{-6\epsilon}\, e^{-i\vec{k}\vec{x}} = 2\pi \int_0^\infty \mathrm{d}r\, r^2\, r^{-6\epsilon} \int_{-1}^{1} \mathrm{d}\cos\theta_k\, e^{-ikr\cos\theta_k} \\
&= 2\pi \int_0^\infty \mathrm{d}r\, r^{-6\epsilon+2}\, \frac{e^{ikr} - e^{-ikr}}{ikr} = \frac{4\pi}{k} \int_0^\infty \mathrm{d}r\, r^{-6\epsilon+1}\, \sin(kr) \\
&= 4\pi\, k^{6\epsilon-1-1-1} \int_0^\infty \mathrm{d}(kr)\, (kr)^{-6\epsilon+1}\, \sin(kr) \\
&= 4\pi\, k^{6\epsilon-3}\, \Gamma(-6\epsilon+2)\, \sin\frac{\pi(2-6\epsilon)}{2}
\end{aligned}
\tag{A.1}
$$

## A.2. From two momenta to one

For most of the loop calculations we used the following identity

$$\int d^3p d^3p' \delta^3(\vec{k}+\vec{p}+\vec{p}')f(k,p,p') = \frac{2\pi}{k}\int_0^\infty dpp \int_{|p-k|}^{p+k} dp'p' f(k,p,p'). \tag{A.2}$$

This follows with $d^3p = 4\pi p^2 dp$ from

$$\int d^3p f(k,p,|\vec{k}+\vec{p}|) = 2\pi \int_0^\infty p^2 \mathrm{d}p \int_0^\pi \mathrm{d}\theta f(k,p,\sqrt{k^2+p^2+2kp\cos\theta}) \tag{A.3}$$

and

$$\mathrm{d}\cos\theta = \frac{2p'\mathrm{d}p'}{2kp}. \tag{A.4}$$

# B. Loop calculations from Meulen and Smit

The following calculation is analogue to [6]. We include it in the Appendix to provide all necessary material in one document to the reader.

## B.1. Diagram $\mathrm{A}^{\mathrm{MS}}$ and $\mathrm{D}^{\mathrm{MS}}$

We use the first two diagrams for determining $\delta_\lambda$ in Section 4.3.2. We only need the UV-contributions of the amputated diagrams.

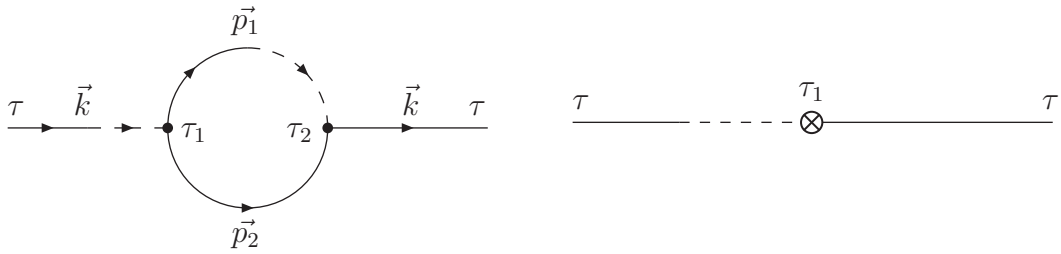


$(A^{MS})$ $(D^{MS})$

The amputated expressions for these two diagrams are

$$\begin{aligned} A^{MS}(k,\tau_1,\tau_2) &= \frac{i\lambda^2}{(2\pi)^3}\, a^4(\tau_1)a^4(\tau_2) \int \mathrm{d}^3p \int \mathrm{d}^3p'\, \delta^3(\vec{k}-\vec{p}-\vec{p}') \\ &\quad \times G^R(p',\tau_1,\tau_2)\, F(p,\tau_1,\tau_2) \\ &= \frac{i\lambda^2}{(2\pi)^2 k}\, a^4(\tau_1)a^4(\tau_2) \int_0^\infty \mathrm{d}p \int_{|p-k|}^{p+k} \mathrm{d}p'\, G^R(p',\tau_1,\tau_2)\, F(p,\tau_1,\tau_2) \end{aligned} \tag{B.1}$$

using Eq. (A.2). For the second diagram we have

$$D^{MS}(k,\tau_1,\tau_2) = -ia^4(\tau_1)\delta_m\delta(\tau_1-\tau_2). \tag{B.2}$$

Using Eq. (4.27) and Eq. (4.28), we find – dropping the prefactor for a moment – the following expression for the large momentum contributions of the amputated $A^{MS}$

diagram

$$
\begin{aligned}
A^{MS}(k,\tau_1,\tau_2) &= \int \mathrm{d}\,p_1 \int \mathrm{d}\,p_2\, F(p,\tau_1,\tau_2)\, G^R(p',\tau_1,\tau_2) \\
&= \Bigg[\frac{\cos p\Delta\tau}{p}\left(\frac{\sin(p+k)\Delta\tau}{p+k} - \frac{\sin(p-k)\Delta\tau}{p-k}\right) \\
&\quad + \frac{1}{2}\tau_1\tau_2 \sin k\Delta\tau\,(2\mathrm{Ci}(2p\Delta\tau) + \mathrm{Ci}(2(p+k)\Delta\tau) + \mathrm{Ci}(2(p-k)\Delta\tau) \\
&\quad + \ln\frac{p^2}{p^2-k^2} - 2\frac{\sin 2p\Delta\tau}{p\Delta\tau}\Bigg) - \frac{(\tau_1\tau_2)}{\Delta\tau}\cos k\Delta\tau\,(\mathrm{Si}(2(p+k)\Delta\tau) \\
&\quad - \mathrm{Si}(2(p-k)\Delta\tau)) + \frac{\tau_1^2\tau_2^2}{\Delta\tau^2}\sin k\Delta\tau \sin^2 p\Delta\tau\Bigg]_{M_{cm}}^{\Lambda a(\tau_2)} \\
&\quad + \int_M^{\Lambda a(\tau_2)} \mathrm{d}p \frac{\cos p\Delta\tau}{p}\left\{\frac{\sin(p+k)\Delta\tau}{(p+k)^2} - \frac{\sin(p-k)\Delta\tau}{(p-k)^2}\right. \\
&\quad \left. - \Delta\tau\left(\frac{\cos(p+k)\Delta\tau}{p+k} - \frac{\cos(p-k)\Delta\tau}{p-k}\right)\right\}.
\end{aligned}
\tag{B.3}
$$

Using the approximation $|M_{cm}\tau_i| \ll 1$, the expression above can be simplified to

$$
\begin{aligned}
&\frac{2k}{3}(\tau_1^3 - \tau_2^3)\left(\frac{7}{3} - \gamma - \ln 2M_{cm}(\tau_1-\tau_2)\right) - \frac{2}{3}\,k\,\tau_1\,\tau_2\,(\tau_1-\tau_2) \\
&+ \frac{\tau_1^2\tau_2^2}{\Delta\tau^2}\,\sin k\Delta\tau\,\sin^2\Lambda\,a(\tau_2)\,\Delta\tau + \mathcal{O}(\tau_i^4).
\end{aligned}
\tag{B.4}
$$

We have a closer look at the term containing $\sin^2\Lambda$. It is logarithmically divergent for $\Lambda\to\infty$. We begin with the following integral

$$
\int_{-\infty}^{\infty} \mathrm{d}\,\Delta\tau\,\theta(\Delta\tau)\,f(\Delta\tau)\,\frac{\sin^2\Lambda\,a(\tau_2)\,\Delta\tau}{\Delta\tau} = \frac{1}{2}\int_0^{\infty}\mathrm{d}\,\Delta\tau\;f(\Delta\tau)\,\frac{1-\cos\left(\frac{-2\Lambda}{H}\frac{\Delta\tau}{\tau_1-\Delta\tau}\right)}{\Delta\tau}
\tag{B.5}
$$

introducting the test function $f(\Delta\tau)$. We split up the integral into two parts to evaluate them separately

$$
\int_0^{\infty} = \lim_{\epsilon\to 0}\int_{\epsilon}^{\eta} + \int_{\eta}^{\infty}.
\tag{B.6}
$$

$\eta$ is the regulator time and will be taken to zero in the end after taking $\Lambda\to\infty$. The

first integral becomes

$$\begin{aligned}\lim_{\epsilon\to 0}\int_{\epsilon}^{\eta} \mathrm{d}\Delta\tau f(0)\frac{1-\cos\left(\frac{-2\Lambda}{H}\frac{\Delta\tau}{\tau_1}\right)}{\Delta\tau} = \lim_{\epsilon\to 0} f(0)\left(\ln\frac{\eta}{\epsilon} - \mathrm{Ci}\left(\frac{-2\Lambda\eta}{H\tau_1}\right) + \mathrm{Ci}\left(\frac{-2\Lambda\epsilon}{H\tau_1}\right)\right)\\ = f(0)\left(\gamma + \ln\frac{-2\Lambda\eta}{H\tau_1}\right)\end{aligned} \tag{B.7}$$

using the approximations

$$\frac{\Delta\tau}{\tau_1-\Delta\tau} \approx \frac{\Delta\tau}{\tau_1}, \quad f(\Delta\tau)\approx f(0) \tag{B.8}$$

and then taking the following limits for the Ci-terms

$$\mathrm{Ci}(-2\Lambda\eta/H\tau_1)\to 0, \quad \mathrm{Ci}(-2\Lambda\epsilon/H\tau_1)\to \gamma + \ln(-2\Lambda\epsilon/H\tau_1). \tag{B.9}$$

This then gives

$$\lim_{\Lambda\to\infty}\int_{\eta}^{\infty}\mathrm{d}\Delta\tau f(\Delta\tau)\frac{1-\cos\left(\frac{-2\Lambda}{H}\frac{\Delta\tau}{\tau_1-\Delta\tau}\right)}{\Delta\tau} = \int_{\eta}^{\infty}\mathrm{d}\Delta\tau\frac{f(\Delta\tau)}{\Delta\tau} \tag{B.10}$$

for the second part of the integral. In the last step, the cosine term vanishes, assuming the test function $f(\Delta\tau)$ vanishes sufficiently fast as $\Delta\tau\to\infty$. In the limit $\Lambda\to\infty$ this gives

$$\begin{aligned}&\int_{-\infty}^{\infty}\mathrm{d}\,\Delta\tau\theta(\Delta\tau)\,f(\Delta\tau)\,\frac{\sin^2\Lambda a(\tau_2)\Delta\tau}{\Delta\tau}\\ &=\int_{-\infty}^{\infty}\mathrm{d}\,\Delta\tau\,f(\Delta\tau)\,\frac{1}{2}\left[\frac{\Theta(-\eta+\Delta\tau)}{\Delta\tau}+\delta(\Delta\tau)\left(\gamma+\ln\frac{-2\Lambda\eta}{H\tau_1}\right)\right],\end{aligned} \tag{B.11}$$

which becomes

$$\theta(\Delta\tau)\,\frac{\sin^2\Lambda a(\tau_2)\Delta\tau}{\Delta\tau} = \frac{1}{2}\left[\frac{\Theta(-\eta+\Delta\tau)}{\Delta\tau}+\delta(\Delta\tau)\left(\gamma+\ln\frac{-2\Lambda\eta}{H\tau_1}\right)\right] \tag{B.12}$$

using distributions. Altogether, we find for the amputated large momentum contributions

$$\begin{aligned}A^{MS}+D^{MS} =&\frac{\mathrm{i}\lambda^2\Theta(\tau_1-\tau_2)}{2(2\pi)^2H^4\tau_1^4\tau_2^4}\left(\frac{2}{3}(\tau_1^3-\tau_2^3)\left(\frac{7}{3}-\gamma-\ln 2M_{cm}\Delta\tau\right)-\frac{2}{3}\tau_1\tau_2(\tau_1-\tau_2)\right.\\ &\left.+\frac{(\tau_1\tau_2)^2}{2}\left[\frac{\Theta(-\eta+\Delta\tau)}{\Delta\tau}+\delta(\Delta\tau)\left(\gamma+\ln\frac{-2\mu\eta}{H\tau_1}\right)\right]\right)\end{aligned} \tag{B.13}$$

with

$$D^{MS}(k,\tau_1,\tau_2) = -\frac{\mathrm{i}\lambda^2}{4(2\pi)^2H^4\tau_1^4}\ln\left(\frac{\Lambda}{\mu}\right)\delta(\tau_1-\tau_2). \tag{B.14}$$

## B.2. Diagrams $\mathrm{B}^{\mathrm{MS}}$ and $\mathrm{C}^{\mathrm{MS}}$

The combination of the internal momenta of these two diagrams is used twice in the main text. First, we need it in Section 4.3.2 for the 4-point function for one-loop, second in Section 4.4.1 for the two-loop calculations.

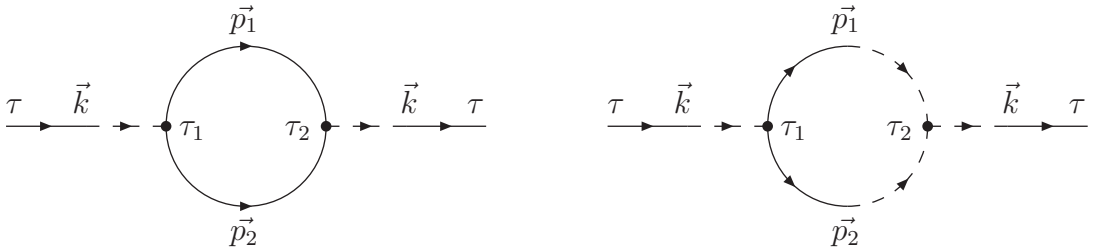


$(B^{MS})$ $(C^{MS})$

The full expressions are

$$\begin{aligned} B^{MS}(k,\tau_1,\tau_2) =& \frac{(-i)^2(-i\lambda)^2}{2H^8\tau_1^4\tau_2^4}\frac{1}{(2\pi)^3}\int \mathrm{d}\tau_1 \int \mathrm{d}\tau_2\, G^R(k,\tau,\tau_1)\, G^R(k,\tau_2,\tau) \\ & \times \int \mathrm{d}^3p_1 \int \mathrm{d}^3p_2\, \delta^3(\vec{k}-\vec{p}_1-\vec{p}_2) F(p_1,\tau_1,\tau_2) F(p_2,\tau_1,\tau_2) \end{aligned} \tag{B.15}$$

and

$$\begin{aligned} C^{MS}(k,\tau_1,\tau_2) =& \frac{(-i)^4(-i\lambda)^2}{8H^8\tau_1^4\tau_2^4}\frac{1}{(2\pi)^3}\int \mathrm{d}\tau_1 \int \mathrm{d}\tau_2\, G^R(k,\tau,\tau_1)\, G^R(k,\tau_2,\tau) \\ & \times \int \mathrm{d}^3p_1 \int \mathrm{d}^3p_2\, \delta^3(\vec{k}-\vec{p}_1-\vec{p}_2) G^R(p_1,\tau_1,\tau_2) G^R(p_2,\tau_1,\tau_2). \end{aligned} \tag{B.16}$$

We begin with the small internal momenta. Here, only diagram $B^{MS}$ contributes. We find

$$\begin{aligned} & \frac{-\lambda^2 H^4(\tau_1\tau_2)^{2\epsilon}}{8(2\pi)^2 k H^8(\tau_1\tau_2)^4} \int_0^{M_{cm}} \mathrm{d}p \int_{|p-k|}^{p+k} \mathrm{d}p' \frac{(pp')^{2\epsilon}}{(pp')^2} \\ & = \frac{-\lambda^2(\tau_1\tau_2)^{2\epsilon}}{8(2\pi)^2 k H^4(\tau_1\tau_2)^4(2\epsilon-1)} \left( \int_0^k \mathrm{d}p p^{-2+2\epsilon} \left( (p+k)^{-1+2\epsilon} - (k-p)^{-1+2\epsilon} \right) \right. \\ & \left. \int_k^{M_{cm}} \mathrm{d}p p^{-2+2\epsilon} \left( (p+k)^{-1+2\epsilon} - (p-k)^{-1+2\epsilon} \right) \right). \end{aligned} \tag{B.17}$$

To evaluate these integrals, we calculate them first for $\epsilon > 1/2$ using analytic continua-

tion to $\epsilon \ll 1$ in the end. We substitute $p = kx$ using the following integrals

$$\begin{aligned}\int_0^1 \mathrm{d}\, x^{-2+2\epsilon}\,(1+x)^{-1+2\epsilon} =& \sum_{n=0}^{\infty} \frac{(-1)^n}{n!}\,\frac{\Gamma(1+n-2\epsilon)}{\Gamma(1-2\epsilon)} \int_0^1 \mathrm{d}\, x\, x^{-2+n+2\epsilon} \\ =& -\frac{1}{2\epsilon} + \ln 2 + \mathcal{O}(\epsilon),\end{aligned} \tag{B.18}$$

$$\int_0^1 \mathrm{d}\, x\, x^{-2+2\epsilon}\,(1-x)^{-1+2\epsilon} = B(-1+2\epsilon, 2\epsilon) = \frac{1}{\epsilon} - 2 + \mathcal{O}(\epsilon), \tag{B.19}$$

with the $\beta$-function

$$B(x,y) = \frac{\Gamma(x)\Gamma(y)}{\Gamma(x+y)}. \tag{B.20}$$

$$\begin{aligned}\int_1^{M_{cm}/k} \mathrm{d}\, x\, x^{-2+2\epsilon}\,(1+x)^{-1+2\epsilon} =& \int_{k/M_{cm}}^1 \mathrm{d}\, y\, \frac{y^{1-4\epsilon}}{(1+y)^{1-2\epsilon}} \\ & 1 - \frac{k}{M_{cm}} - \ln 2 + \ln\left(1 + \frac{k}{M_{cm}}\right) + \mathcal{O}(\epsilon),\end{aligned} \tag{B.21}$$

$$\begin{aligned}\int_1^{M_{cm}/k} \mathrm{d}\, x\, x^{-2+2\epsilon}\,(x-1)^{-1+2\epsilon} =& \int_{k/M_{cm}}^1 \mathrm{d}\, y\, \frac{y^{1-4\epsilon}}{(1-y)^{1-2\epsilon}} \\ =& \int_0^{1-k/M_{cm}} \mathrm{d}\, z\, z^{-1+2\epsilon}\,(1-z) + \mathcal{O}(\epsilon) \\ & \frac{1}{2\epsilon} - 1 + \frac{k}{M_{cm}} + \ln\left(1 - \frac{k}{M_{cm}}\right) + \mathcal{O}(\epsilon),\end{aligned} \tag{B.22}$$

with $y = 1/x$ and $z = 1 - y$. Altogether this gives

$$\begin{aligned}&\frac{-\lambda^2(\tau_1\tau_2)^{2\epsilon}}{8(2\pi)^2 k H^4(\tau_1\tau_2)^4(2\epsilon-1)}\left(-\frac{2}{\epsilon} + 4 - 2\frac{k}{M_{cm}} + \ln\frac{1+k/M_{cm}}{1-k/M_{cm}} + \mathcal{O}(\epsilon)\right) \\ =&\frac{-\lambda^2}{4(2\pi)^2 k^3 H^4(\tau_1\tau_2)^4}\left(\frac{1}{\epsilon} + \frac{k}{M} - \frac{1}{2}\ln\frac{M+k}{M-k} + 2\ln(k^2\tau_1\tau_2) + \mathcal{O}(\epsilon)\right).\end{aligned} \tag{B.23}$$

Now we come to the large internal momenta. For diagram $B^{MS}$ we find

$$\begin{aligned}
B^{MS} &= \int \mathrm{d}\,p \int \mathrm{d}\,p'\, F(p)\, F(p') \\
&= \Bigg[ \frac{\cos p\Delta\tau}{p} \left( \frac{\cos(p+k)\Delta\tau}{p+k} - \frac{\cos(p-k)\Delta\tau}{p-k} \right) \\
&\quad -\tau_1\tau_2 \sin k\Delta\tau \left( \mathrm{Si}(2p\Delta\tau) + 2\frac{\cos^2 p\Delta\tau}{p\Delta\tau} \right) + \frac{(\tau_1\tau_2)^2}{\Delta\tau} \sin k\Delta\tau \left( p + \frac{\sin 2p\Delta\tau}{2\Delta\tau} \right) \Bigg]_M^{\Lambda(\tau_\beta)} \\
&\quad + \int_M^{\Lambda(\tau_\beta)} \mathrm{d}\,p \frac{\cos p\Delta\tau}{p} \left\{ \frac{\cos(p+k)\Delta\tau}{(p+k)^2} - \frac{\cos(p-k)\Delta\tau}{(p-k)^2} \right. \\
&\quad \left. +\Delta\tau \left( \frac{\sin(p+k)\Delta\tau}{p+k} - \frac{\sin(p-k)\Delta\tau}{p-k} \right) - p\,\tau_1\tau_2 \left( \frac{\cos(p+k)\Delta\tau}{p+k} - \frac{\cos(p-k)\Delta\tau}{p-k} \right) \right\}.
\end{aligned} \tag{B.24}$$

The only UV-divergent term here is

$$-\frac{\lambda^2 \sin k\Delta\tau}{8(2\pi)^2 k H^4 (\tau_1\tau_2)^2 \Delta\tau} \left[ p + \frac{\sin 2p\Delta\tau}{2\Delta\tau} \right]_M^{\Lambda a(\tau_\beta)}, \tag{B.25}$$

the only term giving late time contributions is

$$-\frac{\lambda^2}{4(2\pi)^2 k^3 H^4 (\tau_1\tau_2)^4} \left( -\frac{k}{M} + \frac{1}{2} \ln \frac{M+k}{M-k} + \mathcal{O}(\tau_i^2) \right). \tag{B.26}$$

For diagram $C^{MS}$ we proceed similarly:

$$\begin{aligned}
C^{MS} &= \int \mathrm{d}\,p \int \mathrm{d}\,p'\, G^R(p)\, G^R(p') \\
&= \Bigg[ \frac{\sin p\Delta\tau}{p} \left( \frac{\sin(p+k)\Delta\tau}{p+k} - \frac{\sin(p-k)\Delta\tau}{p-k} \right) \\
&\quad +\tau_1\tau_2 \sin k\Delta\tau \left( 3\,\mathrm{Si}(2p\Delta\tau) + 2\frac{\sin^2 p\Delta\tau}{p\Delta\tau} \right) + \frac{(\tau_1\tau_2)^2}{\Delta\tau} \sin k\Delta\tau \left( p - \frac{\sin 2p\Delta\tau}{2\Delta\tau} \right) \Bigg]_M^{\Lambda(\tau_\beta)} \\
&\quad + \int_M^{\Lambda(\tau_\beta)} \mathrm{d}\,p \frac{\sin p\Delta\tau}{p} \left\{ \frac{\sin(p+k)\Delta\tau}{(p+k)^2} - \frac{\sin(p-k)\Delta\tau}{(p-k)^2} \right. \\
&\quad \left. -\Delta\tau \left( \frac{\cos(p+k)\Delta\tau}{p+k} - \frac{\cos(p-k)\Delta\tau}{p-k} \right) - p\,\tau_1\tau_2 \left( \frac{\sin(p+k)\Delta\tau}{p+k} - \frac{\sin(p-k)\Delta\tau}{p-k} \right) \right\}
\end{aligned} \tag{B.27}$$

The only UV-divergent term is

$$\frac{\lambda^2 \Theta(\tau_1-\tau_2) \sin k\Delta\tau}{8(2\pi)^2 k H^4 (\tau_1\tau_2)^2 \Delta\tau} \left[ p - \frac{\sin 2p\Delta\tau}{\Delta\tau} \right]_M^{\Lambda a(\tau_\beta)}. \tag{B.28}$$

Adding the UV-divergent terms of $B^{MS}$ and $C^{MS}$ we see that they add up to something finite

$$\frac{-\lambda^2 \sin k\Delta\tau}{8(2\pi)^2 k H^4 (\tau_1\tau_2)^2 \Delta\tau}\left[\frac{\sin 2p\Delta\tau}{\Delta\tau}\right]_M^{\Lambda a(\tau_\beta)}. \tag{B.29}$$

The complete expression for the amputated diagrams $B^{MS} + C^{MS}$ is

$$-\frac{\lambda^2}{4(2\pi)^2 k^3 H^4 (\tau_1\tau_2)^4}\left(\frac{1}{\epsilon} + 2\ln(k^2\tau_1\tau_2) + \mathcal{O}(\tau_i) + \mathcal{O}(\epsilon)\right). \tag{B.30}$$

Note that the $M_{cm}$ has dropped out completely.

# Bibliography


[1] *The Royal Swedish Academy of Sciences: Press Release*, . 1978, 2006, 2011.

[2] M. R. Douglas, *The statistics of string/M theory vacua*, *JHEP* **05** (2003) 046 [hep-th/0303194].

[3] M. R. Douglas and S. Kachru, *Flux compactification*, *Rev. Mod. Phys.* **79** (2007) 733–796 [hep-th/0610102].

[4] R. Bousso and J. Polchinski, *Quantization of four form fluxes and dynamical neutralization of the cosmological constant*, *JHEP* **0006** (2000) 006 [hep-th/0004134].

[5] L. Susskind, *The Anthropic landscape of string theory*, hep-th/0302219.

[6] M. van der Meulen and J. Smit, *Classical approximation to quantum cosmological correlations*, *JCAP* **0711** (2007) 023 [0707.0842].

[7] K. Dutta, C. Hector, P. M. Vaudrevange and A. Westphal, *More Exact Tunneling Solutions in Scalar Field Theory*, *Phys. Lett.* **B708** (2012) 309–313 [1110.2380].

[8] K. Dutta, C. Hector, T. Konstandin, P. M. Vaudrevange and A. Westphal, *On the Existence of Tunneling Bounce Solutions in Piecewise Linear Potentials*, 1202.2721.

[9] L. Covi, C. Hector and N. Kevlishvili, *in preparation*, .

[10] E. W. Kolb and M. S. Turner, *The Early universe*, *Front.Phys.* **69** (1990) 1–547.

[11] V. Mukhanov, *Physical foundations of cosmology*, . Cambridge, UK: Univ. Pr. (2005) 421 p.

[12] M. Trodden and S. M. Carroll, *TASI lectures: Introduction to cosmology*, astro-ph/0401547.

[13] A. Friedmann, *Über die Krümmung des Raumes*, *Zeitschrift für Physik A* **10 (1)** (1922) 377–386.

[14] A. Friedmann, *Über die Möglichkeit einer Welt mit konstanter negativer Krümmung des Raumes*, *Zeitschrift für Physik A* **21 (1)** (1924) 326–332.

[15] H. P. Robertson, *Kinematics and world structure*, *Astrophysical Journal* **82** (1935) 284–301.

[16] A. G. Walker, *On Milne's theory of world-structure*, *Proceedings of the London Mathematical Society 2* **42 (1)** (1937) 90–127.

[17] **WMAP Collaboration** Collaboration, E. Komatsu *et. al.*, *Seven-Year Wilkinson Microwave Anisotropy Probe (WMAP) Observations: Cosmological Interpretation*, *Astrophys.J.Suppl.* **192** (2011) 18 [1001.4538].

[18] D. Larson *et. al.*, *Seven-Year Wilkinson Microwave Anisotropy Probe (WMAP) Observations: Power Spectra and WMAP-Derived Parameters*, *Astrophys. J. Suppl.* **192** (2011) 16 [1001.4635].

[19] A. H. Guth, *The Inflationary Universe: A Possible Solution to the Horizon and Flatness Problems*, *Phys. Rev.* **D23** (1981) 347–356.

[20] A. D. Linde, *A New Inflationary Universe Scenario: A Possible Solution of the Horizon, Flatness, Homogeneity, Isotropy and Primordial Monopole Problems*, *Phys. Lett.* **B108** (1982) 389–393.

[21] K. Dutta, P. M. Vaudrevange and A. Westphal, *The Overshoot Problem in Inflation after Tunneling*, 1109.5182.

[22] A. A. Penzias and R. W. Wilson, *A Measurement of excess antenna temperature at 4080- Mc/s*, *Astrophys. J.* **142** (1965) 419–421.

[23] J. C. Mather *et. al.*, *Measurement of the Cosmic Microwave Background spectrum by the COBE FIRAS instrument*, *Astrophys. J.* **420** (1994) 439–444.

[24] R. H. Dicke, P. J. E. Peebles, P. G. Roll and D. T. Wilkinson, *Cosmic Black-Body Radiation*, *Astrophys. J.* **142** (1965) 414–419.

[25] **Planck** Collaboration, *Planck: The scientific programme*, astro-ph/0604069.

[26] A. H. Guth and S. Y. Pi, *Fluctuations in the New Inflationary Universe*, *Phys. Rev. Lett.* **49** (1982) 1110–1113.

[27] A. A. Starobinsky, *Dynamics of Phase Transition in the New Inflationary Universe Scenario and Generation of Perturbations*, *Phys. Lett.* **B117** (1982) 175–178.

[28] V. F. Mukhanov, H. A. Feldman and R. H. Brandenberger, *Theory of cosmological perturbations. Part 1. Classical perturbations. Part 2. Quantum theory of perturbations. Part 3. Extensions*, *Phys. Rept.* **215** (1992) 203–333.

[29] E. D. Stewart and D. H. Lyth, *A more accurate analytic calculation of the spectrum of cosmological perturbations produced during inflation*, *Phys. Lett.* **B302** (1993) 171–175 [gr-qc/9302019].

[30] J. M. Bardeen, *Gauge Invariant Cosmological Perturbations*, *Phys. Rev.* **D22** (1980) 1882–1905.

[31] S. J. Huber and T. Konstandin, *Gravitational Wave Production by Collisions: More Bubbles*, *JCAP* **0809** (2008) 022 [0806.1828].

[32] S. R. Coleman, *The Fate of the False Vacuum. 1. Semiclassical Theory*, *Phys. Rev.* **D15** (1977) 2929–2936.

[33] J. Callan, Curtis G. and S. R. Coleman, *The Fate of the False Vacuum. 2. First Quantum Corrections*, *Phys.Rev.* **D16** (1977) 1762–1768.

[34] S. R. Coleman and F. De Luccia, *Gravitational Effects on and of Vacuum Decay*, *Phys. Rev.* **D21** (1980) 3305.

[35] S. Hawking and I. Moss, *Supercooled Phase Transitions in the Very Early Universe*, *Phys.Lett.* **B110** (1982) 35.

[36] F. C. Adams, *General solutions for tunneling of scalar fields with quartic potentials*, *Phys.Rev.* **D48** (1993) 2800–2805 [hep-ph/9302321].

[37] M. J. Duncan and L. G. Jensen, *Exact tunneling solutions in scalar field theory*, *Phys.Lett.* **B291** (1992) 109–114.

[38] T. Hamazaki, M. Sasaki, T. Tanaka and K. Yamamoto, *Selfexcitation of the tunneling scalar field in false vacuum decay*, *Phys.Rev.* **D53** (1996) 2045–2061 [gr-qc/9507006].

[39] G. Pastras, *Exact Tunneling Solutions in Minkowski Spacetime and a Candidate for Dark Energy*, 1102.4567.

[40] K. Dutta, P. M. Vaudrevange and A. Westphal, *An Exact Tunneling Solution in a Simple Realistic Landscape*, 1102.4742.

[41] K.-M. Lee and E. J. Weinberg, *Tunneling without barriers*, *Nucl.Phys.* **B267** (1986) 181.

[42] X. Dong and D. Harlow, *Analytic Coleman-de Luccia Geometries*, 1109.0011.

[43] S. R. Coleman, *Quantum tunneling and negative eigenvalues*, *Nucl.Phys.* **B298** (1988) 178.

[44] M. Cvetic and H. H. Soleng, *Naked singularities in dilatonic domain wall space times*, *Phys.Rev.* **D51** (1995) 5768–5784 [hep-th/9411170].

[45] M. C. Johnson and M. Larfors, *An Obstacle to populating the string theory landscape*, *Phys.Rev.* **D78** (2008) 123513 [0809.2604].

[46] A. Aguirre, M. C. Johnson and M. Larfors, *Runaway dilatonic domain walls*, *Phys.Rev.* **D81** (2010) 043527 [0911.4342].

[47] A. R. Brown and A. Dahlen, *Small Steps and Giant Leaps in the Landscape*, *Phys.Rev.* **D82** (2010) 083519 [1004.3994].

[48] A. R. Brown and A. Dahlen, *The Case of the Disappearing Instanton*, 1106.0527. * Temporary entry *.

[49] J. D. Norton, *The dome: An unexpectedly simple failure of determinism*, *Philosophy of Science* **Vol. 75, No. 5** (December, 2008) 786–798.

[50] L. Randall and R. Sundrum, *A Large mass hierarchy from a small extra dimension*, *Phys.Rev.Lett.* **83** (1999) 3370–3373 [hep-ph/9905221]. 9 pages, LaTex Report-no: MIT-CTP-2860, PUPT-1860, BUHEP-99-9.

[51] M. S. Sloth, *On the one loop corrections to inflation and the CMB anisotropies*, *Nucl. Phys.* **B748** (2006) 149–169 [astro-ph/0604488].

[52] M. S. Sloth, *On the one loop corrections to inflation. II: The consistency relation*, *Nucl. Phys.* **B775** (2007) 78–94 [hep-th/0612138].

[53] K. Enqvist, S. Nurmi, D. Podolsky and G. I. Rigopoulos, *On the divergences of inflationary superhorizon perturbations*, *JCAP* **0804** (2008) 025 [0802.0395].

[54] N. Bartolo, S. Matarrese, M. Pietroni, A. Riotto and D. Seery, *On the Physical Significance of Infra-red Corrections to Inflationary Observables*, *JCAP* **0801** (2008) 015 [0711.4263].

[55] A. Riotto and M. S. Sloth, *On Resumming Inflationary Perturbations beyond One-loop*, *JCAP* **0804** (2008) 030 [0801.1845].

[56] S. Weinberg, *Quantum contributions to cosmological correlations*, *Phys. Rev.* **D72** (2005) 043514 [hep-th/0506236].

[57] S. Weinberg, *Quantum contributions to cosmological correlations. II: Can these corrections become large?*, *Phys. Rev.* **D74** (2006) 023508 [hep-th/0605244].

[58] M. Spradlin, A. Strominger and A. Volovich, *Les Houches lectures on de Sitter space*, hep-th/0110007.

[59] A. D. Dolgov, M. B. Einhorn and V. I. Zakharov, *On Infrared effects in de Sitter background*, *Phys. Rev.* **D52** (1995) 717–722 [gr-qc/9403056].

[60] N. Bartolo, E. Komatsu, S. Matarrese and A. Riotto, *Non-Gaussianity from inflation: Theory and observations*, *Phys. Rept.* **402** (2004) 103–266 [astro-ph/0406398].

[61] E. Calzetta and B. L. Hu, *Closed Time Path Functional Formalism in Curved Space- Time: Application to Cosmological Back Reaction Problems*, *Phys. Rev.* **D35** (1987) 495.

[62] E. Calzetta and B. L. Hu, *Nonequilibrium Quantum Fields: Closed Time Path Effective Action, Wigner Function and Boltzmann Equation*, *Phys. Rev.* **D37** (1988) 2878.

[63] P. Adshead, R. Easther and E. A. Lim, *The 'in-in' Formalism and Cosmological Perturbations*, *Phys.Rev.* **D80** (2009) 083521 [0904.4207].

[64] G. Aarts and J. Smit, *Classical approximation for time-dependent quantum field theory: Diagrammatic analysis for hot scalar fields*, *Nucl. Phys.* **B511** (1998) 451–478 [hep-ph/9707342].

[65] I. Abramowitz, M. and Stegun, *Handbook of Mathematical Functions: With Formulas, Graphs, and Mathematical Tables*, *Dover Publications*.

[66] B. Garbrecht and G. Rigopoulos, *Self Regulation of Infrared Correlations for Massless Scalar Fields during Inflation*, *Phys.Rev.* **D84** (2011) 063516 [1105.0418].

[67] C. P. Burgess, L. Leblond, R. Holman and S. Shandera, *Super-Hubble de Sitter Fluctuations and the Dynamical RG*, *JCAP* **1003** (2010) 033 [0912.1608].

# Acknowledgements

*Du meinst, dann hätten sie doch gleich zu Hause bleiben können?*

*Du meinst, dann hätten sie sich den weiten Weg gespart?*

*O nein, denn sie hätten den Fuchs nicht getroffen, und die Krähe nicht.*

*Und sie hätten den Hasen und den Igel nicht getroffen,*

*und sie hätten nie erfahren, wie gemütlich so ein schönes, weiches Sofa aus Plüsch ist.*

*Und sie hätten nicht gelernt, daß wenn man einen Freund hat, braucht er sich vor nichts zu fürchten.*

**Janosch — Oh wie schön ist Panama**